THE CONTRIBUTION OF DNA INTERSTRAND CROSSLINKS TO AGING

by

Andria Rasile Robinson

B.S. in Pre-medicine, University of Dayton, 2002

Submitted to the Graduate Faculty of the

Department of Human Genetics

Graduate School of Public Health in partial fulfillment

of the requirements for the degree of

Doctor of Philosophy

University of Pittsburgh

2012

UNIVERSITY OF PITTSBURGH

Graduate School of Public Health

This dissertation was presented

by

Andria Rasile Robinson

It was defended on

May 14, 2012

and approved by

Dissertation Advisor:
Laura J. Niedernhofer, M.D., Ph.D.
Associate Professor, Department of Microbiology and Molecular Genetics
School of Medicine, University of Pittsburgh

Committee Member:
Susanne M. Gollin, Ph.D.
Professor, Department of Human Genetics
Graduate School of Public Health, University of Pittsburgh

Committee Member:
M. Ilyas Kamboh, Ph.D.
Professor, Department of Human Genetics
Graduate School of Public Health, University of Pittsburgh

Committee Member:
Paul D. Robbins, Ph.D.
Professor, Department of Microbiology and Molecular Genetics
School of Medicine, University of Pittsburgh

Committee Member:
Bennett Van Houten, Ph.D.
Professor, Department of Pharmacology and Chemical Biology
School of Medicine, University of Pittsburgh

Copyright © by Andria Rasile Robinson

2012

THE CONTRIBUTION OF DNA INTERSTRAND CROSSLINKS TO AGING

Andria Rasile Robinson, Ph.D.

University of Pittsburgh, 2012

DNA damage is hypothesized to be a driver of aging. In support of this, DNA damage and genetic mutations, resulting from replication of that damage, both increase in the nuclear genome as organisms age. Furthermore, long-lived species are relatively resistant to genotoxic stress. Conversely, organisms with DNA repair-deficient or genome instability disorders have decreased lifespans and age rapidly, which supports this theory. One main source of endogenous DNA damage is reactive oxygen species (ROS) generated by mitochondria. While it is true that ROS can damage other macromolecules in the cell, DNA is the only one that is repaired rather than replaced, illustrating the dire consequences of DNA damage. If repair is not 100% complete over a lifetime, it stands to reason that this unrepaired damage could be a major contributor to aging.

Ercc1$^{-/\Delta}$ mice are deficient in multiple DNA repair pathways and therefore suffer more DNA damage than normal mice. As a consequence, they age prematurely, modeling a human progeroid syndrome. This makes them a useful *in vivo* system for studying the contribution of DNA damage to aging. For this reason, we challenged the mice with a chemotherapeutic crosslinking agent to determine if DNA damage promotes aging, with an environmental contaminant and a diet of polyunsaturated fatty acids to see if these promote DNA damage and aging. We found that a particular class of lesions, DNA interstrand crosslinks, accelerate aging-associated changes through a cytostatic, rather than cytotoxic mechanism. We also

exposed the mice to a specialized antioxidant to test the hypothesis that mitochondrial-derived reactive oxygen species are the cause of endogenous DNA damage that promotes aging. Collectively, these studies identified genes, environmental influences and therapeutics that impact lifespan and healthspan. In total, the studies strongly support the hypothesis that DNA damage can promote degenerative changes associated with aging. These studies have public health significance as they reveal multiple novel strategies to decrease the DNA damage burden, therefore presenting potential opportunities to improve quality of life in old age.

TABLE OF CONTENTS

LIST OF TABLES

LIST OF FIGURES

ABBREVIATIONS

8K-NBD, octalysine NEMO binding domain peptide inhibitor

BOSS, Biomarkers of Oxidative Stress Studies

CCl_4, carbon tetrachloride

cdA, cyclodeoxyadenine

cdG, cyclodeoxyguanine

CEA, 2-chloroethylamine

COFS, cerebro-oculo-facio-skeletal syndrome

CPDs, cyclobutane pyrimidine dimers

CS, Cockayne syndrome

CSR, class switch recombination

DNA, deoxyribonucleic acid

DSBs, double strand breaks

EGFP, enhanced green fluorescent protein

EMSA, electrophoretic mobility shift assay

ERCC1, excision repair cross complementation group 1

ERCC4, excision repair cross complementation group 4

FANC, Fanconi anemia, complementation group

GFAP, glial fibrillary acidic protein

γH2AX, phosphorylated H2A histone family, member X

H&E, hematoxylin and eosin

HDL, high density lipoprotein

HGPS, Hutchinson-Gilford progeria syndrome

HR, homologous recombination

ICLs, DNA interstrand crosslinks

Ig, immunoglobulin

IKK, IκB kinase

IR, ionizing radiation

LDL, low density lipoprotein

LOOH, lipid hydroperoxides

LPO, lipid peroxidation

MEC, mechlorethamine

MEFs, mouse embryonic fibroblasts

MitoQ, mitochondrial-targeted coenzyme Q

MitoVitE, mitochondrial-targeted vitamin E

NEMO, NF-κB Essential Modulator

NER, nucleotide excision repair

NF-κB, nuclear factor κB

NHEJ, non-homologous end-joining

PAS, periodic acid Schiff

PUFAs, polyunsaturated fatty acids

ROS, reactive oxygen species

SA β-gal, senescence-associated β-galactosidase

SASP, senescence-associated secretory phenotype

SNK, Student Newman-Keuls

TFIIH, transcription factor IIH

TG, transgenic

TRF2, telomeric repeat binding factor 2

TTD, trichothiodystrophy

TTR, transthyretin

WT, wild-type

XJB, XJB-5-131, mitochondrial-targeted nitroxide radical scavenger

XP, xeroderma pigmentosum

XPA, xeroderma pigmentosum, complementation group A

XPD, xeroderma pigmentosum, complementation group D

XPF, xeroderma pigmentosum, complementation group F

XPG, xeroderma pigmentosum, complementation group G

1.0 INTRODUCTION

Chapter 1, Sections 1.1-1.5, are adapted from a published review in *DNA Repair* with copyright permission from Elsevier.

Gregg, S.Q.[1,2], Robinson, A.R.[1,3], and Niedernhofer, L.J.[1,4] (2011). Physiological consequences of defects in ERCC1-XPF DNA repair endonuclease. *DNA Repair* 10 (7): 781-791.

[1]University of Pittsburgh Cancer Institute, 5117 Centre Avenue, Hillman Cancer Canter 2.6, Pittsburgh, PA 15213, USA.

[2]Department of Cell Biology and Physiology, University of Pittsburgh School of Medicine, S362 Biomedical Science Towers, 3500 Terrace Street, Pittsburgh, PA 15261, USA

[3]Department of Human Genetics, University of Pittsburgh Graduate School of Public Health, 130 DeSoto Street, Pittsburgh, PA 15261, USA.

[4]Department of Microbiology and Molecular Genetics, University of Pittsburgh School of Medicine, 523 Bridgeside Point II, 450 Technology Drive, Pittsburgh, PA 15219, USA.

1.1 FUNCTIONS OF ERCC1-XPF NUCLEASE

The ERCC1–XPF/ERCC4 complex is a structure-specific endonuclease involved in the repair of damaged DNA. ERCC1–XPF performs a critical incision step in nucleotide excision repair (NER), and is also involved in the repair of DNA interstrand crosslinks (ICLs) and some double-strand breaks (DSBs) (Ahmad *et al.*, 2008; Busch *et al.*, 1997; Kuraoka *et al.*, 2000; Petit and Sancar, 1999; Sargent *et al.*, 1997a; Schlake *et al.*, 1993; Sekelsky *et al.*, 1995). A fraction of ERCC1–XPF is localized at telomeres, where it is implicated in recombination of telomeric sequences and loss of telomeric overhangs at deprotected chromosome ends (Munoz *et al.*, 2005; Zhu *et al.*, 2003). Deficiency of either ERCC1 or XPF/ERCC4 in humans results in a variety of conditions, which include the skin cancer-prone disease xeroderma pigmentosum (XP), a progeroid syndrome of accelerated aging, or cerebro-oculo-facio-skeletal syndrome (COFS) (Jaspers *et al.*, 2007; Niedernhofer *et al.*, 2006). These diseases are extremely rare in the general population and therefore mice with low levels of either ERCC1 or XPF have been generated and studied extensively. These murine models clearly illustrate the importance of DNA repair in preventing aging-related tissue degeneration (Diderich *et al.*, 2011). The purpose of this chapter is to provide an overview on the phenotypes of patients with mutations in *ERCC1* or *XPF*, and the mouse models used to study the diseases that result from decreased levels of ERCC1–XPF.

1.1.1 Nucleotide excision repair

Ultraviolet light damages DNA, resulting in a myriad of lesions, most predominantly cyclobutane pyrimidine dimers (CPDs) and (6-4) photoproducts (de Laat *et al.*, 1999). NER is the only mechanism by which these photodimers can be removed from DNA in human cells, and

ERCC1–XPF functions as the nuclease that incises the damaged strand 5′ to the adduct (Bardwell *et al.*, 1994; Park *et al.*, 1995; Sijbers *et al.*, 1996a; Tapias *et al.*, 2004). This incision creates a 3′ end that is used as a primer by the replication machinery to replace the excised nucleotides. XPF contains the catalytic activity with its conserved nuclease domain, and ERCC1 is required for binding to DNA (Enzlin and Scharer, 2002; Fagbemi *et al.*, 2011; Li *et al.*, 1994; Tripsianes *et al.*, 2005; Tsodikov *et al.*, 2005; Tsodikov *et al.*, 2007). Defects in the proteins required for NER can result in xeroderma pigmentosum (XP), trichothiodystrophy (TTD), and Cockayne syndrome (CS), highlighting the importance of DNA repair in preventing UV-induced skin cancer and developmental abnormalities. XP is a disease characterized by extreme photosensitivity and a 10,000-fold increased risk of cutaneous and ocular neoplasms (Kraemer *et al.*, 1994). Cells from all of the XP complementation groups (XP-A to XP-G, and XP-V) are hypersensitive to UV radiation (Itoh *et al.*, 2000; Mayne and Lehmann, 1982; Niedernhofer *et al.*, 2006; Sijbers *et al.*, 1996a; Weeda *et al.*, 1997b). ERCC1–XPF-deficient cells are distinct from other XP patient-derived cells because of their extreme sensitivity to chemicals that induce DNA ICLs (Busch *et al.*, 1997; De Silva *et al.*, 2000; Hoy *et al.*, 1985; Niedernhofer *et al.*, 2004). Another critical piece of evidence indicating that ERCC1–XPF has functions distinct from NER is that ERCC1 and XPF knockout mice exhibit a much more severe phenotype than XPA null mice, which are completely deficient in NER (Busch *et al.*, 1997; de Vries *et al.*, 1995; McWhir *et al.*, 1993; Nakane *et al.*, 1995; Tian *et al.*, 2004).

1.1.2 Intrastrand crosslink repair

The mechanism of DNA ICL repair in mammalian cells is not as well defined as NER. In replicating cells, crosslinking agents lead to DSBs created by an endonuclease(s) near the site of

stalled replication machinery (Raschle *et al.*, 2008). In the absence of ERCC1–XPF, replication-dependent crosslink-induced DSBs occur, indicating that ERCC1–XPF cannot be solely responsible for creating these DSBs (Niedernhofer *et al.*, 2004). There is clear evidence that ERCC1–XPF participates in the same mechanism of ICL repair as the Fanconi anemia proteins. In the absence of ERCC1–XPF, FANCD2 is still monoubiquitylated by FANCL, but translocation of FANCD2 to chromatin is impaired (Bhagwat *et al.*, 2009). In addition, when FANCD2 is depleted, replication-dependent incisions of ICLs are dramatically reduced (Knipscheer *et al.*, 2009).

Recently it was demonstrated that XPF binds SLX4, a related endonuclease, and this interaction is critical for ICL repair (Andersen *et al.*, 2009; Fekairi *et al.*, 2009; Munoz *et al.*, 2009a; Svendsen *et al.*, 2009). Fanconi anemia patients, mice deficient in ERCC1-XPF, and *Slx4(Btbd12)*$^{-/-}$ mice share many spontaneous developmental and degenerative phenotypes, supporting roles for all of these proteins in a common pathway and illustrating the dramatic consequences of failure to repair endogenous ICLs (Auerbach, 2009; Crossan *et al.*, 2011). Recent reports describe the discovery of biallelic mutations in *SLX4* in two patients who exhibited clinical features of Fanconi anemia (Kim *et al.*, 2011; Stoepker *et al.*, 2011). Based on evidence that reintroduction of wild-type SLX4 into the patients' cells rescued sensitivity to crosslinking agents, *SLX4* is considered a new complementation group of Fanconi anemia: FANCP.

1.1.3 Double-strand break repair

Orthologs of ERCC1–XPF in lower eukaryotes such as *Arabidopsis thaliana*, *Drosophila melanogaster*, and *Saccharomyces cerevisiae* play a vital role in the repair of DSBs and meiosis

(Baker *et al.*, 1978; Fishman-Lobell and Haber, 1992; Hefner *et al.*, 2003; Ivanov and Haber, 1995). The two primary mechanisms of DSB repair are non-homologous end-joining (NHEJ) and homologous recombination (HR). Work in budding yeast has contributed tremendously to defining the role of ERCC1–XPF in DSB repair in mammalian cells. Mutation of *rad10* or *rad1*, the orthologs of *ERCC1* and *XPF* in *S. cerevisiae*, suppresses HR between sequence repeats (Klein, 1988; Prado and Aguilera, 1995; Schiestl and Prakash, 1990). The function of the Rad10-Rad1 nuclease in HR is to remove non-homologous 3′ termini of single-stranded overhangs of broken ends to facilitate single-strand annealing, an error-prone sub-pathway of HR (Fishman-Lobell and Haber, 1992; Ivanov and Haber, 1995; Paques and Haber, 1997; Prado and Aguilera, 1995). Like single-strand annealing, there is an error prone sub-pathway of NHEJ that utilizes short stretches of homology to join two broken DNA ends, termed micro-homology mediated end-joining. Rad10-Rad1 also participates in this end-joining pathway in yeast (Ma *et al.*, 2003). Yeast Mre11 and Rad1 proteins define a Ku-independent mechanism to repair double-strand breaks lacking overlapping end sequences (Ma *et al.*, 2003). Mammalian cells deficient in ERCC1–XPF are modestly sensitive to ionizing radiation (IR), a source of DSBs (Ahmad *et al.*, 2008). Like in yeast, HR and end-joining of DSBs is attenuated in ERCC1-XPF-deficient mammalian cells (Adair *et al.*, 2000; Al-Minawi *et al.*, 2008; Niedernhofer *et al.*, 2001; Sargent *et al.*, 2000; Sargent *et al.*, 1997b).

The ERCC1–XPF endonuclease is required for efficient single-strand annealing and gene conversion in mammalian cells (Ahmad *et al.*, 2008; Al-Minawi *et al.*, 2008). Therefore, it is proposed that ERCC1–XPF nuclease facilitates both HR and NHEJ pathways (single-strand annealing and microhomology-mediated end-joining), but only if the broken DNA ends contain

3′-overhanging unmatched sequences or ends that cannot be used to prime DNA synthesis (Ahmad *et al.*, 2008).

1.1.4 At telomeres

ERCC1–XPF deficiency is linked with accelerated aging, and telomere shortening is associated with aging, so therefore it was important to understand if the nuclease impacts telomere length or function (Satoh *et al.*, 1996). Telomeres in humans with mutations in *XPF* or *Ercc1* knockout mice are not shorter than controls (Zhu *et al.*, 2003). Furthermore, there is no difference in sister chromatid exchange at telomeres in the absence of ERCC1–XPF (Hagelstrom *et al.*, 2010). However, ERCC1 co-localizes with TRF2 at telomeres (Zhu *et al.*, 2003). In a TRF2 dominant negative background, ERCC1–XPF deficient cells accumulate telomeric double-minutes. This led to the conclusion that ERCC1–XPF cleaves the G-rich, 3′-overhang, rendering chromosomes vulnerable to end-to-end fusions (Zhu *et al.*, 2003). Hence the absence of ERCC1–XPF apparently does not have a deleterious impact on telomere length or function. Consistent with that, correction of XP-F cells or overexpression of XPF in normal human cells leads to telomere shortening (Wu *et al.*, 2008). Therefore, accelerated aging associated with ERCC1–XPF deficiency is presumed to arise from cellular senescence and cell death and not as a consequence of telomere-dependent replicative senescence.

1.2 XPF-DEFICIENCY IN HUMANS

Humans with mutations in *XPF* can be classified into two groups based on the clinical manifestations of their disease (see Table 1.1). The majority of XP-F patients present with mild symptoms of XP, which include sun sensitivity, freckling of the skin, and basal or squamous cell carcinomas typically occurring after the second decade of life. This is in contrast to many XP-A and XP-C patients, in which skin cancer occurs even before 2 years of age (Kraemer *et al.*, 1987). The second group of XP-F patients exhibit neurological deterioration in addition to their XP-like symptoms. There has been one published case of a patient with mutations in *XPF* with dramatically accelerated aging (Niedernhofer *et al.*, 2006). The mutation in *XPF*, its impact on protein expression, function and subcellular localization are all critical determinants in the clinical manifestations (Ahmad *et al.*, 2010). Of note, all XP-F patients carry a missense mutation in at least one allele, and none of these affect the catalytic domain of the protein (Table 1.1). This has led to speculation that ERCC1–XPF is essential for human life (Jaspers *et al.*, 2007). This is supported by the observation that mice homozygous for null alleles of these genes are not viable except in select genetic backgrounds (see the end of Section 1.3).

The first XPF-deficient human patient was reported in 1979, several years before the *XPF* gene was identified and cloned (Arase *et al.*, 1979). The patient, referred to as XP23OS, was confirmed as XP-F by genetic complementation analysis, and exhibited mild XP symptoms including freckling and photosensitivity. Primary cells from patient XP23OS have only 10% of the normal level of NER as measured by UV-induced unscheduled DNA synthesis (UDS), but only modest sensitivity to UV as measured by clonogenic survival. The seeming discrepancy can be explained by the fact that UDS measures NER that occurs in the first 3 h following UV irradiation, whereas in a clonogenic survival assay, cell growth is measured in the 7–10 days

Table 1.1: List of patients with verified mutations in *XPF* or *ERCC1*

Patient code	Mutation	Amino acid changes	Age[a] (M or F)	% UDS[b]	UV-S[c]	Neuro[d]	Abnormal pigmentation[e]	Skin carcinoma[f]
XP26BR	Base sub 2377 (C → T) Homozygous	Arg799 → Trp Arg799 → Trp		15		–	+	+
XP32BR		Arg589 → Trp Pro379 → Ser	12	10	+ (2×)	–	+	+
XP23OS	1bp insert 1330 Heterozygous	Lys455 → Stop482	45 (F)	10	+ (4×)	–	+	–
XP126LO	Base sub 2377 (C → T)	Arg799 → Trp	22 (F)	45	+	–		–
XP7NE		Pro379 → Ser Silent	28	25	+ (2×)	–	+	
XP25KO			8 (F)	12	+ (3×)	–	+	–
XP27KO			11 (F)	12	+ (2.5×)	–	+	-
XP28KO			8 (F)	12	+ (3×)	–	+	–
XP38KO			44 (F)	20–25	+ (2.3×)	–	+	–
XP46KO			61 (F)	12	+ (2.8×)	–	+	–
XP90TO			42 (M)	12	+ (3×)	–	+	+ (42)
XP92TO			40 (F)	12	+ (3×)	–	+	+ (41)
XP29MA			24 (M)	> 5	+ (6×)	–	+	–
XP30MA			29 (M)	> 5	+ (6×)	–	+	–
XP42RO	Base sub 2377 (C → T) Homozygous	Arg799 → Trp	62 (M)	22	+ (2×)	+ (47)	+	+ (27)
XP24BR	Base sub 2377 (C → T) Homozygous	Arg799 → Trp Arg799 → Trp	29	5	+ (3×)	+	+	+
XP24KY	10bp deletion (1575) Base sub 2377 (C → T)	Val536 → Stop533 Arg799 → Trp	48 (M)	7	+ (3×)	+	+	–
XP62RO	Base sub 2377 (C → T) Homozygous	Arg799 → Trp Arg799 → Trp		20	+ (2×)	+ (late onset)		
AS871		Arg589 → Trp Deletion of Exon 3		15	+ (2×)	+		
XP51RO	Base sub 458 (G → C) Homozygous	Arg153 → Pro	15 (M)	> 5	+ (10×)	+ (6)		–
XP48DC	Base sub 2377 (C → T) Heterozygous	Arg799 → Trp				+		
CO14TA	Base sub 2377 (C → T) Heterozygous	Arg799 → Trp				+		
CO107TA	Base sub 2377 (C → T) Heterozygous	Arg799 → Trp				+		
XP202DC	Nonsense Splice mutation in ERCC1	Lys226 → STOP IVS6-26G → A	15			+		–
165TOR		Glu158 → STOP Phe231 → Leu	congenital	15	+ (5×)	+	–	–

The first 14 patients (XP26BR through XP30MA) are XP-F patients without neurodegeneration. The middle 9 patients (XP42RO through CO107TA) are XP-F patients with neurodegeneration. The last two patients (XP202DC through 165TOR) have a mutation in *ERCC1*.

[a] Age of patient at time of diagnosis and patient's gender.

[b] Unscheduled DNA synthesis as a percentage compared to control cells.

[c] Fold increase in UV sensitivity of patient fibroblasts compared to control cells.

[d] Presence (+) or absence (−) of neurodegenerative symptoms.

[e] Presence (+) or absence (−) of abnormal pigmentation including freckling, blistering, epidermal atrophy and keratoses.

[f] Presence (+) or absence (−) of skin carcinomas (basal cell and squamous cell carinomas).

following UV irradiation. Thus XP23OS cells must have low levels of NER, but that is adequate to prevent cell death and replicative senescence given ample time to repair the genome (Zelle *et al.*, 1980). Furthermore, host cell reactivation of reporter expression following UV damage was only modestly impaired. These results suggest that although the efficiency of NER was impaired

in this patient, the pathway must be intact to explain the relatively mild symptoms in this 45-year-old patient. In the years that followed, several patients with XP group F were described, most of them from Japan, having mild to moderate symptoms, similar to patient XP23OS (Fujiwara *et al.*, 1985a; Fujiwara *et al.*, 1985b; Kondo *et al.*, 1989; Nishigori *et al.*, 1986; Norris *et al.*, 1988; Thielmann *et al.*, 1991; Yamamura *et al.*, 1989). The majority of XP-F patients had UV sensitivity and freckling of the skin, but severe ocular and neurological symptoms were rare in XP (see Table 1.1) (Berneburg *et al.*, 2000; Moriwaki *et al.*, 1993). It is important to note that there have been reports of additional XP-F patients that are not included in Table 1.1 because the mutations have yet to be verified in genomic DNA (Matsumura *et al.*, 1998).

The human *XPF* gene was cloned in 1996 with the identification of a human gene homologous to yeast Rad1 (Brookman *et al.*, 1996; Sijbers *et al.*, 1996a). This cDNA corrected the defect in cells from XP group F patients. Additionally, causative mutations were identified in XP-F patients that corresponded to this gene. Following the cloning of *XPF*, an unusual XP-F patient was described displaying progressive late-onset neurologic decline (Sijbers *et al.*, 1998). This patient, referred to as XP42RO, had mild ocular photophobia with severe erythema on sun exposure. Basal and squamous cell carcinomas were detected in the second decade of life and by the fourth decade the patient exhibited profound neurodegenerative symptoms including ataxia and cerebral and cerebellar atrophy. The mutation found in XP42RO cells is a C → T transition at nucleotide 2377, which results in a change of the conserved arginine residue at 799 to a tryptophan. The R799W mutation was identified in at least eight other XP-F patients, six of whom had reported neurodegeneration (see Table 1.1). Patient XP126LO harbors the R799W mutation, but is without neurologic symptoms to date. One possible explanation is that

neurologic symptoms may not appear until the 4th or 5th decade of life, and this patient was assessed and diagnosed at 22 years of age.

More recently, mutations in *XPF* were linked to a novel progeroid syndrome or disease of accelerated aging (called XFE progeroid syndrome). The patient, referred to XP51RO, had severe photosensitivity, which led investigators to hypothesize that NER was defective, and genetic complementation with XP patient cells revealed that XPF was affected (Niedernhofer *et al.*, 2006). In addition to sun sensitivity and the classical symptoms of XP, patient XFE had severe symptoms of accelerated aging that affected the neurologic, hepatobiliary, musculoskeletal, and hematopoietic systems. Mutation analysis revealed a G → C transversion at position 458 which resulted in a non-conservative substitution of arginine at residue 153 to proline. The mutation in *XPF* was unexpected because patient XFE had severe symptoms of accelerated aging, unlike most other XP-F patients who had mild XP. R153 is located within a conserved helicase motif of XPF which is also a leucine-rich region postulated to be important for protein–protein interactions. Primary fibroblasts from patient XP51RO are highly sensitive to UV and the crosslinking agent mitomycin C. Patient XP51RO had normal early postnatal development, but progeroid symptoms began to appear in early prepubescence. The symptoms included an old, wizened appearance, loss of subcutaneous fat, liver dysfunction, vision and hearing loss, renal insufficiency, muscle wasting, osteopenia, kyphosis and cerebral atrophy. These symptoms of accelerated aging are strikingly similar to those seen in *Ercc1*$^{-/-}$ and *Xpf*$^{m/m}$ mice (see Figure 1.1).

Very recently, a patient with features similar to XP51RO was identified in the UK. The patient has the facial appearance of CS, sun-sensitivity, microcephaly, neurological problems and developmental delay, together with pancytopenia and renal failure. Cellular studies revealed low

UDS and assignment to the XP-F group (D. Pilz, D. McGibbon, R. Sarkany, M. Stefanini and A Lehmann, *personal communication*). XP-F patients with early onset and more severe symptoms

A

B

Symptom	*Ercc1*$^{-/-}$	*Ercc1*$^{-/\Delta}$	XP51RO	Human Aging
Loss of subcutaneous fat	+	+	+	+
Atrophic epidermis	+	+	+	+
Hearing loss	+	+	+	+
Visual impairment	+	+	+	+
Tremors	+	+	+	+
Ataxia	+	+	+	+
Cerebral atrophy	+	+	+	+
Hypertension	?	?	+	+
Renal acidosis	+	+	+	+
Bone marrow degeneration	+	+	+	+
Osteoporosis	+	+	+	+
Kyphosis	+	+	+	+
Dystonia	+	+	+	-
Sarcopenia	+	+	+	+
Frailty	+	+	+	+
Urinary Incontinence	?	+	+	+
Disc degeneration	+	+	?	+
Maximum Lifespan	4 weeks	28 weeks	16 years	120 years

Figure 1.1: Images and symptoms of ERCC1-deficient mice and symptoms of patient XP51RO

(A) Representative images of *Ercc1*$^{-/-}$ (left; 3 weeks of age) and *Ercc1*$^{-/\Delta}$ (right; 18 weeks of age) mice. (B) Table listing the symptoms of aging observed in *Ercc1*$^{-/-}$ mice, *Ercc1*$^{-/\Delta}$ mice, and patient XP51RO who had a progeroid syndrome (or disease of accelerated aging) due to a homozygous mutation in *XPF*. Symptoms are compared to normal human aging. (+) Indicates presence and (-) indicates absence of the symptom. References are listed in the right hand column. Also indicated are whether or not the same symptoms are associated with old age in humans and (+) or (-) indicates presence of absence in the *Ercc1*$^{-/-}$ mice, *Ercc1*$^{-/\Delta}$ mice, or progeroid patient XP51RO.

appear to have mutations that lead to mislocalization of ERCC1–XPF to the cytoplasm, thereby decreasing the cellular capacity for efficient repair of nuclear DNA (Ahmad *et al.*, 2010).

1.3 ERCC1 MUTATIONS IN HUMANS

ERCC1 was the first human DNA repair gene cloned (Westerveld *et al.*, 1984). For decades, however, no patients were identified with *ERCC1* mutations; hence the gene does not have the standard XP nomenclature (XP-x) like other NER factors associated with xeroderma pigmentosum. Recently, a single patient was discovered who had mutations in *ERCC1* resulting in severe pre- and postnatal developmental defects (Jaspers *et al.*, 2007). The patient, referred to as 165TOR, had severe skeletal defects at birth, including microcephaly, arthrogryposis and rocker-bottom feet. These abnormalities were seen in conjunction with neurological alterations including cerebellar hypoplasia and blunted cortical gyri. The clinical diagnosis was cerebro-oculo-facio-skeletal syndrome, or COFS syndrome. COFS syndrome was first reported by Lowry in 1971, and further characterized in the Manitoba aboriginal population by Pena and Shokeir in 1974 (Lowry *et al.*, 1971; Pena and Shokeir, 1974). COFS syndrome is a rare autosomal recessive disorder in which patients undergo rapid neurologic decline. Symptoms include but are not limited to microcephaly and brain atrophy with calcifications, cataracts, optic atrophy, progressive joint contractures, and severe postnatal growth failure (Graham *et al.*, 2001). Patients with COFS syndrome are reported to have mutations in genes encoding DNA repair proteins *ERCC6*/*CSB*, *ERCC5*/*XPG* and *ERCC2*/*XPD* (Meira *et al.*, 2000; Nouspikel *et al.*, 1997).

Two mutations were found in the coding region of *ERCC1* in patient 165TOR. The maternal allele harbors a C → T transition that converts Gln158 into an amber translational stop codon. The result is a truncated polypeptide that lacks the entire C-terminal domain, essential for binding XPF (de Laat *et al.*, 1998). The paternal allele has a C → G transversion, resulting in the conversion of Phe231 to leucine. This amino acid falls within the C-terminal tandem helix–hairpin–helix domain of ERCC1, critical for binding XPF, and is conserved in invertebrates and mammals (de Laat *et al.*, 1998). *ERCC1* mRNA levels were normal in this patient, although the protein levels of ERCC1 and XPF in the nucleus were reduced 4–5-fold. The truncated protein was not detectable by immunoblot. Accordingly, fibroblasts from patient 165TOR had 15% of the normal level of NER, representing a modest defect, suggesting that the missense mutation affects stability of ERCC1–XPF and/or its nuclear localization, but not enzymatic activity.

Unexpectedly, the expression of ERCC1–XPF in 165TOR cells is reduced but comparable to a patient with mild XP-F. Several hypotheses have been proposed to explain this incongruity, the simplest being that ERCC1 and XPF play distinct roles *in vivo*. Evidence against this hypothesis includes the fact that *Ercc1*$^{-/-}$ and *Xpf*$^{m/m}$ mice have apparently identical phenotypes (McWhir *et al.*, 1993; Tian *et al.*, 2004). Additionally, ERCC1 and XPF are required to stabilize one another *in vivo* (de Laat *et al.*, 1998; Sijbers *et al.*, 1996b). It is important to note that COFS is also caused by mutations in the TFIIH subunit XPD and the NER endonuclease XPG that stabilizes TFIIH (Graham *et al.*, 2001; Hamel *et al.*, 1996; Thorel *et al.*, 2004; Zafeiriou *et al.*, 2001). ERCC1–XPF and the other members of the NER machinery have been demonstrated to play a role in regulating transcription that has been suggested to be independent of their role in DNA repair (Le May *et al.*, 2010). Therefore, the clinical severity of patient 165TOR may be due to a transcription-coupled nucleotide excision repair defect during

development. It is also possible that 165TOR was genetically replete of functional ERCC1–XPF during development, but selective pressure led to partial reversion of the cellular phenotype postnatally. Reversion with mosaicism has been reported in many genome instability disorders including Fanconi anemia, Werner and Bloom syndromes, and observed for ERCC1–XPF deficient cells chronically exposed to crosslinking agents (Auerbach, 2009; Bosma *et al.*, 2003; Ellis *et al.*, 2001; Hirschhorn, 2003). In addition, there are undoubtedly modifier genes that affect the severity of symptoms caused by mutations in ERCC1 or XPF as illustrated by the fact that *Ercc1*$^{-/-}$ mice are not viable in inbred C57Bl/6 or FVB/n backgrounds, but are born with Mendelian frequency in an f1 mixed background (Niedernhofer *et al.*, 2006). Finally, little is known about regulation of ERCC1–XPF expression, which could be tissue-specific and therefore, contribute to heterogeneous phenotypes. Identifying modifier genes, identifying regulators of nuclease expression, and modeling additional patient mutations in mice will be essential for deciphering genotype:phenotype correlations. A second patient with mutations in ERCC1 was briefly described recently (Imoto *et al.*, 2007). The patient had a nonsense mutation affecting amino acid 226, which lies early in the helix–hairpin–helix domain necessary for binding XPF. The second allele contains a splice-site mutation (IVS6-G → A). The patient displayed neurologic symptoms beginning at age 15 years and died by the age of 37. Neurodegeneration was progressive and severe, resulting in dementia and cortical atrophy. The symptoms are very similar to XPF patients with neurologic involvement (Table 1.1), supporting the conclusion that ERCC1 and XPF function exclusively as a complex *in vivo*.

1.4 MOUSE MODELS OF ERCC1-XPF DEFICIENCY

1.4.1 ERCC1 knockout mice

To understand the biological significance of ERCC1, the gene was knocked-out in the mouse by two independent laboratories (McWhir *et al.*, 1993; Weeda *et al.*, 1997a). The two knockout alleles were created by interrupting different exons. McWhir *et al.* (1993) created the first knockout mouse model by disrupting exon 5 of *Ercc1*, leading to a truncated transcript missing the last four exons, which contain the XPF interaction domain (Enzlin and Scharer, 2002; McWhir *et al.*, 1993; Sijbers *et al.*, 1996b). The second knockout strain was generated by inserting a *neomycin* resistance cassette into exon 7 of *Ercc1* (Weeda *et al.*, 1997a). The result was a truncation in the helix–hairpin–helix motif required for interaction with XPF (de Laat *et al.*, 1998). *Ercc1* mRNA was not detected in these mice (Weeda *et al.*, 1997a). The former strain is born with Mendelian frequency; the latter is sub-Mendelian, likely due to differences in the genetic background (McWhir *et al.*, 1993; Weeda *et al.*, 1997a). Deletion of ERCC1 is lethal in a fully inbred genetic background, indicating that there are modifier genes that influence the severity of the phenotype (Niedernhofer *et al.*, 2006). In both knockout strains, postnatal growth is severely retarded and the mice die at approximately 3 weeks of age when they weigh only about 20% compared to their normal littermates (McWhir *et al.*, 1993; Weeda *et al.*, 1997a). The median lifespan of $Ercc1^{-/-}$ mice in an f1 mixed genetic background of 50:50 C57BL/6:FVB/n is 21 days and the maximum lifespan 28 days (Niedernhofer *et al.*, 2006). The $Ercc1^{-/-}$ mice spontaneously develop symptoms characteristic of progressive neurodegeneration, including dystonia, trembling and ataxia (Niedernhofer *et al.*, 2006).

The hematopoietic system of *Ercc1*$^{-/-}$ mice develops normally (Prasher *et al.*, 2005). However, by the end of life, *Ercc1*$^{-/-}$ mice are leukopenic and thrombocytopenic, and there is extensive adipose transformation of the bone marrow, hallmark features of normal aging in mice (Prasher *et al.*, 2005). Proliferation of multi-potent and lineage-committed progenitors from *Ercc1*$^{-/-}$ mice is profoundly impaired (Prasher *et al.*, 2005). Collectively, these data suggest that ERCC1-deficient mice undergo rapid turnover of hematopoietic cells leading to premature exhaustion of stem cell reserves. In addition, bone marrow progenitors from *Ercc1*$^{-/-}$ mice are exquisitely sensitive to crosslinking agents, similar to murine models of Fanconi anemia (Parmar *et al.*, 2009; Prasher *et al.*, 2005).

The liver of *Ercc1*$^{-/-}$ mice is prominently affected, with hepatocellular polyploidy, aneuploidy and G2 arrest (Chipchase *et al.*, 2003; McWhir *et al.*, 1993; Nunez *et al.*, 2000). The structural changes correlate with impaired liver function as demonstrated by significantly increased liver enzymes in the serum (McWhir *et al.*, 1993). *Ercc1*$^{-/-}$ mice develop kyphosis, sarcopenia, dystonia and ataxia, indicative of musculoskeletal and nervous system defects (Niedernhofer *et al.*, 2006). There is a suppression of the somatotroph, lactotroph and thyrotroph hormonal axes in the *Ercc1*$^{-/-}$ mice, which explains their growth delay and diminutive size (Niedernhofer *et al.*, 2006). Many of the degenerative and endocrine abnormalities are similar to what occurs with old age in mice (Caruso and Silliman, 2006; Schumacher *et al.*, 2008). To further investigate the relationship of DNA repair deficiency to normal aging, genome-wide expression changes in *Ercc1*$^{-/-}$ mice relative to wild-type littermates were compared to changes that occur with natural aging (differences in gene expression between old wild-type and young wild-type mice). There is a highly significant overlap between these two profiles, whether comparing gene-by-gene or over-represented biological pathways (Niedernhofer *et al.*, 2006).

This provided some of the early support for the notion that DNA damage may contribute to aging.

1.4.2 XPF mutant mice

Tian et al. (2004) recreated the *XPF* mutation in patient XP23OS in the mouse (Tian *et al.*, 2004). The patient had a single base insertion after nucleotide 1330 leading to a frameshift mutation after lysine 455 and a stop codon 38 residues later (Matsumura *et al.*, 1998). This leads to truncation of XPF upstream of the catalytic domain and its ERCC1-interaction domain (Enzlin and Scharer, 2002). The clinical phenotype of the patient was mild, having reached her 4th decade without neurodegeneration or skin cancer (Matsumura *et al.*, 1998). In keeping with this, the level and length of the *XPF* transcript in XP23OS cells are comparable to normal cells, illustrating that the patient must have a second normal *XPF* allele. To further emphasize this, a mouse homozygous for the frameshift mutation has undetectable levels of *Xpf* mRNA and a severe phenotype identical to that of ERCC1 null mice (Tian *et al.*, 2004). The $Xpf^{m/m}$ mice develop normally and are born with Mendelian frequency. However, postnatal growth is delayed such that by two weeks of age the $Xpf^{m/m}$ mice are approximately 25% the size of littermates, and die by three weeks of age. Hepatocellular polyploidy was prominent, as in the $Ercc1^{-/-}$ mice (Tian *et al.*, 2004). The phenotypic parallels between ERCC1 and XPF null mice strongly suggest that the proteins function exclusively as a complex.

Importantly, ERCC1 and XPF-deficient mice appear to have a normal complement of mature and immature B cells (Schrader *et al.*, 2004; Tian *et al.*, 2004; Winter *et al.*, 2003). This provides definitive evidence that ERCC1–XPF is not essential for NHEJ, the DSB repair pathway required for class switch recombination (CSR) (Kotnis *et al.*, 2009). However, *ex vivo*

CSR is mildly attenuated in splenocytes isolated from *Ercc1*$^{-/-}$ mice and the mutation pattern in the switch region of the immunoglobulin locus is significantly different from that of normal littermate mice, suggesting that ERCC1–XPF may contribute to DNA end-processing of DSBs at the Ig locus (Schrader *et al.*, 2004). Consistent with this, ERCC1-deficient mice are hypersensitive to IR, which induces DNA DSBs (Ahmad *et al.*, 2008).

1.4.3 Liver corrected *Ercc1*$^{-/-}$ mice

To investigate the cause of death in *Ercc1*$^{-/-}$ mice, Selfridge et al. (2001) crossed the mice with a transgenic strain expressing ERCC1 specifically in the liver, using transthyretin (TTR) regulatory sequences to control ERCC1 expression (Selfridge *et al.*, 2001). The resulting mice (*Ercc1*$^{-/-}$ + TG) have dramatically improved growth, reaching 58% of normal body weight for their age. Furthermore, their lifespan is significantly increased, with a median survival of ~75 days. Hepatocellular polyploidy and abnormal liver functions are largely corrected by expression of ERCC1 in the liver. Interestingly, by 7 weeks of age, the transgenic mice begin to display evidence of renal dysfunction (significantly elevated serum creatinine and proteinuria) and renal histopathology (glomerulosclerosis, hyaline casts, renal tubular epithelial anisokaryosis, karyomegaly, hyperchromasia, pyknosis and keryorrhexis) (Lawrence *et al.*, 2008; Selfridge *et al.*, 2001). These data suggest that *Ercc1*$^{-/-}$ mice die of liver failure, and that hepatocytes and renal cells are the most vulnerable to loss of ERCC1-XPF-dependent DNA repair.

Since the *Ercc1*$^{-/-}$ + TG mice live longer than *Ercc1*$^{-/-}$ mice, they are a practical system for identifying other tissues affected by ERCC1-deficiency. Performance of *Ercc1*$^{-/-}$ + TG mice on an opto-kinetic response test to measure visual acuity is impaired by 4 weeks and worsens with age (Selfridge *et al.*, 2001). Structural abnormalities of the eye were not detected, indicating

that loss of vision is not due to a developmental defect (Selfridge *et al.*, 2001). Also, there is no evidence for retinal degeneration typical of CSB mice, another NER-defective mutant strain (Lawrence *et al.*, 2008).

Like *Ercc1*$^{-/-}$, symptoms associated with neurodegeneration were observed in *Ercc1*$^{-/-}$ + TG mice. The *Ercc1*$^{-/-}$ + TG mice displayed dystonia and ataxia indicative of a cerebellar defect. While mild atrophy of the neocortex and cerebellum were observed, there were no abnormalities or loss of Purkinje cells to explain these phenotypes. Also, there were no signs of degeneration at the neuromuscular junctions. Therefore these symptoms were attributed to uremic encephalopathy, caused by kidney failure (Lawrence *et al.*, 2008).

Male and female *Ercc1*$^{-/-}$ + TG mice were found to be infertile (Hsia *et al.*, 2003). Testes of these mice were approximately 50% the normal size at puberty and contained significantly fewer spermatocytes. Spermatogenesis is not arrested at a particular stage, as expected for a meiotic defect, but instead there is abundant apoptosis in these rapidly dividing cells (Hsia *et al.*, 2003; Paul *et al.*, 2007). This leads to a 97% reduction in the sperm count (Paul *et al.*, 2007). Ovaries from adult *Ercc1*$^{-/-}$ + TG mice showed a reduced number of oocytes and an absence of primary follicles (Hsia *et al.*, 2003).

1.4.4 *Ercc1* mutant mice

To further probe the DNA repair function of ERCC1 *in vivo*, a premature stop codon was engineered at position 292 of *mErcc1* (Weeda *et al.*, 1997a). This results in a C-terminal deletion of seven amino acids of the murine protein, including a phenylalanine residue at position 293, thought to be essential for binding to XPF (de Laat *et al.*, 1998). Thus, the prediction was that this mutation would ablate DNA repair function without compromising the protein stability

(Sijbers *et al.*, 1996b). Unlike either of the null alleles, normal levels of the mutant *Ercc1* transcript are detected in the tissues from the mutant mice (Weeda *et al.*, 1997a). Homozygous *Ercc1*^{*292} (also referred to as *Ercc1*$^{\Delta/\Delta}$) mice live up to six months, which is six-times longer than ERCC1 null mice. Similar to the *Ercc1*$^{-/-}$ mice, the *Ercc1*^{*292} mice are infertile and their skin is atrophic and lacks subcutaneous fat (Weeda *et al.*, 1997a). The spleen of *Ercc1*^{*292} mice contains increased ferritin and hemosiderin deposits, indicative of a high turnover of erythrocytes. The kidney exhibits dilated renal tubules with hyaline casts. Nuclear polyploidy is common in the liver and kidney. Thus, virtually all of the phenotypes of *Ercc1*$^{-/-}$ mice are recapitulated in this longer-lived mutant strain. Primary mouse embryonic fibroblasts (MEFs) from the *Ercc1*$^{-/-}$ mice are modestly more sensitive to the crosslinking agent mitomycin C than MEFs from *Ercc1*^{*292} mice, suggesting that their increased longevity is due to increased DNA repair capacity (Weeda *et al.*, 1997a). Despite this, topical application of the tumor initiator, DMBA to *Ercc1*^{*292} mice leads to acute toxicity rather than carcinogenesis, illustrating a dramatic difference from other NER-deficient mice (Weeda *et al.*, 1997a).

1.4.5 *Ercc1* hypomorphic mice

Combination of one null and one mutant *Ercc1* allele yields mice (*Ercc1*$^{-/*292}$; *Ercc1*$^{-/\Delta}$ or *Ercc1*$^{d/-}$) that are born with Mendelian frequency and have an even greater maximal lifespan of seven months in an f1 background of 50:50 C57Bl/6J:FVB/n (Dolle *et al.*, 2006). *Ercc1*$^{-/\Delta}$ mice are runted compared to their wild-type littermates (de Waard *et al.*, 2010). However, they develop normally until sexual maturity, at which point they began to exhibit signs of rapid aging (Nevedomskaya *et al.*, 2010). They live 24–30 weeks while progressively developing dystonia, tremors, kyphosis and ataxia (de Waard *et al.*, 2010).

The *Ercc1*$^{-/\Delta}$ mice were crossed with a transgenic lacZ reporter strain to measure the mutation frequency *in vivo* (Dolle *et al.*, 2006). The mutation frequency is modestly elevated in the liver of 5–6 month old *Ercc1*$^{-/\Delta}$ mice compared to normal littermates. Interestingly, the mutations are primarily chromosomal rearrangements characteristic of old wild-type mice rather than point mutations, characteristic of NER-deficient mice (Dolle *et al.*, 2006). This observation extends the parallels between the progeroid *Ercc1*$^{-/\Delta}$ mice and aged normal mice.

Ercc1$^{-/\Delta}$ mice are hypersensitive to IR (Ahmad *et al.*, 2008). Even though these mice are hypomorphic for ERCC1–XPF, they were equally as sensitive to IR as DNA-PKcs knockout mice (Li *et al.*, 2002). IR causes persistent γH2AX foci in ERCC1-deficient cells and mice, supporting a role for ERCC1–XPF in the repair of DSBs. The involvement of ERCC1–XPF in DSB repair is presumably a Ku-independent pathway, since *Ercc1*$^{-/-}$*Ku86*$^{-/-}$ mice are not viable (Ahmad *et al.*, 2008). *Ercc1*$^{-/-}$ MEFs have normal levels of spontaneous and mitomycin C-induced sister chromatid exchanges, illustrating that ERCC1–XPF is not essential for homologous recombination (Niedernhofer *et al.*, 2001; Sonoda *et al.*, 1999). In contrast, DSBs with 3′ overhangs cause large deletions in *Ercc1*$^{-/-}$ cells (Ahmad *et al.*, 2008; Niedernhofer *et al.*, 2001). These genetic and *in vitro* data support a role for ERCC1–XPF in processing a subset of DSBs (those with 3′ overhangs) and a role in the alternative end-joining pathway of DSB repair (McVey and Lee, 2008).

Ercc1$^{-/-}$, *Ercc1*$^{-/-}$ + TG, and *Ercc1*$^{-/\Delta}$ mice all develop progressive dystonia, tremors and ataxia, highly suggestive of neurodegeneration (de Waard *et al.*, 2010; Lawrence *et al.*, 2008; Niedernhofer *et al.*, 2006). The former strains display cerebellar hypoplasia, similar to the ERCC1 patient 165TOR, but this could not be completely dissected from developmental abnormalities, due to their young age (Jaspers *et al.*, 2007; Lawrence *et al.*, 2008; Niedernhofer

et al., 2006). Evidence for degenerative processes in the central nervous system is quite clear in *Ercc1*$^{-/\Delta}$ mice (de Waard *et al.*, 2010). De Waard *et al.* (2010) found profound astrocytosis and microgliosis in the spinal cord of 4 month old *Ercc1*$^{-/\Delta}$ mice, compared to normal littermates and 1 month old mutant animals. This is accompanied by a significant reduction in the number of motor neurons in the ventral horn of the spinal cord and a concomitant denervation of the skeletal muscle. There is an approximately 50% reduction in neurons from 4 to 8 weeks of life, and then again from 8 to 16 weeks of life in the *Ercc1*$^{-/\Delta}$ mice. It is also evident that the pre-synaptic motor nerve terminals have degenerated in the aged *Ercc1*$^{-/\Delta}$ mice with characteristics similar to those seen in amyotrophic lateral sclerosis and aging motor neurons (de Waard *et al.*, 2010).

Genome-wide expression profiling of *Ercc1*$^{-/\Delta}$ mice revealed a highly significant correlation with the transcriptome of numerous long-lived models, including Ames and Snell dwarf mice and/or calorically restricted mice (Schumacher *et al.*, 2008). In addition, there is a significant correlation with the transcriptome of old wild-type mice. This indicates that *Ercc1*$^{-/\Delta}$ mice look biologically "old", but also that the failure to repair DNA damage in these mice triggers activation of a stress response that is transcriptionally regulated and promotes longevity. Schumacher et al. showed that this same stress response is also triggered by nutritional deprivation and is mediated through suppression of growth hormone–insulin-like growth factor 1 signaling as evidenced by the significant correlation with Ames and Snell dwarf mice. All of these mice displayed suppression of the somatotroph axis, oxidative metabolism and peroxisomal biogenesis coupled with an upregulation of antioxidants, DNA damage and apoptosis (Schumacher *et al.*, 2008).

This was further supported by analysis of metabolites in the serum and urine of *Ercc1*$^{-/\Delta}$ mice (Nevedomskaya *et al.*, 2010). There is no difference between *Ercc1*$^{-/\Delta}$ mice and normal littermates at 8 and 12 weeks of age. However by 16 weeks, there are significant differences, which become further amplified by 20 weeks of age. Collectively, these data support the conclusion that *Ercc1*$^{-/\Delta}$ mice develop normally into adulthood, but then undergo degenerative changes. Several of the metabolic changes mimic those that occur with caloric restriction, including increased HDL, decreased LDL and VLDL, and ketosis. However, a number of metabolic changes in the *Ercc1*$^{-/\Delta}$ mice are also consistent with degeneration, such as increased glucose, citrate and succinate in the urine, indicative of kidney dysfunction, and metabolic alkalosis, indicative of liver dysfunction (Nevedomskaya *et al.*, 2010). These observations are consistent with the model that DNA damage accumulates in *Ercc1*$^{-/\Delta}$ mice leading to metabolic reprogramming in response to stress (Schumacher *et al.*, 2008). This may be beneficial, but in the long-run is insufficient to sustain the organism in the face of continued DNA damage (Niedernhofer *et al.*, 2006).

Remarkably, *Ercc1*$^{-/\Delta}$ mice spontaneously develop numerous diseases associated with old age in humans. This includes osteoporosis and intervertebral disc degeneration (Vo *et al.*, 2010). There is progressive attrition of disc extracellular proteoglycans with age, leading to loss of disc height and its cushioning function (Roughley, 2004; Roughley *et al.*, 2002). Similar changes were observed in discs of 5-month-old *Ercc1*$^{-/\Delta}$ mice and these alterations were exacerbated in mice treated with genotoxic chemotherapeutic agents (Vo *et al.*, 2010). These observations support the conclusion that DNA damage, if not repaired, can promote common aging-related degenerative diseases, even in post-mitotic tissues.

1.4.6 Tissue-specific deletion of ERCC1

Tissue-specific deletion of a gene is a powerful tool for dissecting a complex phenotype, such as that of the ERCC1-deficient mice, allowing for dissection of whether a particular symptom or pathology is a direct consequence of a deletion of a gene or merely a secondary consequence (e.g., is neurodegeneration due to loss of ERCC1 in neurons or uremic encephalopathy due to loss of ERCC1 in the kidneys?). Tissue-specific knockout of protein expression occurs if the gene of interest (or an exon vital to its function) is flanked (floxed) by recombination signals (loxP or FRT) and mice expressing the two copies of the floxed allele are crossed with transgenic mice expressing recombinase (CRE or FLP, respectively) under a tissue-specific promoter (Tronche *et al.*, 2002). Another important attribute of this approach is that it is possible to distinguish developmental from degenerative changes by selecting promoters that are active only postnatally.

A floxed allele of *Ercc1* was generated by inserting loxP sites in intron 2 and 5, such that Cre recombinase excises exons 3–5 of the *Ercc1* locus (Doig *et al.*, 2006). Mice harboring two floxed alleles of *Ercc1* were crossed with transgenic mice expressing Cre-recombinase under a tyrosinase promoter (Selfridge *et al.*, 2010). The goal was to knockout expression of ERCC1 in melanocytes to generate a murine melanoma model. Unexpectedly, the mice die by 6 months of age due to severe colonic obstruction. Tyrosinase is expressed in all neural crest cell-derived lineages, including parasympathetic neurons that innervate the gastrointestinal tract and are required for colonic peristalsis. Knocking-out ERCC1 expression in neural crest cells causes p53 activation and apoptosis of ganglion cells in the mesenteric plexus. Denervation of the bowel explains the colonic obstruction and demonstrates that ERCC1–XPF dependent DNA repair is critical for protecting neurons from degeneration (Selfridge *et al.*, 2010). This provides strong

evidence that the neurological symptoms observed in ERCC1-deficient mice are due, at least in part, to loss of functional neurons rather than a defect in supportive glial cells.

ERCC1 was also knocked-out specifically in the skin to create a model of UV-induced skin cancer. *Ercc1*$^{flox/-}$ mice were crossed with transgenic mice expressing Cre recombinase under the keratin 5 (K5) promoter, which is only expressed in the basal layer of the epidermis (Doig *et al.*, 2006). To facilitate UV carcinogenesis studies, these mice were produced in an albino, hairless background. Deletion of *Ercc1* in the skin leads to a 20-fold reduction in the minimal erythemal dose in response to UV-B irradiation, leading to dramatic, but transient hyperplasia (Doig *et al.*, 2006). Furthermore, the mice develop significantly more skin tumors, early, and at a lower dose of UV-B than normal controls. The cumulative dose of UV-B required to induce tumors in half of the ERCC1-deficient mice was 37-times lower than normal controls in a chronic exposure study (Doig *et al.*, 2006). The mice also developed actinic keratosis and squamous cell carcinomas. Thus, this tissue-specific knockout strain offers an accurate and rapid (tumors within 8 weeks) model of UV-induced skin cancer, which may be useful in the study of XP. Subsequently, these mice have been used to test topical treatments that protect against UV-induced skin cancer (Lawrence *et al.*, 2009).

1.4.7 Double mutant mice

TRF1 and TRF2 are shelterin proteins required to protect telomeres at chromosomal ends (Smogorzewska *et al.*, 2000). Overexpression of either protein leads to a dominant negative effect exemplified by telomere shortening, loss of telomeric 3′ G-rich overhangs and end-to-end fusions (Munoz *et al.*, 2009b; Munoz *et al.*, 2005). Overexpression of TRF2 in the skin of mice by putting the cDNA under control of the keratin 5 promoter (K5TRF2), leads to skin atrophy,

hyperpigmentation and increased skin cancer in sun-exposed areas. These results demonstrate that dysregulation of telomeres promotes UV-induced skin cancer (Munoz *et al.*, 2005). Skin and keratinocytes isolated from either K5TRF1 or K5TRF2 mice contain telomeric defects, which were rescued by knocking-out *Xpf* (Munoz *et al.*, 2009b; Munoz *et al.*, 2005). This strongly supports the previous observation that the absence of ERCC1–XPF does not negatively impact telomere length or function, but instead has an unexpected beneficial effect (Zhu *et al.*, 2003).

1.5 CONCLUDING REMARKS

This chapter provides a comprehensive overview of the physiological impact of reduced expression or activity of ERCC1–XPF DNA repair endonuclease. There is tremendous variability between patients with mutations in ERCC1 or XPF, ranging from mild cutaneous symptoms to severe neurodegeneration. ERCC1 patient 165TOR had severe developmental abnormalities that are not normally seen in XP-F patients. These differences cannot be fully predicted by the patients' mutations or the level of residual NER (UDS) in patient fibroblasts. Clearly, further work is needed to decipher how expression and activity of ERCC1–XPF is regulated. This in turn is likely to yield better methods for predicting the physiological consequences of a particular mutation (Fan *et al.*, 2008). The studies in mice have been crucial for a number of reasons. First, the identical phenotypes of *Ercc1*$^{-/-}$ and *Xpf*$^{m/m}$ mice, which are null for XPF, provide the strongest possible evidence that ERCC1 and XPF must function exclusively as a heterodimer. Second, the unexpected premature aging phenotypes of the ERCC1 mutant mice led to the discovery of a new rare genetic disease (XFE progeroid syndrome) and contributed to the body of evidence that DNA damage is one type of cellular damage that

promotes aging-related degenerative changes (e.g., neurodegeneration). Third, it is clear that the severity of symptoms associated with ERCC1–XPF deficiency are somehow linked to variable levels of expression or activity. This implies that functional single nucleotide polymorphisms in either gene may be important for predicting risk of cancer or degenerative diseases. Fourth, ERCC1 mutant mice are unique amongst the NER-deficient mutant strains because they spontaneously develop neurodegeneration, which may be used to screen therapies for treating XP, CS and TTD patients. Finally, tissue-specific ERCC1 knockout strains will be crucial for identifying which tissues and cell types are most vulnerable to DNA damage and are responsible for triggering systemic stress responses.

1.6 THEORIES OF AGING

In the 21st century, there has been a global demographic shift, such that the number of individuals over the age of 60 is increasing rapidly in both developed and non-developed nations (2001b). In 1950, there were approximately 205 million persons over the age of 60 worldwide. In 2000, this number nearly tripled to 606 million persons age 60+. However, by 2050 that number is predicted to reach nearly 2 billion and comprise nearly 20% of the population (2001b; Greenberg, 2011). Aging is the number one risk factor for numerous chronic degenerative diseases, including cardiovascular disease, arthritis, cataracts, glaucoma, osteoporosis, type 2 diabetes, and neurodegenerative disorders such as Alzheimer's disease and Parkinson's disease. Eighty percent of individuals over the age of 65 have at least one chronic disease, whereas greater than 50% have two or more (2011a). In the United States alone, the direct medical costs associated with these chronic diseases is estimated to be $582 billion annually (Hoffman and

Rice, 1996). Therefore, in order to improve the quality of life for the elderly by reducing the disease burden, and to minimize the economic burden from the medical care of the aged population, it is critical to identify the molecular mechanisms that underlie aging.

The amount of DNA damage and resulting genetic mutations found in the nuclear genome increases with age in a variety of tissues in aged organisms (Dolle *et al.*, 2002; Hamilton *et al.*, 2001; Mecocci *et al.*, 1999; Wang *et al.*, 2012). Interestingly, multiple mouse models that are long-lived are resistant to stressors that cause DNA damage (i.e., UV light and oxidative stress) (Murakami, 2006). Conversely, mouse models of DNA repair deficiency or genome instability disorders have short lifespans, including strains with mutations in *Ercc1, Xpf, Xpd, Wrn, Blm, Ku80,* and *Terc* (de Boer *et al.*, 2002; de Waard *et al.*, 2010; Hasty *et al.*, 2003b; Kirkwood, 2005; McWhir *et al.*, 1993; Tian *et al.*, 2004; Warner and Sierra, 2003; Weeda *et al.*, 1997a). In fact, many human progerias, or diseases of accelerated aging, are caused by mutations in genes that are required for genomic maintenance (Hasty *et al.*, 2003b; Niedernhofer *et al.*, 2006). This supports the theory that damage to nuclear DNA contributes to the functional decline and loss of an ability to maintain homeostasis that invariably occurs with aging (Kirkwood, 2005; Warner and Sierra, 2003).

The main cause of endogenous DNA damage is reactive oxygen species (ROS), the majority of which are generated by mitochondria (Balaban *et al.*, 2005; Kirkwood, 2005). This led to the theory that free radicals, produced endogenously as part of normal cellular metabolism, can cause damage to lipids, DNA and other cellular components (Chakravarti and Chakravarti, 2007; Cooke *et al.*, 2003; Cui *et al.*, 2012; Mandavilli *et al.*, 2002), thereby promoting aging-related functional decline of an organism's tissues (Harman, 1956; Muller *et al.*, 2007). This is supported by research showing that mitochondria from aged and post-mitotic cells exhibit loss of

membrane potential and accumulate damage to their genome (Jendrach *et al.*, 2005). Some ROS produced by mitochondria diffuse throughout the cell, resulting in oxidative damage to cellular macromolecules, even in the nucleus (Chakravarti and Chakravarti, 2007; Cooke *et al.*, 2003; Cui *et al.*, 2012; Mandavilli *et al.*, 2002). Because DNA is the only cellular macromolecule that is repaired instead of replaced, it stands to reason that damage to DNA could be a major contributor to aging.

As discussed above, *Ercc1*$^{-/\Delta}$ mice are a particularly useful model to study the aging process and how DNA damage contributes to aging. ERCC1-deficient mice mimic natural aging of the hepatobiliary, renal, neurological, musculoskeletal, hematopoietic, and epidermal systems over the span of seven months rather than the normal mouse lifespan, which can be up to three years (de Waard *et al.*, 2010; Goss *et al.*, 2011; Gregg *et al.*, 2012a; Nevedomskaya *et al.*, 2010; Niedernhofer *et al.*, 2006). Therefore, this model accelerates the aging process by >5-fold in a mammalian system. Also, the primary defect causing accelerated aging is well-defined in *Ercc1*$^{-/\Delta}$ mice: they are defective in the repair of nuclear DNA. This enables testing of hypotheses about what exposures in our environmental or diet may induce DNA damage and thereby promote aging. Likewise the *Ercc1*$^{-/\Delta}$ mice are amenable to rapid screening of therapeutics intended to attenuate DNA damage and therefore, aging (e.g., anti-oxidants). Finally, *Ercc1*$^{-/\Delta}$ mice can be used to test whether signaling pathways identified as important modifiers of lifespan in other model systems are similarly important for regulating lifespan/healthspan in response to DNA damage accumulation (e.g, mTOR, sirtuins, NF-κB transcription factor).

ERCC1-deficient mice are extremely sensitive to crosslinking agents (Niedernhofer *et al.*, 2006) and their phenotype differs largely from mice deficient solely in NER, *Xpa*$^{-/-}$ mice (de

Vries *et al.*, 1995). Therefore, damage repaired by ERCC1-XPF that is not repaired by the NER pathway, is hypothesized to be causing the premature aging phenotype of this mouse model. It has been shown that ERCC1-XPF is required for the unhooking of ICLs from one strand of DNA during the repair process (Bhagwat *et al.*, 2009). Therefore, the aim of Chapter 2 was to test the hypothesis that DNA ICLs promote cellular senescence and aging. If crosslinks are indeed driving aging, then reducing endogenous crosslinks should delay aging-associated changes. The free radical theory states that cells age because of free radical damage to cells and tissues over time (Harman, 1956). Therefore the aim of Chapter 3 was to test the hypothesis that mitochondrial-derived ROS promote aging in a DNA repair-deficient mouse model. If crosslinks promote aging and reduction of oxidative damage attenuates aging-related symptoms, then the next step is to find a source of endogenous crosslinks. The aim of Chapter 4 was to test the hypothesis that lipid peroxidation, a potential source of endogenous ICLs, promotes age-related decline. Finally, if a reduction of oxidative damage attenuates aging, NF-κB, which is activated in response to oxidative stress (Miyamoto, 2011), may be involved in the aging process. Therefore, the aim of Chapter 5 was to test the hypothesis that NF-κB drives systemic aging and is a therapeutic target for attenuating and/or delaying aging-related degenerative changes.

In total, the studies provide strong evidence that nuclear DNA damage can promote degenerative changes associated with aging. Furthermore, the studies reveal multiple unanticipated strategies that can be used to reduce the DNA damage burden and thereby potentially improve health in old age.

2.0 DNA INTERSTRAND CROSSLINKS PROMOTE CELLULAR SENESCENCE AND AGING-RELATED DEGENERATIVE CHANGES

Andria Rasile Robinson[1,2], Chelsea H. Feldman[2], Christin E. Burd[3], Siobhán Q. Gregg[2,4], Norman E. Sharpless[3], and Laura J. Niedernhofer[2,5]

[1]Department of Human Genetics, University of Pittsburgh Graduate School of Public Health, 130 DeSoto Street, Pittsburgh, PA 15261, USA.

[2]University of Pittsburgh Cancer Institute, 5117 Centre Avenue, Hillman Cancer Canter 2.6, Pittsburgh, PA 15213, USA.

[3]Department of Genetics, The Lineberger Comprehensive Cancer Center, University of North Carolina School of Medicine, Campus Box 7295, Chapel Hill, NC 27599, USA.

[4]Department of Cell Biology and Physiology, University of Pittsburgh School of Medicine, S362 Biomedical Science Towers, 3500 Terrace Street, Pittsburgh, PA 15261, USA

[5]Department of Microbiology and Molecular Genetics, University of Pittsburgh School of Medicine, 523 Bridgeside Point II, 450 Technology Drive, Pittsburgh, PA 15219, USA.

2.1 INTRODUCTION

DNA interstrand crosslinks (ICL) covalently link both strands of DNA together, rendering them inseparable (Dronkert and Kanaar, 2001). Strand separation is essential for DNA replication and transcription (Hoeijmakers, 2001; Osawa *et al.*, 2011). Therefore, ICLs are generally accepted to be highly cytotoxic, in particular, to rapidly dividing cells. Less than 40 ICLs can kill a cell (Grillari *et al.*, 2007), while tens of thousands of single-strand breaks, abasic sites and oxidative lesions are tolerated by cells (Ames, 1989; Grillari *et al.*, 2007; Lindahl and Barnes, 2000). This forms the conceptual basis for why drugs that induce ICLs are thought to be so effective for treating cancer (McHugh *et al.*, 2001).

Environmental exposures that crosslink DNA can be from industrial exposures, dietary sources, inhalation of atmospheric contaminants or due to cancer chemotherapy (2009). The unifying feature is that crosslinking agents must be bi-functional, having two reactive groups (Dronkert and Kanaar, 2001). They all react with DNA in a two-step fashion, first forming a monoadduct by reacting with a nucleobase in one strand of DNA then, if the sequence context is appropriate, reacting with a second nucleobase on the opposite strand to form an ICL (Anderson and Walker; Hartley *et al.*, 1991). Crosslinking agents, without exception, form multiple types of DNA lesions in addition to ICLs, including monoadducts, intrastrand crosslinks and DNA:protein crosslinks (Friedberg *et al.*, 2006). This has made it particularly challenging to decipher the biological impact of ICL lesions.

Mechlorethamine (MEC) is a chemotherapeutic agent used to treat multiple myeloma and ovarian cancer (2012a). It is a bifunctional nitrogen mustard (Figure 2.1A) that crosslinks deoxyguanosine residues at 5′-GNC sequences (Millard *et al.*, 1990; Ojwang *et al.*, 1989; Rink *et al.*, 1993). 2-Chloroethylamine (CEA) is a structurally similar monofunctional compound (Wijen

et al., 2000) (Figure 2.1B). Both compounds can form monoadducts, however only MEC has the ability to further react with protein to form DNA-protein crosslinks (Michaelson-Richie *et al.*, 2011) or an additional DNA base to form intra- and interstrand crosslinks (Wijen *et al.*, 2000) (Figure 2.1C). While the ICLs that are formed only make up 1-5% of the total types of damage induced (Dronkert and Kanaar, 2001), they are thought to be responsible for the cytotoxicity to cells after chemotherapeutic treatment. Direct comparison of the impact of MEC and CEA on cells and organisms offers a unique opportunity to dissect the unique impact of ICLs on cells.

To accomplish this, we utilized mice and cells that are genetically engineered to be DNA repair deficient and therefore hypersensitive to genotoxic agents such as MEC and CEA. ERCC1-XPF is a nuclease required for nucleotide excision repair (NER) of monoadducts (Sijbers *et al.*, 1996a) as well as the repair of ICLs (Bhagwat *et al.*, 2009; Grillari *et al.*, 2007; Niedernhofer *et al.*, 2004). XPA is a DNA damage recognition protein required only for NER (de Vries *et al.*, 1995). Comparing the impact of MEC and CEA on ERCC1-XPF-deficient and *Xpa*$^{-/-}$ mice offers a second approach for deciphering the specific effect of ICLs on tissues. Any response to MEC observed exclusively in ERCC1-XPF deficient mice will be attributable to ICLs.

Another rationale for testing the effect of ICLs on aging is that genetic deletion of *Xpa* in mice ablates NER but results in a very mild phenotype (de Vries *et al.*, 1995; Melis *et al.*, 2008). In contrast, mutation in *Ercc1*, reducing but not knocking-out expression of ERCC1-XPF in mice, leads to dramatic accelerated aging (Goss *et al.*, 2011; Gregg *et al.*, 2012a; Niedernhofer *et al.*, 2006; Schumacher *et al.*, 2008; Vo *et al.*, 2010). This difference in phenotypes has been ascribed to ICL repair deficiency or ICLs in the ERCC1-XPF deficient mice. This suggests that

ICLs may drive aging, which has important implications for cancer survivors treated with crosslinking agents.

In this study, *Ercc1*$^{-/\Delta}$ mice, with reduced expression of ERCC1-XPF (Weeda *et al.*, 1997a), and *Xpa*$^{-/-}$ mice (Melis *et al.*, 2008), along with wild-type littermates were chronically exposed to MEC or CEA and the impact on their health in terms of pre-mortem symptoms and post-mortem pathology was measured. Likewise primary fibroblasts from these mice were exposed to MEC and CEA to measure the impact on cell viability, growth and function. MEC, but not CEA, induced cell senescence *in vitro* and *in vivo*. In addition, MEC, but not CEA, promoted early onset of aging-related symptoms in all of the mouse strains. *Ercc1*$^{-/\Delta}$ mice were more severely affected than wild-type or *Xpa*$^{-/-}$ mice. Collectively, these data support the conclusion that crosslinking agents promote cell senescence and aging. This in turn implies that ICLs may be cytostatic rather than frankly cytotoxic and that chemotherapeutic agents such as mechlorethamine and cisplatin accelerate the onset of aging-related degenerative changes in cancer survivors.

2.2 RESULTS

2.2.1 Exposure paradigm

To measure the effect of MEC and CEA on cells, early passage, congenic wild-type (WT), *Ercc1*$^{-/-}$ and *Xpa*$^{-/-}$ MEFs (n = 3 independent cell lines per group) were exposed to 0.1 μM MEC (Figure 2.1A) or 0.16 μM CEA (Figure 2.1B) to induce equivalent numbers of DNA adducts based on the mustards' ability to alkylate DNA in rat 9L gliosarcoma cells (Tokuda and Bodell, 1987). Using this approach, differences in outcomes could be ascribed to ICLs, which are unique to MEC (Figure 2.1C). The cells were treated at passages 3, 4 and 5 and the impact on cell proliferation was measured (Fig. 1d). Apoptosis, cellular senescence (senescence-associated β-galactosidase) and DNA damage (γH2AX) were measured at passage 4 (Figure 2.1D). Similarly, DNA repair-deficient mice and their WT littermates (n ≥ 5 mice per genotype per treatment group) were treated once a week for six weeks with 8 μg/kg of either MEC or CEA, beginning at 8 weeks of age (Figure 2.1E). We previously reported that ERCC1-deficient mice have a 100-fold increased sensitivity to the crosslinking agent, mitomycin C (Niedernhofer *et al.*, 2006), therefore, this dose of MEC was chosen as it is approximately 100-fold lower than the dose that affects the health of WT mice (Heston, 1950). The mice were monitored daily for the onset of symptoms until the age of 20 weeks, at which time they were sacrificed and tissues were collected for pathologic analysis. Alternatively, to assess *in vivo* senescence, *Ercc1*$^{-/\Delta}$ mice were crossed with p16-luciferase reporter (*p16*$^{Luc\text{-}reporter}$) mice and treated once a week for four weeks with 8 μg/kg of either MEC or CEA. They were imaged weekly to measure p16 expression, a marker of senescence until 15 weeks of age, at which time they were sacrifice (Figure 2.1F).

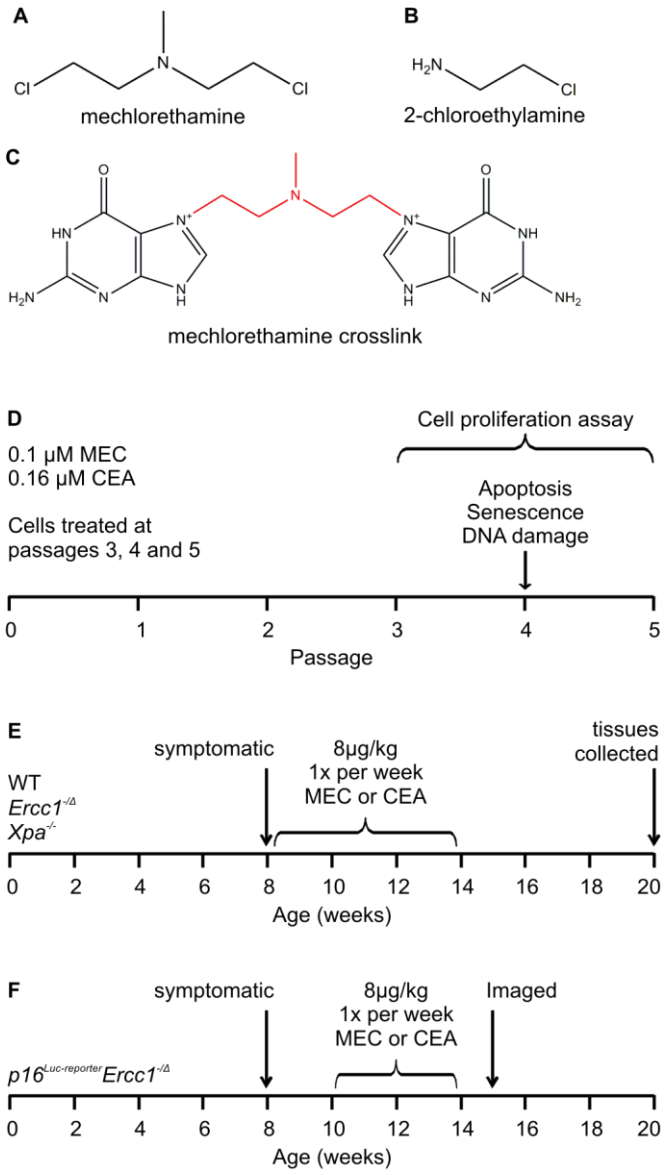

Figure 2.1: Chemical structures and exposure paradigms

Chemical structures of (**A**) mechlorethamine (MEC), (**B**) 2-chloroethylamine (CEA) and (**C**) a MEC DNA crosslink. (**D**) *In vitro* treatment schematic of wild-type (WT), *Ercc1*$^{-/-}$ and *Xpa*$^{-/-}$ primary mouse embryonic fibroblasts (MEFs). Cells were treated for one hour with 0.1µM MEC and 0.16 µM CEA, calculated to induce the same number of monoadducts lesions, such that the difference in outcomes could be ascribed to ICLs. Cells were counted, reseeded at equal density and treated with MEC and CEA at passage 3, 4 and 5 to assess cellular proliferation. At passage 4, MEFs were either fixed and stained, or analyzed by flow cytometry to assess DNA damage, senescence and apoptosis. (**E**) *In vivo* treatment schematic of WT, *Ercc1*$^{-/\Delta}$ and *Xpa*$^{-/-}$ mice. Subcutaneous injections of MEC and CEA were administered once a week for six weeks starting at 8 weeks of age. Animals were monitored daily and tissues were collected at 20 weeks of age when the mice were moribund. (**F**) *p16*$^{Luc\text{-}reporter}$*Ercc1*$^{-/\Delta}$ mice were injected with MEC once a week for four weeks, starting at 10 weeks of age. Mice were injected with luciferin and imaged prior to sacrifice and tissue collection at 15 weeks of age.

2.2.2 MEC, but not CEA, promotes senescence *in vitro*

Proliferation of WT, *Ercc1*$^{-/-}$ and *Xpa*$^{-/-}$ primary MEFs untreated or exposed to MEC or CEA was measured by counting the cells at each passage and re-seeding at equal density. The growth of all of the cell lines exposed to CEA was equivalent (Figure 2.2A), indicating that at this dose, CEA did not induce enough DNA damage to cause replicative senescence even if the damage was not repaired (i.e., in *Ercc1*$^{-/-}$ or *Xpa*$^{-/-}$ cells). Likewise MEC, did not affect the proliferation of *Xpa*$^{-/-}$ cells compared to WT, corroborating the CEA data. However, MEC did cause a significant drop in proliferation of *Ercc1*$^{-/-}$ cells compared to all over genotypes and treatments ($p \leq 0.01$, Student Newman-Keuls (SNK) test), suggesting that ICLs, when not repaired, inhibit proliferation.

Next, DNA damage was measured at passage 4 in untreated, MEC- or CEA-treated MEFs by counting the fraction of nuclei containing γH2AX foci by immunofluorescence staining. Thirty-three percent of untreated *Ercc1*$^{-/-}$ cells contained γH2AX foci (Figure 2.2B). This was significantly more than CEA-treated WT ($p \leq 0.01$, SNK test), *Ercc1*$^{-/-}$ ($p \leq 0.05$, SNK test) and *Xpa*$^{-/-}$ ($p \leq 0.001$, SNK test) cells, containing 8%, 13% and 4%, respectively, as well as the 5% of MEC-treated *Xpa*$^{-/-}$ cells ($p \leq 0.01$, SNK test). In addition, *Ercc1*$^{-/-}$ cells treated with MEC contained the highest percentage of γH2AX, with 61% of cells staining positive. This was significantly different from *Ercc1*$^{-/-}$ MEFs treated with CEA as well as untreated, which contained 13% and 33% cells positive for γH2AX foci, respectively ($p \leq 0.001$, SNK test). Furthermore, MEC-treated *Ercc1*$^{-/-}$ MEFs were also significantly different from all treatment groups of WT and *Xpa*$^{-/-}$ cells, which ranged from 4-18% cells positive for γH2AX foci ($p \leq 0.001$, SNK test). Indicating that treatment with MEC significantly increases that amount of cellular DNA damage.

To test whether the observed decreased cellular proliferation of *Ercc1*$^{-/-}$ MEFs treated with MEC was due to cell death, the fraction of apoptotic cells was measured. Adherent and non-adherent cells were stained for Annexin-V and quantitated by flow cytometry. The fraction of apoptotic cells in *Ercc1*$^{-/-}$ MEFs treated with MEC was approximately 13% and did not significantly differ between treatment groups or cell types (Figure 2.2C). Interestingly, however, when the cells were treated with a 10-fold higher dose of CEA or MEC there was an increase in apoptosis in all cell types treated with CEA compared to MEC as measured by immunodetection of cleaved caspase-3 (Figure 2.2D).

Senescence-associated β-galactosidase (SA β-gal) staining of p4 MEFs was used to measure the fraction of senescent cells. In untreated WT samples, 10% of the cells in culture were senescent (Figure 2.2E). After treatment with CEA, the level in WT cells remained the same. However, MEC induced a 2-fold increase in the amount of senescence detected in WT cells. In contrast, approximately 30% of *Xpa*$^{-/-}$ cells were found to be senescent regardless of treatment. At p4 15% of the untreated *Ercc1*$^{-/-}$ MEFs were senescent. Upon treatment with CEA, one quarter of the cells senesced. However, in the absence of ICL repair, MEC was a potent inducer of senescence. 70% of MEC-treated *Ercc1*$^{-/-}$ cells were SA β-gal-positive compared to 25% in the CEA-treated ERCC1-deficient MEFs. This was significantly greater than all other treatments and genotypes ($p \leq 0.001$, SNK test). Interestingly, growth, DNA damage, apoptosis and senescence data of cells treated with CEA is comparable to data from untreated cells (Gregg *et al.*, 2012b), which indicates that CEA is the baseline for which to measure MEC-induced phenotypes. These data indicate that CEA promotes cell death through apoptosis, while MEC promotes cellular senescence.

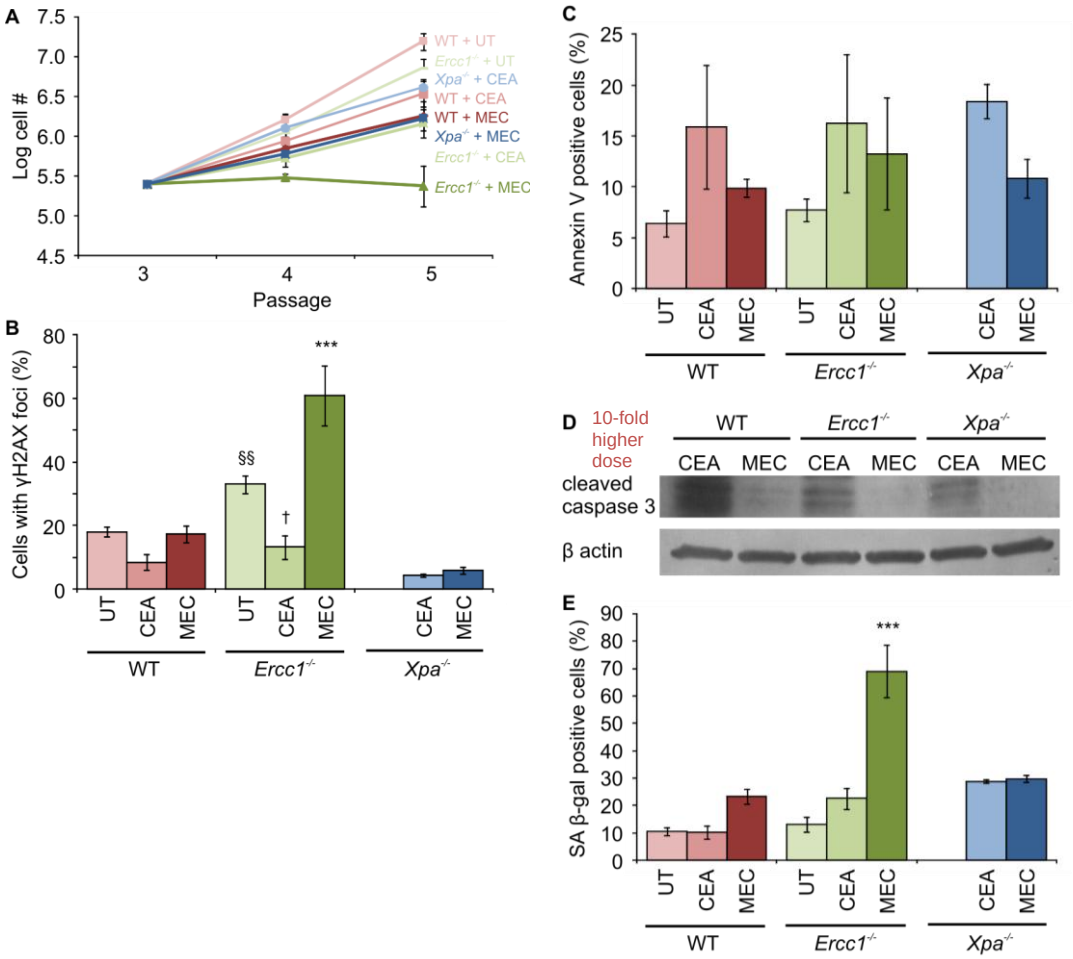

Figure 2.2: MEC, but not CEA, promotes senescence *in vitro*

(**A**) Cellular proliferation assay to measure growth in MEFs after treatment with 0.1μM MEC and 0.16μM CEA. Cells were counted and an equal number of cells were plated at each passage. Red triangles represent WT, green triangles represent *Ercc1*$^{-/-}$, blue squares represent *Xpa*$^{-/-}$ MEFs, light color indicates untreated cells, medium color indicates cells treated with CEA, and dark color indicates cells treated with MEC. (**B**) DNA damage of MEFs treated at p3 with 0.1μM MEC and 0.16μM CEA and allowed to recover one passage was assessed by γH2AX staining. Cells containing γH2AX foci were counted and compared back to total cell number. Values indicate the mean ± S.E.M. '†', $p \leq 0.05$; '§§', $p \leq 0.01$; '***', $p \leq 0.001$; Student Newman-Keuls test. (**C**) Adherent and non-adherent MEFs treated for 1 hour with 0.1μM MEC and 0.16μM CEA at p3 were allowed to recover to p4 and were stained for flow cytometry with Annexin V and propidium iodide to look for apoptosis. Values indicate the mean ± S.E.M. (**D**) Immunoblot for cleaved caspase-3 to measure apoptosis on p4 cells treated with 1μM MEC and 1.6μM CEA at p3 and allowed to recover. B-actin was used as a loading control. (**E**) p3 MEFs were treated with 0.1μM MEC and 0.16μM CEA were allowed to recover to p4. Cells were fixed and stained for senescence-associated β-galactosidase (SA β-gal). The percentage of cells stained positive were counted and compared back to the total cell number. Values indicate the mean ± S.E.M. '***', $p \leq 0.001$; Student Newman-Keuls test.

2.2.3 Chronic exposure of *Ercc1*$^{-/\Delta}$ mice to MEC, but not CEA, accelerates the onset of symptoms and pathologies associated with aging

WT, *Ercc1*$^{-/\Delta}$ and *Xpa*$^{-/-}$ mice were administered 8 μg/kg MEC or CEA via subcutaneous injection, once a week for six weeks (Figure 2.1E). This dose was not acutely toxic, as the weight of the animals was not affected throughout the treatment course (Figure 2.3). *Ercc1*$^{-/\Delta}$ mice spontaneously develop progeroid symptoms (de Waard *et al.*, 2010). Hence we asked if the onset of these symptoms from untreated mice was affected by chronic exposure to CEA or MEC. While the onset of progeroid symptoms were the same between untreated and CEA-treated *Ercc1*$^{-/\Delta}$ mice, multiple symptoms of ERCC1-deficient mice treated with MEC were significantly accelerated (Table 2.1, $p \leq 0.05$, SNK test). The onset of ataxia, priapism and urinary incontinence, all symptoms associated with neurodegeneration, were accelerated, as well as sarcopenia (loss of muscle mass in the hind-limbs). These data suggest that inducing ICLs can accelerate the aging symptoms in this mouse model.

Tissue sections from liver, kidney and brain (cerebellum) of WT *Ercc1*$^{-/\Delta}$ and *Xpa*$^{-/-}$ mice chronically exposed to CEA and MEC were compared. At 20 weeks of age, when the tissues were harvested, only the *Ercc1*$^{-/\Delta}$ mice were moribund. The sections were stained with hematoxylin and eosin and examined for aging-related degenerative changes. The liver of WT and *Xpa*$^{-/-}$ mice treated with CEA revealed normal hepatocellular architecture (Figure 2.4A). In comparison, liver sections from MEC-treated WT and *Xpa*$^{-/-}$ mice, as well as CEA-treated *Ercc1*$^{-/\Delta}$ mice, showed evidence of early ballooning degeneration of hepatocytes, indicative of steatosis (Ding *et al.*, 2010; Lackner *et al.*, 2008). All images were taken at 20x magnification, demonstrating extremely large nuclei in the hepatocytes of *Ercc1*$^{-/\Delta}$ mice compared to other

strains. However, the *Ercc1*$^{-/\Delta}$ mice treated with MEC compared to CEA had dramatically more ballooning hepatocyte degeneration, as well as increased necrosis (Figure 2.4A).

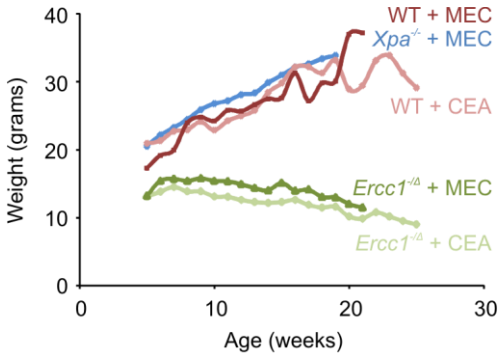

Figure 2.3: Weights of WT, *Ercc1*$^{-/\Delta}$ and *Xpa*$^{-/-}$ mice treated with MEC and CEA

Weights in grams of CEA- (medium red) and MEC treated (dark red) WT mice; CEA- (medium green) and MEC-treated (dark green) *Ercc1*$^{-/\Delta}$ mice; MEC-treated (blue) *Xpa*$^{-/-}$ mice starting at five weeks of age, three weeks before injections started.

Table 2.1: Chronic exposure of *Ercc1*$^{-/\Delta}$ mice to a crosslinking agent accelerates the onset of symptoms associated with aging

Symptoms	*Ercc1*$^{-/\Delta}$ Untreated	*Ercc1*$^{-/\Delta}$ + CEA	*Ercc1*$^{-/\Delta}$ + MEC	n = (UT, CEA, MEC)
Dystonia	8.6	12.5	10.7	5, 4, 6
Trembling	8.2	10.7	9.7	6, 6, 6
Kyphosis	11.9	13.4	13.8	6, 5, 6
Ataxia*	14.4	15.8	11.5	6, 6, 6
Hind limb wasting*	15.4	15.3	12.3	4, 4, 6
Priapism**	25.7	> 24.0	20.0	2, 2, 3
Incontinence**	>25.0	> 24.0	20.3	2, 2, 3

Significantly accelerated symptoms due to treatment of mice with MEC; '*', $p < 0.05$; '**', $p < 0.01$; Student Newman-Keuls test.

H&E-stained kidney sections from CEA-treated WT, MEC-treated WT and CEA-treated *Xpa*$^{-/-}$ revealed normal renal pathology (Figure 2.4B). In comparison, kidney samples from MEC-treated *Xpa*$^{-/-}$ and both treatment groups of *Ercc1*$^{-/\Delta}$ mice had enlarged tubular cells. In addition, both CEA- and MEC-treated *Ercc1*$^{-/\Delta}$ mice showed increased proteinaceous hyaline cast formation in the renal tubules, as well as glomerulosclerosis compared to WT and *Xpa*$^{-/-}$ mice. However, MEC treatment of *Ercc1*$^{-/\Delta}$ mice resulted in more severe glomerulosclerosis than CEA treatment (Figure 2.4B). Additionally, kidney functional tests revealed an elevation of urea nitrogen in MEC-treated *Ercc1*$^{-/\Delta}$ mice, above the normal limit found in the WT blood serum (Figure 2.4C). This increase was significantly different from *Ercc1*$^{-/\Delta}$ mice treated with CEA ($p < 0.05$, Student's *t*-test). Indicating that treatment with a crosslinking agent can deleteriously affect kidney function.

Finally, H&E stained brains were analyzed for cerebellar changes. Analysis of WT and *Xpa*$^{-/-}$ cerebella revealed no change in neuropathology upon treatment with MEC or CEA (Figure 2.4D). A decrease in the number of Purkinje cells was noted upon investigation of the *Ercc1*$^{-/\Delta}$ brains. In order to quantify this change, nucleated Purkinje cells were counted and the ratio of Purkinje cell number to linear Purkinje cell layer was analyzed (Axelrad *et al.*, 2008). There was no measurable difference in Purkinje cell count between untreated, CEA-treated and MEC-treated WT and *Xpa*$^{-/-}$ mice (Figure 2.4E). However, there was a significant decrease of cerebellar Purkinje cells in untreated *Ercc1*$^{-/\Delta}$ mice compared to all treatment groups of WT and *Xpa*$^{-/-}$ mice ($p < 0.01$, SNK test). There was no difference in the number of cells in CEA-treated *Ercc1*$^{-/\Delta}$ mice compared to untreated. In addition, *Ercc1*$^{-/\Delta}$ mice treated with MEC had a further reduction in Purkinje cell number compared to untreated and CEA-treated *Ercc1*$^{-/\Delta}$ mice (Figure

2.4E; $p < 0.05$, SNK test). This supports the acceleration of neurodegenerative changes seen in these mice prior to sacrifice (Table 2.1) and indicates that ICLs promote neurodegeneration.

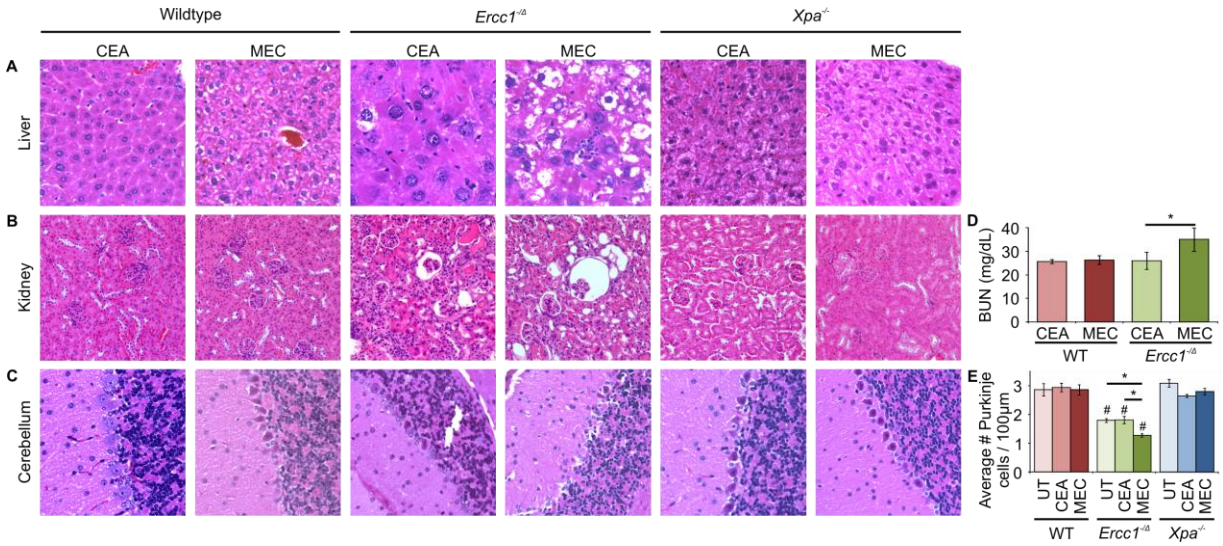

Figure 2.4: Chronic exposure of *Ercc1*$^{-/\Delta}$ mice to MEC accelerates the onset of symptoms and pathologies associated with aging

(**A**) Liver and (**B**) kidney were stained with hematoxylin and eosin (H&E) and imaged by brightfield microscopy at 20x magnification. (**C**) Blood urea nitrogen (BUN) levels were measured in the WT and *Ercc1*$^{-/\Delta}$ mice treated with MEC or CEA. '*', $p < 0.05$ Student's *t*-test. (**D**) Cerebella were stained with H&E and imaged by brightfield microscopy at 40x magnification to visualize Purkinje cells (PC). (**E**) To quantify PC loss, untreated, CEA- and MEC-treated WT, *Ercc1*$^{-/\Delta}$ and *Xpa*$^{-/-}$ PCs were counted in at least ten cerebellar images for three mice per treatment. The cell counts were normalized to the linear PC layer. '*', $p \leq 0.05$ for differences between the treatment groups of *Ercc1*$^{-/\Delta}$ mice; '#', $p \leq 0.01$ comparing the *Ercc1*$^{-/\Delta}$ to WT and *Xpa*$^{-/-}$ mice of all treatment groups; Student Newman-Keuls test.

2.2.4 CEA promotes apoptosis in the liver and kidney

To investigate the mechanism by which MEC induced aging-related pathology, liver and kidney sections from the exposed animals were subjected to TUNEL assay to measure apoptosis (Figure 2.5A and B). Interestingly, none of the MEC-treated liver or kidney samples from WT, *Ercc1*$^{-/\Delta}$ or *Xpa*$^{-/-}$ mice stained TUNEL-positive (Figure 2.5A). In the liver sections from CEA-treated mice, there were similar levels of TUNEL-positive cells between genotypes. Analysis of the

kidneys revealed TUNEL-positive staining in renal tubules from *Ercc1*$^{-/\Delta}$ and *Xpa*$^{-/-}$ mice (Figure 2.5B). This supports the *in vitro* data, which showed that high doses of CEA in culture can cause increased apoptotic changes (Figure 2.2D). This indicates that cell death is not driving the aging-related degenerative phenotype of the *Ercc1*$^{-/\Delta}$ mice that is accelerated by induction of ICLs.

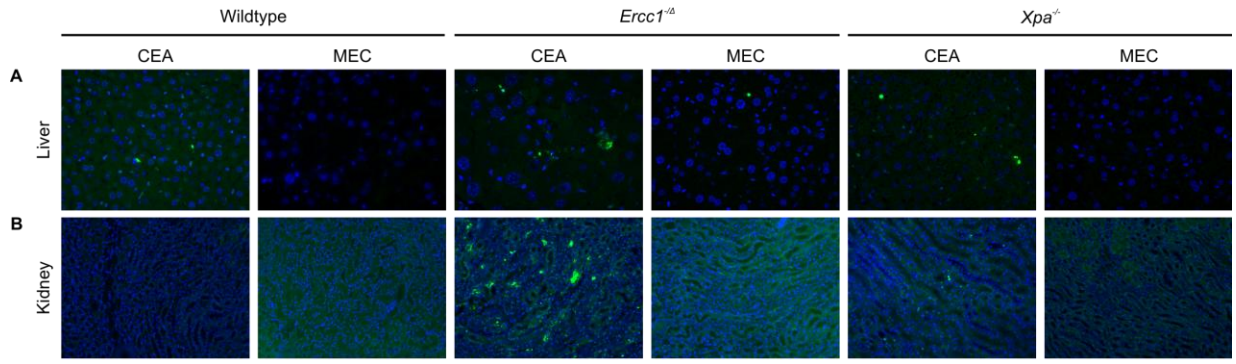

Figure 2.5: CEA, but not MEC, increases apoptosis

TUNEL staining (green) to detect apoptosis in (**A**) liver (40x objective) and (**B**) kidney (20x objective) from WT, *Ercc1*$^{-/\Delta}$ and *Xpa*$^{-/-}$ mice treated with 8 µg/kg MEC and CEA. Nuclei were counterstained with DAPI (blue).

2.2.5 *Ercc1*$^{-/\Delta}$ mice show tissue-specific senescence after treatment with MEC

Cells expressing p16 were recently demonstrated to drive aging (Baker *et al.*, 2011). Hence a p16 reporter was used to measure expression of this senescence marker in *Ercc1*$^{-/\Delta}$ mice treated with MEC. *Ercc1*$^{-/\Delta}$ mutant mice containing a p16-Luciferase reporter (*p16*$^{Luc\text{-}reporter}$) were chronically exposed to MEC for four weeks. They were monitored weekly for p16 expression and sacrificed at 15 weeks (Figure 2.1F). *p16*$^{Luc\text{-}reporter}$*Ercc1*$^{-/\Delta}$ mice (n = 4) did not show evidence of p16 expression at 14 weeks of age, when some progeroid symptoms are already evident (Table 2.1). However, by 20 weeks of age, p16 expression is evident in the lung and bladder regions of the mice (Figure 2.6A). In contrast, the 15 week-old MEC-treated *p16*$^{Luc\text{-}reporter}$*Ercc1*$^{-/\Delta}$ mice,

displayed increased levels of luciferase signal in the lung, pancreas and bladder regions compared to untreated mice of similar age (Figure 2.6B). The MEC-treated animals revealed an acceleration of the onset of senescence by almost four weeks. This is in accord with the acceleration of the aging-related symptoms, ataxia, sarcopenia, priapism and incontinence, which were apparent more than 3 weeks earlier than those of control mice (Table 2.1).

At 15 weeks, the animals were also sacrificed to further investigate the senescence pattern in the organs of MEC-treated $p16^{Luc\text{-}reporter}Ercc1^{-/\Delta}$ mice. The luciferase reporter levels in the lungs, bladder and pancreas were similar to, if not higher than, tissues imaged from untreated 18 week-old $p16^{Luc\text{-}reporter}Ercc1^{-/\Delta}$ mice (Figure 2.7). This also supports the accelerated onset of the progeroid phenotype in MEC-treated $Ercc1^{-/\Delta}$ mice (Table 2.1). Unfortunately, because of differential uptake of luciferin by tissues and because hemoglobin absorbs visible light which can mask the luciferase signal, "dark" organs, such as the liver and kidneys, were nearly impossible to analyze by this method (Berger *et al.*, 2008; Carlsen *et al.*, 2002).

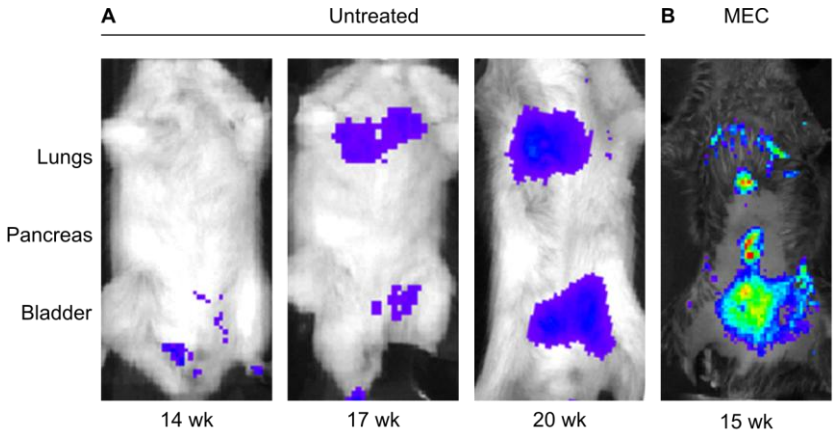

Figure 2.6: Treatment with MEC revealed tissue-specific senescence in *Ercc1*$^{-/\Delta}$ mice

(**A**) Untreated $p16^{Luc\text{-}reporter}Ercc1^{-/\Delta}$ mice at 14, 17 and 20 weeks of age, represent the natural progression of senescence in ERCC1-deficient mice ($n \geq 3$ at each timepoint). (**B**) $p16^{Luc\text{-}reporter}Ercc1^{-/\Delta}$ mice were administered subcutaneous injections of 8 ug/mg MEC for 4 weeks ($n = 3$). At 15 weeks of age, the mice were injected with luciferin and imaged.

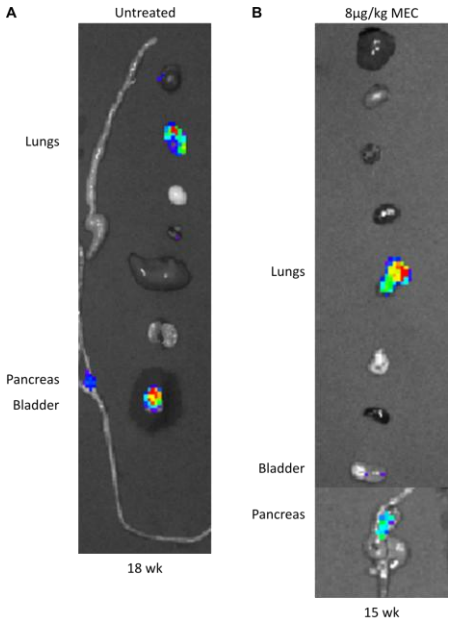

Figure 2.7: Post-mortem tissue-specific senescence in *Ercc1*$^{-/\Delta}$ mice treated with MEC

Mice were injected with luciferin and tissues harvested 15 minutes later to image organs. (**A**) Representative image of organs from an untreated *p16*$^{Luc\text{-}reporter}$*Ercc1*$^{-/\Delta}$ mouse at 18 weeks of age. The lungs, bladder and pancreas luminesce. (**B**) Representative image of organs from a MEC-treated *p16*$^{Luc\text{-}reporter}$*Ercc1*$^{-/\Delta}$ mouse at15 weeks of age. Luminesce is apparent in the lungs, bladder and pancreas.

2.2.6 MEC treatment of *Ercc1*$^{-/\Delta}$ mice increases neurodegeneration

To investigate the acceleration of the neurodegenerative phenotype of the *Ercc1*$^{-/\Delta}$ mice by treatment with MEC, cerebellar sections were stained by TUNEL assay to label apoptotic cells (Figure 2.8A). There was no evidence of increased apoptosis in the brains of WT or *Xpa*$^{-/-}$ mice regardless of the treatment. However, TUNEL-positive neurons were present in the cerebella of *Ercc1*$^{-/\Delta}$ mice. As seen in the liver and kidney (Figure 2.5A and B), there was increased apoptosis in the CEA-treated *Ercc1*$^{-/\Delta}$ mice compared to MEC treatment (Figure 2.8A).

To further investigate the neurodegenerative symptoms that were accelerated by MEC treatment (Table 2.1), the cerebella from the MEC- and CEA-treated mice were stained with Fluoro-Jade® B, a fluorescein derivative that preferentially binds to degenerating neurons. WT,

Ercc1$^{-/\Delta}$ and *Xpa*$^{-/-}$ mice treated with MEC did not reveal FluoroJade®-positive neurons (Figure 2.8B). However, CEA-treated cerebellar sections of all three genotypes showed increased staining, indicative of neurodegeneration. In fact, *Xpa*$^{-/-}$ mice treated with CEA had the highest level of degenerating neurons, as measured by Fluoro-Jade® B (Figure 2.8B). This could indicate that the timepoint of 20 weeks old, when we sacrificed the mice to look at histopathologic changes is too late to visualize the accelerated neurodegenerative phenotype. The symptoms assessed when they were alive presented themselves almost four weeks earlier than those of untreated and CEA-treated *Ercc1*$^{-/\Delta}$ mice (Table 2.1). Therefore an earlier timepoint may be necessary to investigate the neurodegenerative changes induced by DNA ICLs.

Finally, the *Ercc1*$^{-/\Delta}$ brain sections were also stained with a glial fibrillary acidic protein (GFAP) antibody to identify gliosis, another marker of neurodeneration (Figure 2.8C). There was staining in the cerebellum of CEA-treated *Ercc1*$^{-/\Delta}$ mice. The staining was increased in the *Ercc1*$^{-/\Delta}$ mice treated with MEC.

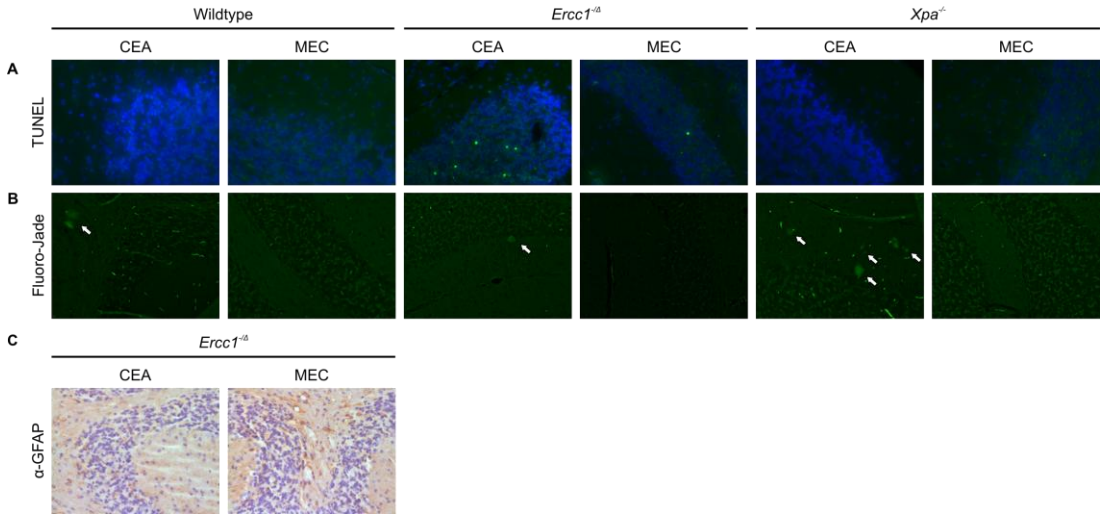

Figure 2.8: MEC treatment of *Ercc1*$^{-/\Delta}$ mice increases neurodegeneration

(**A**) TUNEL staining (green) of cerebellar sections (40x magnification) from MEC and CEA treated WT, *Ercc1*$^{-/\Delta}$ and *Xpa*$^{-/-}$ mice. Nuclei were counterstained with DAPI (blue). (**B**) Cerebellar sections of mice treated with CEA as stained by Fluoro-Jade B®, a stain that preferentially binds to degenerating neurons (40x magnification). (**C**) Immunohistochemical detection of glial fibrillary acidic protein (GFAP) antibody in cerebella from *Ercc1*$^{-/\Delta}$ mice after treatment with MEC and CEA (40x magnification). Nuclei were counterstained with hematoxylin.

2.3 DISCUSSION

Accumulation of DNA damage is one contributor to aging. Because of the fact that mutations in DNA repair genes result in premature aging of tissues, DNA damage is implicated as a contributor to the aging process (Hasty *et al.*, 2003b). However, the type of nuclear damage and mechanism by which this occurs is unknown. Herein, we utilize two murine models of human diseases, one of xeroderma pigmentosum and the other of XFE progeroid syndrome, to analyze the response to DNA damage and assess their effect on the aging process.

Furthermore, because early clinical chemotherapy trials were started in the late 1970s and early 1980s, long-term toxicity has since been assessed in cancer survivors (Maccormick, 2006). These patients have suffered from a number of health problems that are typically associated with advanced age, including neurodegenerative, musculoskeletal and osteoporotic symptoms, as well as skin changes and fatigue. Therefore, chemotherapies have been identified as a possible source of premature aging in long-term cancer survivors (Grillari *et al.*, 2007; Maccormick, 2006). Consequently, identifying the causes of aging and strategies to ameliorate the diseases, while preserving tissue homeostasis, is a pressing healthcare issue, not only for cancer survivors, but the population as a whole.

Mechlorethamine was the first chemotherapeutic agent to be developed at Yale University during World War II and is still in use today to treat multiple myeloma and ovarian cancer (2012a; Christakis, 2011; Gilman, 1963). Despite previous studies indicating that DNA interstrand crosslinks are cytotoxic to tumor cells (Geleziunas *et al.*, 1991; Hansson *et al.*, 1987; Ross *et al.*, 1978), little is known about the mechanism by which ICLs induce premature aging side effects seen in chemotherapeutic patients. Herein we describe the method by which the

DNA interstrand crosslink-inducing nitrogen mustard, mechlorethamine, contributes to age-related degeneration.

Interestingly, our *in vitro* data indicate that MEC, but not CEA, treatment of ICL repair-deficient MEFs results in severe growth arrest (Figure 2.2A). This dramatic reduction in proliferating cells is not a result of cell death, but rather a result of high levels of senescence in cells unable to repair the DNA interstrand crosslinks (Figure 2.2B-E). In fact, cells deficient in the nucleotide excision repair pathway alone (i.e., $Xpa^{-/-}$), which are able to repair ICLs and do not exhibit signs of premature aging, show no difference between treatment with MEC compared to CEA (Figure 2.2).

We further demonstrate that MEC-induced DNA interstrand crosslinks accelerate the aging phenotype of our progeroid mice (Table 2.1). Because ERCC1 deficiency leads to exquisite sensitization to DNA ICLs (Niedernhofer *et al.*, 2006), we were able to treat mice with a low dose of MEC to investigate the effects this crosslinking agent has on the aging phenotype of these mice. Specifically there were significant changes in ataxia, priapism and incontinence, signs of neurodegeneration, as well as hind-limb wasting, a musculoskeletal symptom. These data fit with the aging symptoms seen in long-term cancer survivors (Grillari *et al.*, 2007; Maccormick, 2006). We also demonstrate that after treatment with MEC the liver, kidney and brain of ICL repair-deficient mice show signs of impaired function (Figure 2.4). In addition we establish that this *in vivo* accelerated aging occurs as a result of senescence and not apoptosis (Figure 2.5 and Figure 2.6). These data strongly support the conclusion that DNA interstrand crosslinks promote aging through a cytostatic, rather than a cytotoxic method.

In conclusion, individual cells undergo senescence after treatment with MEC, both *in vitro* and *in vivo*. We found no evidence of increased apoptosis or cytotoxicity, as was previously

described (Grillari *et al.*, 2007). We did however, find evidence that 2-chloroethylamine, a monoadducting chemical, can induce apoptosis *in vitro* and *in vivo* (Figure 2.2, Figure 2.5 and Figure 2.8), perhaps through an error-prone mutagenic DNA repair pathway (Wijen *et al.*, 2000). Additionally, the MEC-treated cells and tissues exhibited a high level of senescence (Figure 2.2 and Figure 2.6), which may induce the senescence-associated secretory phenotype (SASP) (Rodier *et al.*, 2009). This signaling further propagates senescence in surrounding cells leading to tissue dysfunction and organismal aging. Therefore, strategies must be developed to diminish the aging-related side effects that long-term cancer survivors experience by preventing senescence in otherwise healthy tissue.

2.4 METHODS

2.4.1 Cell Culture

Mouse embryonic fibroblasts (MEFs) were isolated at pre-natal day 15 from heterozygous C57Bl/6 mice bred to yield wild-type (WT), *Ercc1*$^{-/-}$, and *Xpa*$^{-/-}$ as previously described (Ahmad *et al.*, 2008; Niedernhofer *et al.*, 2006). Cells were cultured in a 1:1 mixture of Dulbecco's modified Eagle medium and Ham's F-10 supplemented with 10% fetal bovine serum, 1% non-essential amino acids and 1% penicillin and streptomycin. MEFs were incubated in MEC (0.1 μM) and CEA (0.16 μM) for 1h in serum-free medium, with a minimum recovery period of 24h. To assay proliferation, 250,000 cells were plated and quantified using an automated cell counter (Millipore, Billerica, MA) as previously described (Ahmad *et al.*, 2008). Experiments were repeated using three independent cell lines.

2.4.2 Detection of apoptotic cells by flow cytometry

WT, *Ercc1*$^{-/-}$, and *Xpa*$^{-/-}$ MEFs treated with MEC or CEA (as described above) and trypsinized at confluence. 1 million cells from each treatment group were washed in PBS and stained for apoptosis markers FITC Annexin V and Propidium Iodide (BD Pharmingen, Franklin Lakes, NJ) according to manufacturer's instructions. Apoptotic cells were measured on a Beckman Coulter (Cytomation) CyAN 9-Color High Speed Analyzer (Beckman Coulter, Inc., Brea, CA) and quatified using Summit v.4.3 software.

2.4.3 *In vitro* detection of senescent cells

Nitrogen mustard-treated cells were plated on glass coverslips and fixed in 2% paraformaldehyde + 0.25% glutaraldehyde in PBS for 10 minutes. Senescence-associated β-galactosidase (SA β-gal) staining was performed as previously described (Debacq-Chainiaux *et al.*, 2009; Dimri *et al.*, 1995). Nuclei were counterstained with DAPI, and senescent cells were imaged using an Olympus BX51 fluorescent microscope (Olympus America Inc., Center Valley, PA) at 40X magnification. Mean percentages of SA β-gal positive cells were graphed ± S.E.M.

2.4.4 *In vitro* immunohistochemistry

MEC- or CEA-treated MEFs were grown on glass coverslips to 50-60% confluency. Cells were fixed in 2% paraformmaldehyde + 0.25% glutaraldehyde in PBS and permeabilized with 0.2% Triton X-100 solution. Immunofluorescence was performed for γH2AX following 45min block in 2% bovine serum albumin (BSA). Primary antibody for γH2AX (clone JBW 301, Millipore, Billerica, MA) was applied overnight at 4°C at a 1:500 dilution. Secondary antibody was applied for 1h at room temperature. Nuclei were counterstained with DAPI, and fluorescent images were taken using an Olympus BX51 fluorescence microscope at 20X magnification. Mean percentages of cells containing γH2AX foci were plotted ± S.E.M.

2.4.5 Immunoblotting

MEC- or CEA-treated WT, *Ercc1*$^{-/-}$, and *Xpa*$^{-/-}$ MEFs were trypsinized, pelleted and resuspended in ice cold NETT buffer (100mM NaCl, 50mM Tris pH 7.5, 5mM EDTA pH 8.0, 0.5% Triton-

X) containing Protease Inhibitor Cocktail Set III (Calbiochem, Gibbstown, NJ). 50µg samples were boiled for 10min in 4X loading buffer (0.25mol/L Tris-HCl (pH 8.5), 8% SDS, 1.6mmol/L EDTA, 0.1mol/L DTT, 0.04% bromophenol blue, 40% glycerol) and separated via SDS-PAGE on a 4-20% Mini-PROTEAN gradient gel (Bio-Rad, Hercules, CA). Protein was transferred to a nitrocellulose membrane. Primary antibody for cleaved caspase-3 (clone 9664, Cell Signaling Technology, Beverly, MA) was applied overnight at 4°C at a 1:1000 dilution. This was followed by a 1:1000 dilution of HRP-conjugated goat anti-rabbit IgG (Promega, Madison, WI) for 1h at room temperature. Blots were developed and imaged using Alpha Innotech Red gel imaging system.

2.4.6 Mice

Ercc1$^{-/\Delta}$ mice were generated in an f1 hybrid background by crossing *Ercc1*$^{+/-}$ and *Ercc1*$^{+/\Delta}$ from inbred C57Bl/6 and FVB/n backgrounds, respectively. The mice were genotyped by PCR as previously described (Ahmad *et al.*, 2008). *p16*$^{Luc\text{-}reporter}$*Ercc1*$^{-/\Delta}$ were generated by crossing *p16*$^{Luc\text{-}reporter}$ with *Ercc1*$^{+/-}$ C57Bl/6 mice. These were then bred with *Ercc1*$^{+/\Delta}$ FVB/n mice to generate *p16*$^{Luc\text{-}reporter}$*Ercc1*$^{-/\Delta}$ mice in an f1 hybrid background. The mice were genotyped by PCR using the following primers to amplify the WT and *p16*$^{Luc\text{-}reporter}$ alleles using the forward primer: 5'-CTA TGG CGG GCT GTG GAG and 2 reverse primers: 5'-CAC GGT AGG CTG CGA AAT G and 5'-TGG GAC ACT CCT TGC CTA CC. The resulting PCR products were 312 bp for the WT allele and 543 bp for the *p16*$^{Luc\text{-}reporter}$ allele.

2.4.7 Treatment of mice with nitrogen mustards

WT, *Ercc1*$^{-/\Delta}$, and *Xpa*$^{-/-}$ were injected subcutaneously with 8 μg/kg of either MEC or CEA dissolved in sunflower seed oil from *Helianthus annuus* (Sigma-Aldrich, St. Louis, MO). Mice were treated once a week for six weeks starting at eight weeks of age. They were monitored daily, with weights taken once a week and symptom development noted twice a week. Tissues were collected at 20 weeks of age for analysis.

2.4.8 Histochemistry

Liver, kidney and brain were fixed overnight in 10% formalin, embedded in paraffin and sectioned using a microtome by standard procedures. Hematoxylin and eosin (H&E) was done according to standard procedures. Liver, kidney and brain sections were also permeablized with 0.1% Triton X-100 + 0.1% sodium citrate and stained using an *In Situ* Cell Death Detection Kit, Fluorescein (Roche Applied Science, Indianapolis, IN) according to manufacturer's instructions to label apoptotic cells. Nuclei were counter-stained with DAPI. Apoptotic-positive cells were imaged on an Olympus BX51 fluorescent 4 microscope (Olympus America Inc., Center Valley, PA).

2.4.9 *In vivo* senescence detection

p16$^{Luc\text{-}reporter}$ and *p16*$^{Luc\text{-}reporter}$*Ercc1*$^{-/\Delta}$ mice were injected with MEC starting at 10 weeks of age and lasting four weeks. Mice were injected with 300 mg/kg of Luciferin (Gold Biotechnologies, St. Louis, MO) 15min prior to imaging. Animals were anesthetized with isoflurane and

luciferase intensity was measured using an IVIS 200 imaging system (Caliper Life Sciences, Hopkinton, MA). Mice were imaged weekly for onset of premature senescence and sacrificed one week after the completion of injections.

2.4.10 Purkinje cell counts

H&E stained cerebellar sections were imaged on an Olympus BX51 fluorescence microscope (Olympus America Inc., Center Valley, PA) at 40x magnification. Purkinje cells were counted as previously described (Axelrad *et al.*, 2008). Briefly, nucleated Purkinje cells were counted and normalized to linear Purkinje cell layer which was measured using SPOT software (v.4.6, Diagnostic Instruments, Inc., Sterling Heights, MI). This ratio was obtained from at least 10 non-overlapping random fields of view from three mice per treatment group.

3.0 A MITOCHONDRIAL-TARGETED NITROXIDE DELAYS MULTIPLE DEGENERATIVE DISEASES IN A MURINE MODEL OF ACCELERATED AGING

Andria Rasile Robinson[1,2], Jin Wang[3], Erin M. Skoda[4], Marie-Céline Frantz[4], Salony Maniar[5], Jeremy S. Tilstra[6], Luigi A. Nasto[7], Siobhán Q. Gregg[5], Arvydas Usas[7], Nam Vo[7], Claudette St. Croix[5], Yinsheng Wang[3], Paul D. Robbins[6,7], Peter Wipf[4], and Laura J. Niedernhofer[2,6]

[1]Department of Human Genetics, University of Pittsburgh Graduate School of Public Health, 130 DeSoto Street, Pittsburgh, PA, 15261, USA.

[2]University of Pittsburgh Cancer Institute, 5117 Centre Avenue, Hillman Cancer Center 2.6, Pittsburgh, PA, 15213, USA.

[3]Department of Chemistry, University of California, Riverside, CA 92521, USA.

[4]Department of Chemistry, University of Pittsburgh, 219 Parkman Avenue, Pittsburgh, PA, 15260, USA.

[5]Department of Cell Biology and Physiology, University of Pittsburgh School of Medicine, S362 Biomedical Science Towers, 3500 Terrace Street, Pittsburgh, PA 15261, USA.

[6]Department of Microbiology and Molecular Genetics, University of Pittsburgh School of Medicine, 523 Bridgeside Point II, 450 Technology Drive, Pittsburgh, PA, 15219, USA.

[7]Department of Orthopaedic Surgery, University of Pittsburgh School of Medicine, 3471 Fifth Avenue, Pittsburgh, PA, 15213, USA.

3.1 INTRODUCTION

Aging is accompanied by a universal and progressive decline in the function of tissues, leading to a decreased ability to maintain homeostasis under stress; therefore, a dramatically increased risk of morbidity and mortality (Kirkwood, 2005). These inevitable changes are thought to arise as a direct or indirect consequence of cellular damage, which accumulates over time. One of the main sources of endogenous damage is reactive oxygen species (ROS), which form the basis of the free radical theory of aging (Harman, 1956). Within cells, mitochondria are the main source of ROS, and some ROS can diffuse throughout the cell, resulting in oxidative damage to lipids, proteins, RNA and DNA (Chakravarti and Chakravarti, 2007; Cooke *et al.*, 2003; Cui *et al.*, 2012; Mandavilli *et al.*, 2002). DNA lesions caused by ROS include oxidized bases, abasic sites, single-strand breaks and lipid peroxidation-induced adducts including interstrand crosslinks (Maynard *et al.*, 2009; Niedernhofer *et al.*, 2003). Thus, mitochondrial dysfunction, which leads to an increase in ROS production, has been hypothesized to be central to the aging process (Cui *et al.*, 2012). Though there is extensive evidence to support ROS as a driver of aging in lower eukaryotes, it remains highly controversial in mammals (Muller *et al.*, 2007). Critically evaluating whether mitochondrial-generated ROS play a causal role in aging is, therefore, important for devising strategies to prevent or delay age-related degenerative diseases.

ERCC1-XPF is a structure-specific endonuclease required for nucleotide excision repair, interstrand crosslink repair and the repair of some double-strand breaks in the nuclear genome (Ahmad *et al.*, 2008; Niedernhofer *et al.*, 2004; Sijbers *et al.*, 1996a). In humans, reduced expression of ERCC1-XPF causes a severe progeroid syndrome or disease of accelerated aging. This affects the endocrine, epidermal, hematopoietic, hepatobiliary, musculoskeletal, neurologic and renal systems (Niedernhofer *et al.*, 2006). *Ercc1*$^{-/\Delta}$ mice model this progeroid syndrome and

spontaneously develop progressive degenerative changes that mimic those seen in aged humans (de Waard *et al.*, 2010; Goss *et al.*, 2011; Gregg *et al.*, 2012a; Vo *et al.*, 2010). The mice are asymptomatic during development, only showing aging-related symptoms after reaching adulthood (2 months of age) and have a maximum lifespan of 7 months (de Waard *et al.*, 2010). These mice, therefore, offer a sensitive model for investigating endogenous sources of damage that may drive aging.

To investigate the hypothesis that mitochondrial-derived ROS play a causal role in aging, *Ercc1*$^{-/\Delta}$ mice were chronically treated with the mitochondrial-targeted ROS scavenger XJB-5-131 (XJB). Treatment with XJB was intended to reduce ROS before they could damage the nuclear genome. XJB has previously been shown to prolong survival in rat models of ischemia, a type of inflammatory oxidative stress (Macias *et al.*, 2007). XJB caused a significant reduction in oxidative DNA damage and a significant delay in the onset of aging symptoms and pathologies in the *Ercc1*$^{-/\Delta}$ mice. This provides strong experimental evidence that oxidative damage caused by mitochondrial-derived ROS drives aging and that targeted anti-oxidants can be used therapeutically to attenuate damage and extend healthspan.

3.2 RESULTS

3.2.1 XJB-5-131 concentrates in mitochondria

4-Hydroxy-2,2,6,6,-tetramethyl piperidine-1-oxyl (TEMPOL) is a stable nitroxide radical that acts as a superoxide dismutase mimetic (Goldstein *et al.*, 2003; Krishna *et al.*, 1996), which converts superoxide radical anion to oxygen and hydrogen peroxide. The intermediate hydroxylamine, which is also generated from nitroxide radical and biological reductants can act itself as a scavenger of ROS, in particular of the highly reactive hydroxyl radical, and cycle back and forth between nitroxide, nitroxonium cation, and hydroxylamine forms (Charloux *et al.*, 1995; Fink *et al.*, 2007; Mitchell *et al.*, 2000). TEMPOL was conjugated to a fragment of the antibiotic gramicidin S, to create XJB-5-131 (XJB) (Figure 3.1A) (Goldstein *et al.*, 2003; Wipf *et al.*, 2005). The gramicidin S fragment is intended to target the radical scavenger to the mitochondrial membrane (Frantz and Wipf, 2010; Jiang *et al.*, 2007; Kagan *et al.*, 2009). To test if this was the case, a fluorescently-labeled version of XJB was synthesized by conjugation to the dye, BODIPY-FL. This agent was added to monolayers of primary mouse embryonic fibroblasts, and the fluorescent signal was monitored every 3 min using confocal, live cell imaging. Beginning at 1.5 h post-addition of BODIPY-FL-XJB-5-131 to the culture media, a peri-nuclear punctuate pattern of fluorescence signal was observed (Figure 3.1B). The BODIPY-FL signal co-localized with MitoTracker®, indicating that XJB was concentrated in the mitochondria. Three hours after addition of BODIPY-FL-XJB-5-131, the signal was unchanged, suggesting that XJB stably associates with mitochondria.

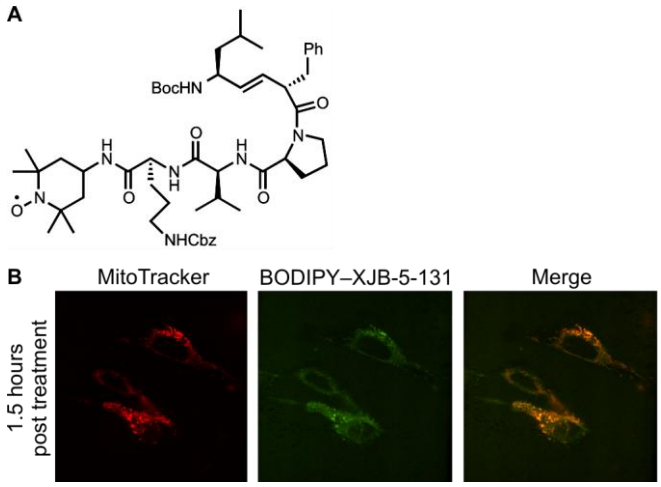

Figure 3.1: XJB-5-131 is a nitroxide radical scavenger conjugated to a mitochondrial-targeting moiety derived from gramicidin S

(**A**) Structure of XJB-5-131. (**B**) XJB-5-131 was covalently labeled with BODIPY-FL (green) to enable tracking its subcellular localization. It was added to primary mouse embryonic fibroblasts grown on MatTek glass bottom plates with MitoTracker® (red) to identify mitochondria. The cells were monitored by live cell imaging for 3 h. Shown is an image from 1.5 h post-addition of the fluorescently tagged XJB to the culture medium.

3.2.2 XJB-5-131 extends the healthspan of *Ercc1*$^{-/\Delta}$ mice

To determine if the mitochondrial-targeted radical scavenger ameliorates signs of premature aging in *Ercc1*$^{-/\Delta}$ mice, the animals were treated with 2 mg/kg XJB, three times per week, by intraperitoneal injection, starting at five weeks of age (Figure 3.2A). Alternatively, control *Ercc1*$^{-/\Delta}$ mice were treated with vehicle only (sunflower seed oil). Importantly, there was no difference in the weights of the animals between the two treatment groups throughout the study, indicating that there is no toxicity associated with chronic treatment with XJB (Figure 3.3). The animals were monitored daily for the onset of their progeroid symptoms, by an investigator blinded as to treatment groups. The mice treated with XJB exhibited a significant delay in the onset of aging-related symptoms, in particular those associated with neurodegeneration (dystonia

and ataxia), as well as kyphosis, lethargy (or reduced spontaneous activity) and hind-limb muscle wasting (Table 3.1 and Figure 3.2B). The majority of the mice were treated in a pair-wise fashion, in which littermate *Ercc1*$^{-/\Delta}$ mice housed together were treated with XJB or vehicle only, to remove genetic and environmental variables. The ages at onset of symptoms were compared between these eight littermate pairs to determine the percent of symptoms delayed in the XJB treatment group, as a measure of healthspan. Sixty-six percent of symptoms assessed in live animals were significantly delayed in the *Ercc1*$^{-/\Delta}$ mice treated with XJB compared to their littermates treated with vehicle only (Table 3.1).

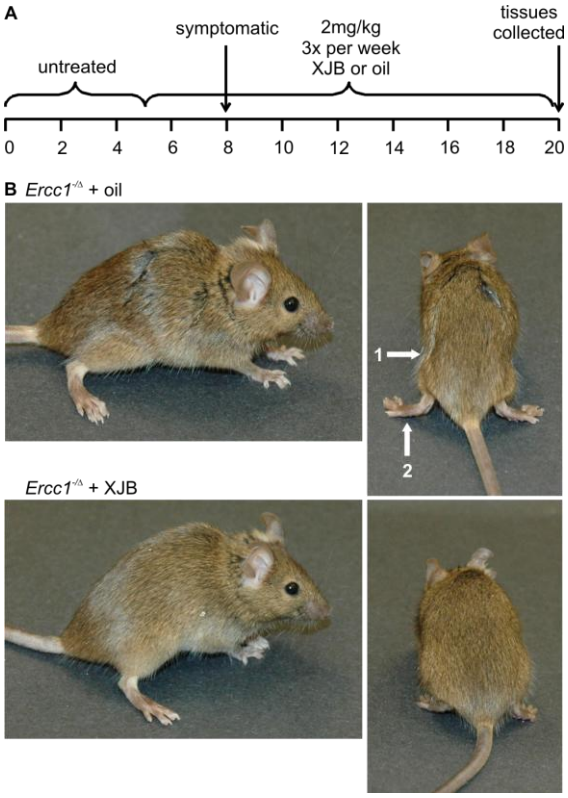

Figure 3.2: Progeroid DNA repair-deficient mice treated with XJB are healthier than littermate animals treated with vehicle only

(**A**) Treatment scheme for *Ercc1*$^{-/\Delta}$ mice. Littermate pairs were injected with either vehicle (sunflower seed oil) or 2 mg/kg XJB in a blinded fashion, three times per week, intraperitoneally starting at five weeks and lasting until 20 weeks of age. (**B**) Photographs of a 20 week-old *Ercc1*$^{-/\Delta}$ littermate pair treated with either XJB or vehicle only. Shown are examples of hind-limb wasting (1) and ataxia (2) in mice treated with vehicle only.

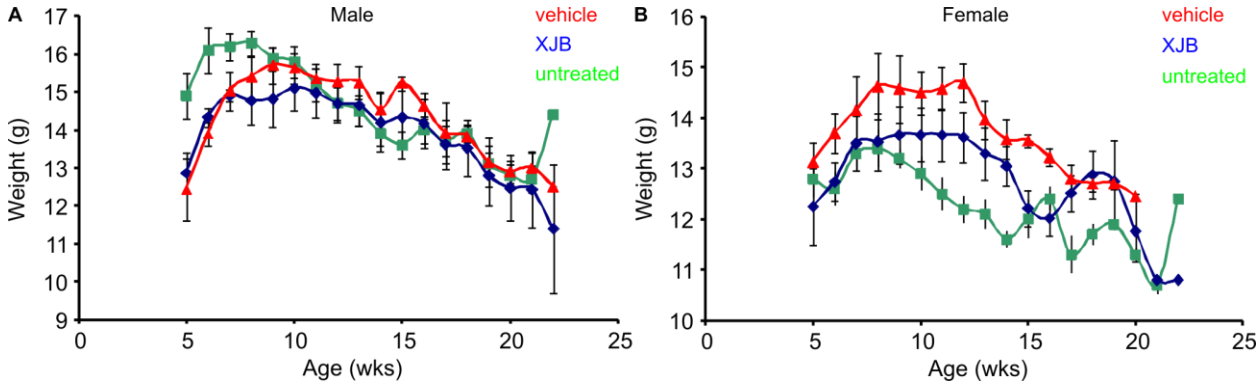

Figure 3.3: Weights of *Ercc1*$^{-/\Delta}$ mice

Weights in grams of untreated (green), vehicle- (red), and XJB-treated (blue) *Ercc1*$^{-/\Delta}$ mice starting at five weeks of age, when treatment began, and lasting until 22 weeks of age, when the last mice were sacrificed.

Table 3.1: XJB delays the onset of age-related degeneration

	Age at onset (wk)			
Symptom	***Ercc1*$^{-/\Delta}$ + Vehicle**	**n^{A}**	***Ercc1*$^{-/\Delta}$ + XJB**	**n^{B}**
Dystonia^{C}	7.4	8	8.6	10
Trembling	7.7	8	8.9	10
Kyphosis^{C}	11.7	8	13.2	10
Ataxia^{C}	14.5	8	16.3	10
Hind-limb wasting^{C}	14.0	8	16.0	10
Priapism	17.6	2	17.0	1
Lethargy^{C}	17.5	5	20.9	5
Urinary incontinence	12.4	2	N/A	0
Delayed Symptoms^{C}	**10%**	8	**66%**	8

^{A}*Ercc1*$^{-/\Delta}$ + Vehicle: n = 8; 5 males, 3 females;
^{B}*Ercc1*$^{-/\Delta}$ + XJB: n = 10; 6 males, 4 females;
^{C}Symptoms that are significantly delayed after treatment with XJB; $p \leq 0.05$, one-tailed Student's *t*-test.

3.2.3 XJB delays the onset of multiple age-related degenerative symptoms

The mice in both treatment groups were euthanized at 20 weeks of age in order to compare histopathology between them. At this age, the livers of *Ercc1*$^{-/\Delta}$ mice display significant levels of necrosis, apoptosis and ballooning degeneration of hepatocytes (Ding *et al.*, 2010; Lackner *et al.*, 2008). Both necrosis and ballooning degeneration were reduced in the liver of *Ercc1*$^{-/\Delta}$ mice treated with XJB compared to those treated with vehicle only (Figure 3.4A).

Apoptosis and hyaline cast formation occurs in the renal tubules as a result of advanced age (Gregg *et al.*, 2012a; Silva, 2005). In the kidneys of *Ercc1*$^{-/\Delta}$ mice, by 20 weeks of age, there was evidence of extensive loss of renal tubule epithelial cells and hyaline casts (Figure 3.4B). In mice chronically treated with XJB, tissue architecture was preserved and casts were reduced (Figure 3.4B).

The brains of XJB-treated mice were stained with an antibody against glial fibrillary acidic protein (GFAP), a marker of neurodegeneration (Qin and Crews, 2012). GFAP staining in the cerebellum of *Ercc1*$^{-/\Delta}$ mice was greatly reduced in XJB-treated animals compared to those that received vehicle only (Figure 3.4C). This data is consistent with the delay of neurodegenerative symptoms, ataxia and dystonia, in animals treated with XJB (Table 3.1).

XJB treatment also delayed the loss of pancreatic islets in *Ercc1*$^{-/\Delta}$ mice (Figure 3.4D). Furthermore, microcomputed tomography of the spine revealed that osteoporotic changes were reduced in *Ercc1*$^{-/\Delta}$ mice treated with XJB versus vehicle only (Figure 3.4E). This correlated with a significant increase in the thickness of the trabecular bone (Figure 3.5) and a significant delay in onset of kyphosis (Table 3.1).

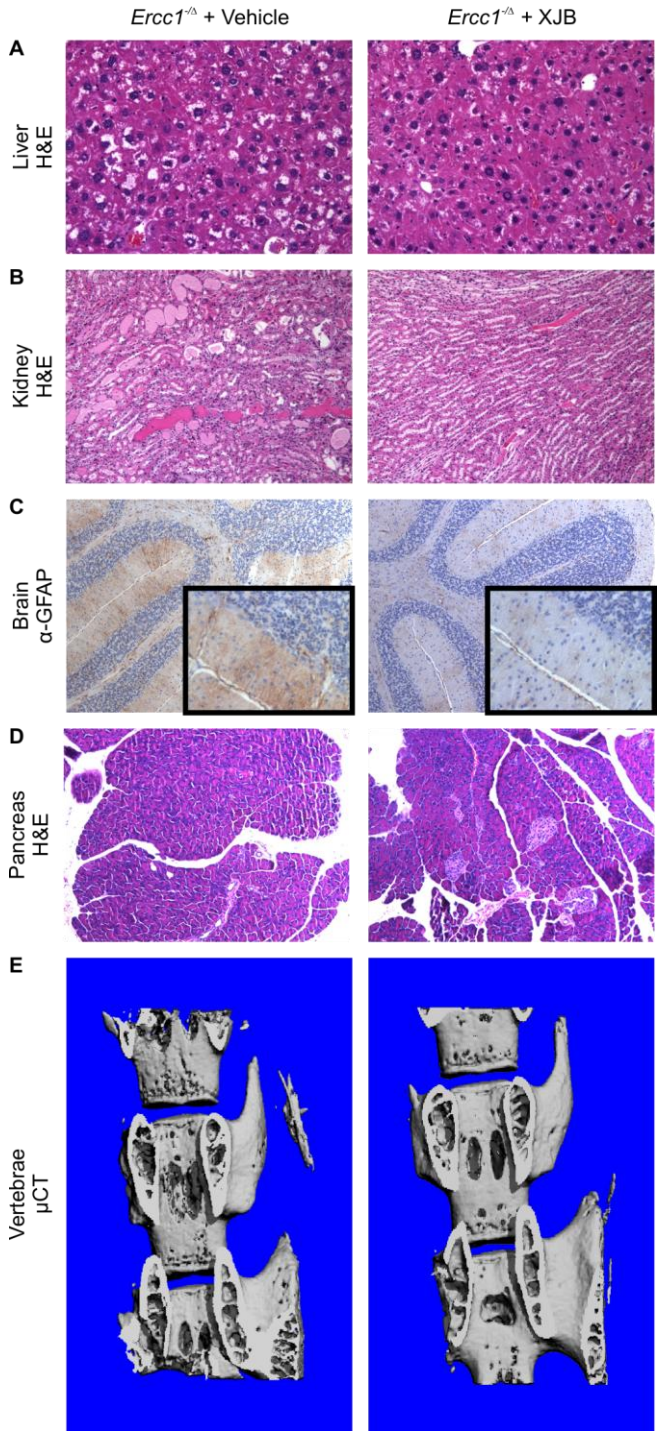

Figure 3.4: Delay in onset of age-related degenerative diseases in *Ercc1*$^{-/\Delta}$ tissues after treatment with XJB

(**A**) Liver and (**B**) kidney sections from vehicle- or XJB-treated *Ercc1*$^{-/\Delta}$ mice were stained with H&E to visualize histopathologic changes. (**C**) An antibody against glial fibrillary acidic protein (GFAP, brown) was used to visualize neurodegeneration in the cerebellum of vehicle- or XJB-treated *Ercc1*$^{-/\Delta}$ mice. Nuclei were counter-stained with hematoxylin. (**D**) H&E stained pancreas sections to visualize beta-islet cells. (**E**) µCT analysis of vertebrae from *Ercc1*$^{-/\Delta}$ mice treated with vehicle or XJB to detect osteoporotic pore formation.

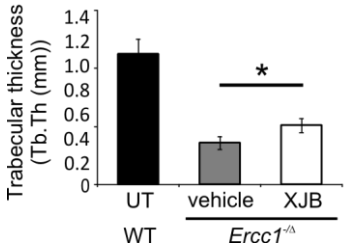

Figure 3.5: Osteoporotic changes in *Ercc1*$^{-/\Delta}$ mice

Trabecular thickness of the vertebrae of *Ercc1*$^{-/\Delta}$ mice treated with either vehicle or XJB. '*', $p = 0.04$, one-tailed Student's *t*-test. The values represent the mean ± standard error of the mean obtained from three mice per group.

3.2.4 XJB reduces oxidative DNA damage

Accelerated aging in DNA repair-deficient *Ercc1*$^{-/\Delta}$ mice presumably arises as a consequence of failure to repair DNA damage (Wang *et al.*, 2012). Accordingly, oxidative DNA damage should be reduced in XJB-treated mice with delayed aging phenotypes. To test this hypothesis, we measured cyclopurine adducts, which are spontaneous, endogenous oxidative lesions normally repaired by nucleotide excision repair (Brooks *et al.*, 2000; Romieu *et al.*, 1999). Cyclopurines are formed when a hydroxyl radical attacks guanine or adenine residues. XJB-5-131 scavenges hydroxyl radicals (Brooks, 2007; Charloux *et al.*, 1995). Both diastereomers of cyclodeoxyadenine (cdA) and cyclodeoxyguanine (cdG) were measured in nuclear DNA isolated from livers of *Ercc1*$^{-/\Delta}$ mice chronically treated with XJB or vehicle only. The level of all four oxidative lesions ranged on the order of 1-2 per 10^6 nucleosides in liver of mice treated with the vehicle only (Figure 3.6). The level of all four cyclopurine adducts was significantly lower (at least 3-fold) in mice treated with XJB. This demonstrates a strong correlation between DNA damage levels and the onset of aging-related degenerative changes. It also demonstrates that a mitochondrial-targeted radical scavenger can significantly reduce oxidative DNA damage in the nucleus.

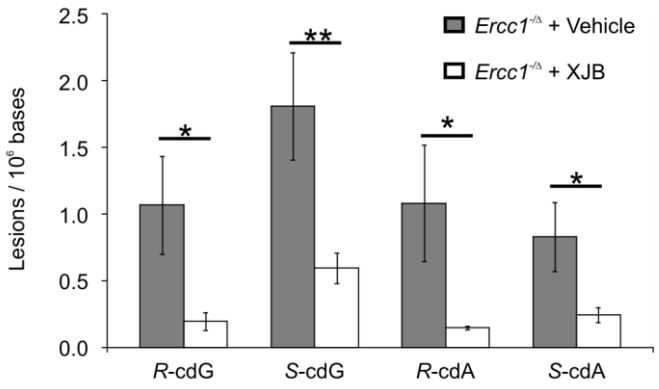

Figure 3.6: Amelioration of oxidative DNA damage in the liver of ERCC1-deficient mice treated with XJB

The levels of the (5′*R*)- and (5′*S*)-diastereomers of 8,5′-cyclo-2′-deoxyguanosine (cdG) and 8,5′-cyclo-2′deoxyadenosine (cdA) in nuclear DNA isolated from the livers of 20 week-old vehicle- and XJB-treated *Ercc1*$^{-/\Delta}$ mice. '*', $p < 0.05$; '**', $p < 0.01$. The *p*-values were calculated using two-tailed Student's *t*-test. The values represent the mean ± standard error of results obtained from DNA of three mice per group.

3.2.5 XJB attenuates cellular senescence and apoptosis

Loss of functional cells either through senescence or apoptosis promotes aging (Baker *et al.*, 2011). Therefore, we next asked if XJB attenuates cellular senescence and/or apoptosis in tissues where histopathology was improved (Figure 3.4). Senescence-associated β-galactosidase activity, a marker of cell senescence, was dramatically reduced in the liver of *Ercc1*$^{-/\Delta}$ mice chronically treated with XJB, compared to littermate mutant mice that received vehicle only (Figure 3.7A). Liver, kidney and cerebellar sections were also stained with an antibody that recognizes cleaved caspase-3 to measure apoptosis (Figure 3.7B-D). In the liver, no apoptotic signal was detected in any animals (Figure 3.7B). In the kidney, there was intense staining of the collecting ducts in the inner medulla / pyramid area indicative of apoptotic cells in *Ercc1*$^{-/\Delta}$ mice treated with vehicle only (Figure 3.7C). This pathology was significantly attenuated in mice treated with XJB. Numerous apoptotic cells were also observed scattered throughout the

cerebellum of *Ercc1*$^{-/\Delta}$ mice treated with vehicle only (Figure 3.7D). Fewer apoptotic cells were detected in the cerebellum of *Ercc1*$^{-/\Delta}$ mice treated with XJB.

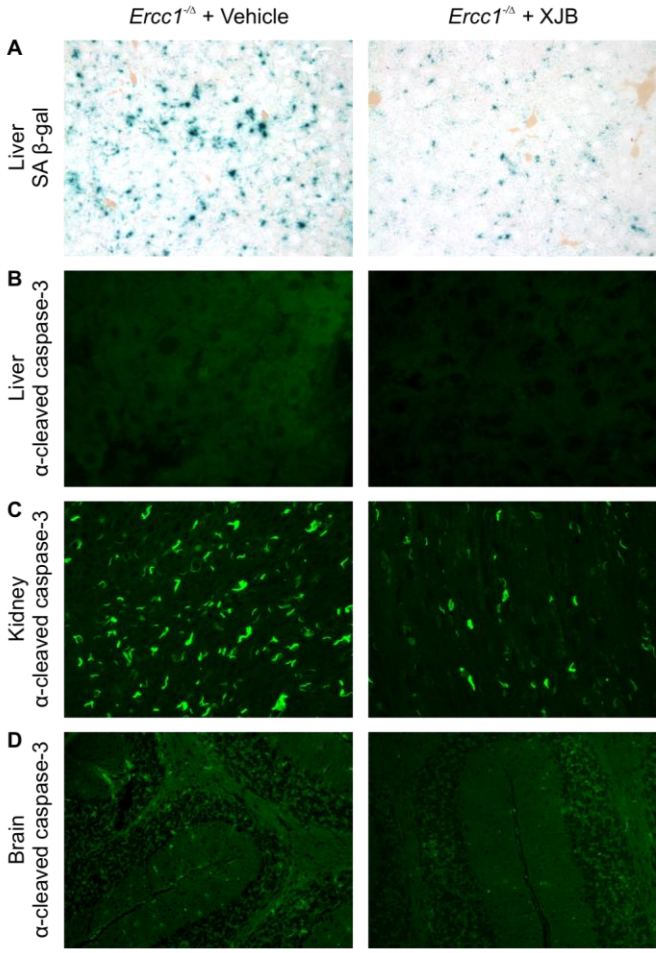

Figure 3.7: Delayed loss of functional tissue in *Ercc1*$^{-/\Delta}$ mice after treatment with XJB

(A) Senescence-associated β-galactosidase (SA β-gal) staining of fixed-frozen liver sections from vehicle- or XJB-treated *Ercc1*$^{-/\Delta}$ mice. Immunofluorescence detection of α-cleaved caspase-3 in (B) liver, (C) kidney and (D) cerebellum of *Ercc1*$^{-/\Delta}$ mice treated with vehicle or XJB.

3.3 DISCUSSION

In the mid 1950's, Harman proposed the free radical theory of aging which posits that much of the "spontaneous" or endogenous damage that drives aging is a direct consequence of highly reactive free radicals generated during normal metabolism (Harman, 1956, 1992a, b). This was modified to include mitochondria when it was realized that these organelles are the major source of free radicals and ROS in most cells (Chance *et al.*, 1979). Thus, decline of mitochondrial function, and a subsequent increase in ROS, is envisioned to be a chief contributor of oxidative stress associated with a broad spectrum of diseases associated with aging (Van Houten *et al.*, 2006). If mitochondrial dysfunction and ROS production is important for aging, then it might be expected that increasing or decreasing mitochondrial oxidant defenses should affect the healthspan and/or lifespan of an organism (Harper, 2008). Despite clear evidence that disrupting the vicious cycle of mitochondrial dysfunction and increased ROS production in lower organisms extends healthspan and lifespan (Muller *et al.*, 2007), the evidence for a similar effect in mammals remains equivocal (Jang and Remmen, 2009; Salmon *et al.*, 2010).

To test the free radical theory of aging, we chronically treated *Ercc1*$^{-/\Delta}$ mice with a mitochondrial-targeted radical scavenger XJB-5-131. *Ercc1*$^{-/\Delta}$ mice are defective in nucleotide excision repair and interstrand crosslink repair (de Waard *et al.*, 2010; Niedernhofer *et al.*, 2006; Niedernhofer *et al.*, 2004), both of which are implicated in protecting against DNA damage induced by oxidative stress (Niedernhofer *et al.*, 2003; Wang, 2008). Chronic XJB treatment led to significant reduction in the levels of cyclopurine adducts, DNA lesions caused by ROS, in the nuclear genome (Figure 3.6). These data support previous evidence that mitochondrial ROS promotes nuclear DNA damage (Van Remmen *et al.*, 2003). The data also reveal a method by which to attenuate oxidative DNA damage in the nucleus. This is important because the

cyclopurine adducts measured were recently shown to accumulate in the liver, kidney and brain of wild-type mice as they age (Wang *et al.*, 2012). These lesions may contribute to aging or be a biomarker of it as *Ercc1*$^{-/\Delta}$ mice, which age rapidly, compared to wild-type littermates (Wang *et al.*, 2012).

Chronic treatment of *Ercc1*$^{-/\Delta}$ mice with XJB also reduced degenerative changes in the liver and kidney parenchyma (Figure 3.7). It also delayed the loss of insulin-producing cells in the pancreas, as well as histopathologic signs of neurodegeneration and osteoporosis. This was accompanied by a significant delay in the majority of progeroid symptoms in mice treated with XJB compared to mutant sibling animals treated with vehicle only (Table 3.1). This includes kyphosis (hunched posture), ataxia (unsteady gait), proximal muscle wasting, and reduced spontaneous activity. These changes are all characteristic of old age in humans as well (de Waard *et al.*, 2010; Ding *et al.*, 2010; Gregg *et al.*, 2012a; Lackner *et al.*, 2008; Silva, 2005). The fact that XJB treatment led to improvement in multiple tissues, delayed the onset of several aging-related chronic degenerative diseases and improved organism function strongly argues that XJB delays aging *per se* in *Ercc1*$^{-/\Delta}$ mice. The data therefore provide novel evidence to support the free radical theory of aging and the concept that mitochondrial ROS promote aging.

Numerous studies have examined the effect of other anti-oxidants for treating aging-related diseases. Vitamin C is marketed as an oral and topical antioxidant. It was tested in several clinical trials for its ability to prevent cardiovascular disease, yielding no clear positive results (Wojcik *et al.*, 2010). Importantly, Vitamin C, can also act as a pro-oxidant that promotes oxidative DNA damage (Podmore *et al.*, 1998). Vitamin E appears to be efficacious in Alzheimer's disease and for reducing risk of atherosclerosis, but only in a subset of patients at high risk (Behl, 1999; Robinson *et al.*, 2006). However, meta-analyses of multiple clinical trials

reveal that both vitamins C and E can increase risk of mortality (Miller *et al.*, 2005; Vivekananthan *et al.*, 2003). The lack of a clear beneficial effect may be due to the fact that in some tissues, cell types or subcellular domains these anti-oxidants become pro-oxidant. Alternatively, it may because without targeting them to sites of non-enzymatic production of deleterious ROS, ROS required for essential signaling pathways are also reduced (Bae *et al.*, 2011). XJB-5-131 bypasses both of these potential problems.

Coenzyme Q and vitamin E have both been targeted to the mitochondria by use of mitochrondrial membrane potential, i.e., MitoQ (mitochondrial-targeted coenzyme Q) and MitoVitE (mitochondrial-targeted vitamin E). When applied to mitochondria, MitoVitE decreases lipid peroxidation and protein damage (Smith *et al.*, 1999), while MitoQ decreases lipid peroxidation and apoptosis when used to treat cells (Kelso *et al.*, 2001). In a rodent model of Parkinson's disease, MitoQ preserved motor function, but in clinical trials it had no effect on disease progression yet caused nausea and vomiting (Snow *et al.*, 2010). MitoQ improved liver function in hepatitis C patients, suggesting it can attenuate tissue-specific inflammation (Gane *et al.*, 2010). This has led to additional clinical trials for a variety of human pathologies, currently underway (Smith *et al.*, 2011). Importantly, both MitoQ and MitoVitE are positively charged and can cause mitochondrial depolarization at high doses, which might cause poor long term tolerance (Kelso *et al.*, 2001; Smith *et al.*, 1999). In contrast, XJB is neutral.

TEMPOL, the reactive portion of XJB, attenuates damage in a number of aging-related pathologies in rodent models including hypertension, ischemia, neurodegeneration and chronic inflammation (Wilcox, 2010). In addition, chronic treatment with TEMPOL significantly extends the lifespan of *Drosophila* and mice (Wilcox, 2010). However, weight loss has been found as a consequence of long-term TEMPOL administration (Soule *et al.*, 2007). Additionally, its use in

rats induced systemic hypotension (Rashid *et al.*, 2011). Therefore, clinical trials of TEMPOL have been limited to topical application to treat alopecia associated with radiotherapy for brain cancer (Metz *et al.*, 2004). We observed no side-effects as a consequence of chronic treatment with XJB, supported by the fact that the weight of mice treated with XJB, is identical to that of mice given vehicle only (Figure 3.3).

What may set XJB apart from previous anti-oxidants directed to the mitochondria is that it is targeted by a neutral gramicidin S analog, while other mitochondrial-targeted compounds rely on plasma membrane potential to drive uptake (Smith *et al.*, 1999). Therefore, XJB has the unique ability to target damaged mitochondria, which have lost membrane potential and have the greatest likelihood of producing excess ROS. In addition, the nitroxide radical moiety of XJB can oscillate between different redox states and adapt itself to the local environment during the process of reducing oxidative stress (Fink *et al.*, 2007). Finally, XJB recycles and therefore, can remain active while at the mitochondrial membrane (Figure 3.1), which is advantageous over stoichiometric anti-oxidants. Based on our results, XJB represents a lead agent in a novel class of anti-oxidants with apparent efficacy for delaying symptoms and pathologies associated with neurodegeneration, progeroid syndromes, and potentially the aging in the general population.

3.4 METHODS

3.4.1 XJB-5-131 and BODIPY-FL-XJB-5-131

XJB-5-131 was synthesized as described previously (Wipf *et al.*, 2005). BODIPY-FL-XJB-5-131 was prepared in an analogous fashion and purified by chromatography on SiO_2 (ISCO, 4 g column, liquid load in CH_2Cl_2, MeOH/CH_2Cl_2 gradient) to give an impure, red oil. The material was then purified a second time by chromatography on SiO_2 (ISCO, 4 g column, liquid load in CH_2Cl_2, MeOH/CH_2Cl_2 gradient) to give BODIPY-FL-XJB-5-131 as a reddish orange oil: R_f 0.57 (10% MeOH/CH_2Cl_2); HRMS (ESI) *m/z* calcd for $C_{62}H_{86}BN_9O_8F_2$ (M+H) 1133.6660, found 1133.6678.

3.4.2 Mice

Ercc1$^{-/\Delta}$ mice were generated by breeding *Ercc1*$^{+/-}$ and *Ercc1*$^{+/\Delta}$ mice in inbred C57Bl/6J and FVB/n backgrounds, respectively, to create a cohort of mice that were in an f1 hybrid background and genetically identical. The mice were genotyped by PCR as previously described (Ahmad *et al.*, 2008). All experiments were reviewed and approved by the University of Pittsburgh (Pittsburgh, PA) Institutional Animal Care and Use Committee and in accordance with the National Institutes of Health guidelines for the humane care of animals.

3.4.3 Live cell imaging of XJB-treated cells

Ercc1$^{-/-}$ mouse embryonic fibroblasts were grown on MatTek glass bottom culture dishes and allowed to adhere overnight. At 60% confluence, MitoTracker® was added to the media to label mitochondria, as well as 500 μM BODIPY-FL-XJB-5-131, and images of the cells were captured every 3 min for 3 h at 40X magnification using a Nikon Eclipse Ti microscope equipped with a Photometrics CoolSnap HQ2 camera.

3.4.4 XJB treatment of mice

The *Ercc1*$^{-/\Delta}$ mice were given intraperitoneal injections of 2 mg/kg XJB dissolved in sunflower oil (S5007 Sigma-Aldrich, St. Louis, MO) or an equivolume of vehicle only (sunflower oil) three times per week, beginning at five weeks of age, by an investigator blinded to the treatment group. Whenever possible, littermate pairs of *Ercc1*$^{-/\Delta}$ mice were used, with one mouse in each treatment group, to minimize variability. The mice were weighed twice a week and monitored for the onset of age-related symptoms, including dystonia, trembling, ataxia, priapism and urinary incontinence (neurodegenerative symptoms), hind-limb muscle wasting, lethargy (reduced spontaneous activity) and kyphosis (hunched posture). Data only from littermate pairs were evaluated to determine the fraction of symptoms delayed in the mouse treated with XJB vs. its sibling treated with vehicle only using a paired Student's *t*-test. All mice were euthanized at 20 weeks of age and their tissues were isolated for pathological analysis.

3.4.5 Immunofluorescence

Tissues were fixed in 10% formalin for 2 h, cryoprotected in 30% sucrose overnight, frozen using chilled 2-methylbutane, and sectioned by standard procedures using a cryostat. Cleaved caspase-3 (9664 Cell Signaling Technology, Beverly, MA) was used at a dilution of 1:250 with a 4°C overnight incubation. SA β-gal staining was done overnight at 37°C as previously described (Dimri *et al.*, 1995) with one modification, the final solution was pH 5.8 for murine samples.

3.4.6 Immunohistochemistry

Tissues were fixed in 10% formalin overnight, embedded in paraffin and sectioned using a microtome by standard procedures. They were then deparaffinized using xylenes, rehydrated in ethanol baths and stained. Tissues were stained with H&E by standard procedure. Anti-GFAP (13-0300 Invitrogen, Carlsbad, CA) was used a dilution of 1:250 with a 4°C overnight incubation.

3.4.7 Micro-computed tomography

Imaging of spines isolated from *Ercc1*$^{-/\Delta}$ mice treated with XJB or vehicle only were acquired using a VivaCT 40 (Scanco Medical) with 15 μm isotropic voxel size resolution, 55 kVp of energy and 145 μA of current. After the acquisition of transverse two-dimensional image slices, three-dimensional reconstruction of the lumbar vertebrae was performed using a constant threshold value of 235, which was selected manually for the bone voxels by visually matching the threshold areas to the gray-scale images.

3.4.8 Measurement of 8,5′-cyclopurine-2′-deoxynucleosides in nuclear DNA of mouse livers

Nuclear DNA was isolated from mouse livers using a high-salt method (Miller *et al.*, 1988a) and analyzed for DNA damage as described previously (Wang *et al.*, 2011b). In brief, nuclear DNA was digested using a four-enzyme cocktail, and to the digestion mixture was added uniformly ^{15}N-labeled cdA and cdG. The resulting nucleoside mixture was subjected to off-line high performance liquid chromatography (HPLC) separation for the enrichment of the lesions under study, following previously described procedures (Wang *et al.*, 2011b). The LC-MS/MS/MS experiments were conducted using an LTQ linear ion trap mass spectrometer using recently described conditions (Wang *et al.*, 2011b).

4.0 EXOGENOUS AND ENDOGENOUS SOURCES OF LIPID PEROXIDATION PROMOTE AGING

Andria Rasile Robinson[1,2], Lora H. Rigatti[3], Hillary L. Shane[2], and Laura J. Niedernhofer[2,4]

[1]Department of Human Genetics, University of Pittsburgh Graduate School of Public Health, 130 DeSoto Street, Pittsburgh, PA 15261, USA.

[2]University of Pittsburgh Cancer Institute, 5117 Center Avenue, Hillman Cancer Center 2.6, Pittsburgh, PA 15213, USA.

[3]Department of Pathology, University of Pittsburgh School of Medicine, S417 Biomedical Science Tower, 200 Lothrop Street, Pittsburgh, PA 15261, USA.

[4]Department of Microbiology and Molecular Genetics, University of Pittsburgh School of Medicine, 523 Bridgeside Point II, 450 Technology Drive, Pittsburgh, PA 15219, USA.

4.1 INTRODUCTION

The free radical theory of aging, first proposed by Denham Harman in 1956, states that aging and age-related disease are associated with the attack of free radicals on cellular components (Harman, 1956). Free radicals damage cell membranes by modification of the lipids in the phospholipid bilayer. Polyunsaturated fatty acids (PUFAs) are particularly vulnerable to hydrogen abstraction by free radicals because the methylene hydrogens at double bonds are highly reactive. The product of this abstraction is a carbon-based radical, which rapidly reacts with molecular oxygen to produce a lipid peroxyl radical. This can react with a second neighboring fatty acid in a chain reaction to produce one lipid hydroperoxide and a second lipid peroxy radical. Alternatively, an epoxide can form via intramolecular reaction of the peroxide with another methylene carbon. This can lead to scission and the release of products such as malondialdehyde and α-β-unsaturated aldehydes. These products are more stable than free radicals, yet still reactive. These lipid peroxidation-derived hydroperoxides and aldehydes react with DNA to produce a variety of DNA lesions, including DNA interstrand crosslinks (Buege and Aust, 1978; Niedernhofer *et al.*, 2003; Stone *et al.*, 2008). Therefore free radical damage to membrane lipids can be particularly damaging because the affect membranes, the nuclear and mitochondrial genomes, and can act at long distances via stable products.

Lipid peroxyl radicals have been proposed to play a role in the aging process (Rikans and Hornbrook, 1997). Indeed the levels of lipid hydroperoxides are 2-fold greater in liver and kidney from old wild-type mice compared to young (Tokumaru *et al.*, 1996). Furthermore, lipid peroxidation is a major source of lipofuscin (Yin, 1996), an aging-related pigment consisting of oxidized cellular debris that collects in cells. Finally, defects in the repair of DNA interstrand crosslinks leads to dramatically accelerated aging in humans and mice (Niedernhofer *et al.*,

2006). This must arise from endogenous processes and has been attributed to DNA interstrand crosslinks caused by lipid peroxidation (Niedernhofer *et al.*, 2006; Weeda *et al.*, 1997a). This study was designed to directly test the hypothesis that lipid peroxidation promotes aging.

To test this, we challenged mice with two common environmental exposures that promote lipid peroxidation *in vivo*. The first is carbon tetrachloride (CCl_4). CCl_4 is a chemical solvent historically used in the production of refrigerants and building materials, in aerosol propellants (i.e., fire extinguishers), in the dry cleaning industry, and in cleaning fluids, as well as for the oral treatment of hookworm (Faroon *et al.*, 2005; Pooranaperundevi *et al.*, 2010). Use of CCl_4 diminished dramatically since 1990 as a result of toxicology studies indicating that CCl_4 is a carcinogen in rodents (2001a). However, CCl_4 is used in building materials and cleaning supplies. Therefore, the primary source of exposure to CCl_4 is inhalation during its manufacture and use (Faroon *et al.*, 2005). High exposures to CCl_4 can result in hepatic toxicitiy (1992; Kadiiska *et al.*, 2000). This is because the liver is the primary target as a result of the metabolism that occurs there. Cytochrome P450 is required to reduce CCl_4 to the trichloromethyl free radical, which in the presence of oxygen is converted into a peroxy radical (Kadiiska *et al.*, 2000). Both of these radicals are capable of oxidizing lipids. Exposure is not limited to manufacturing. White-collar workers can be exposed to fumes from cleaning products used in the workplace (Faroon *et al.*, 2005). Furthermore CCl_4 is in our water supply at a background level of approximately 1 μg/liter in the United States (Fawell and Mascarenhas, 2004).

Another environmental exposure that promotes lipid peroxidation is dietary PUFAs. Cell membranes are made up of a mixture of saturated and unsaturated lipids acquired largely from the diet. PUFAs, harboring conjugated double bonds, are particularly prone to lipid peroxidation (Buege and Aust, 1978). A diet rich in PUFAs can promote endogenous lipid peroxidation

(Jump, 2002). Dietary PUFAs include linoleic, α-linolenic, arachidonic, eicosapentaenoic, docosahexaenoic and n-3 docosapentaenoic acids (2011b; Astorg *et al.*, 2004). Major dietary sources of PUFAs include vegetable oils (i.e. poppyseed, safflower, sunflower and corn oils), nuts and animal fats (2011b; Astorg *et al.*, 2004). Therefore, by feeding mice a diet enriched with PUFAs derived from safflower oil, it is possible to increase endogenous LPO.

To increase the sensitivity of our *in vivo* studies, we used *Ercc1*$^{-/\Delta}$ mice, which have reduced expression of ERCC1-XPF DNA repair endonuclease (Weeda *et al.*, 1997a). ERCC1-XPF is required for interstrand crosslink repair, as well as other DNA repair mechanisms (Ahmad *et al.*, 2008; Bhagwat *et al.*, 2009; Niedernhofer *et al.*, 2004; Sijbers *et al.*, 1996a). As a consequence the mice show premature aging of the hepatobiliary, renal, neurological, hematopoietic, musculoskeletal, epidermal and endocrine systems (de Waard *et al.*, 2010; Goss *et al.*, 2011; Gregg *et al.*, 2012a; Niedernhofer *et al.*, 2006; Vo *et al.*, 2010). These mice model a human progeroid syndrome caused by a mutation in XPF, affecting expression of ERCC1-XPF (Niedernhofer *et al.*, 2006), demonstrating the relevance of this model to human health. Chronic exposure of *Ercc1*$^{-/\Delta}$ mice with either a sub-lethal dose (Faroon *et al.*, 2005) of CCl_4 or a diet enriched for PUFAs promoted LPO, accelerated the onset aging-related pathologies and reduced lifespan. These data support the conclusion that LPO can promote aging and does so, at least in part, by inducing DNA damage.

4.2 RESULTS

4.2.1 Chronic exposure to CCl_4 causes LPO and reduced lifespan in *Ercc1*$^{-/\Delta}$ mice

Ercc1$^{-/\Delta}$ mice, which are defective in nucleotide excision repair of helix-distorting monoadducts and the repair of interstrand crosslinks, and their wild-type (WT) littermates were chronically exposed to CCl_4 (80 mg/kg) biweekly via subcutaneous injection for five weeks, which is a cumulative dose of 800 mg/kg (Figure 4.1A). *Xpa*$^{-/-}$ mice, which are defective only in nucleotide excision repair, were also exposed to the same regiment in order to facilitate identifying the impact of LPO-induced DNA interstrand crosslinks. The mice were monitored three times a week and sacrificed when the *Ercc1*$^{-/\Delta}$ mice were considered end-stage (reduced spontaneous activity). CCl_4 treatment of the ERCC1-deficient mice resulted in a decreased median lifespan compared to untreated *Ercc1*$^{-/\Delta}$ mice ($p = 0.08$, one-tailed Student's *t*-test; Figure 4.1B). The same dose had no detrimental effects on WT or *Xpa*$^{-/-}$ mice, with the single *Xpa*$^{-/-}$ death being unrelated to the treatment. The lifespan data support the hypothesis that unrepaired LPO-induced ICLs have a negative health impact.

To determine if CCl_4 was inducing LPO, lipid hydroperoxides (LOOH) were measured in liver samples from untreated 20 week-old *Ercc1*$^{-/\Delta}$ and WT mice (n = 3 per group) using an LOOH assay (Gregg *et al.*, 2012a). Surprisingly, untreated mutant animals had a 7-fold increase in LPO compared to their WT littermates (Figure 4.1C; $p < 0.01$, one-tailed Student's *t*-test). Upon analysis of liver samples from 19-23 week old *Ercc1*$^{-/\Delta}$ and WT mice 4-8 weeks after treatment with CCl_4 ended (n = 3 per group), there was a significant increase in the mutant LOOH levels compared to their WT littermates ($p < 0.05$, one-tailed Student's *t*-test). Treatment

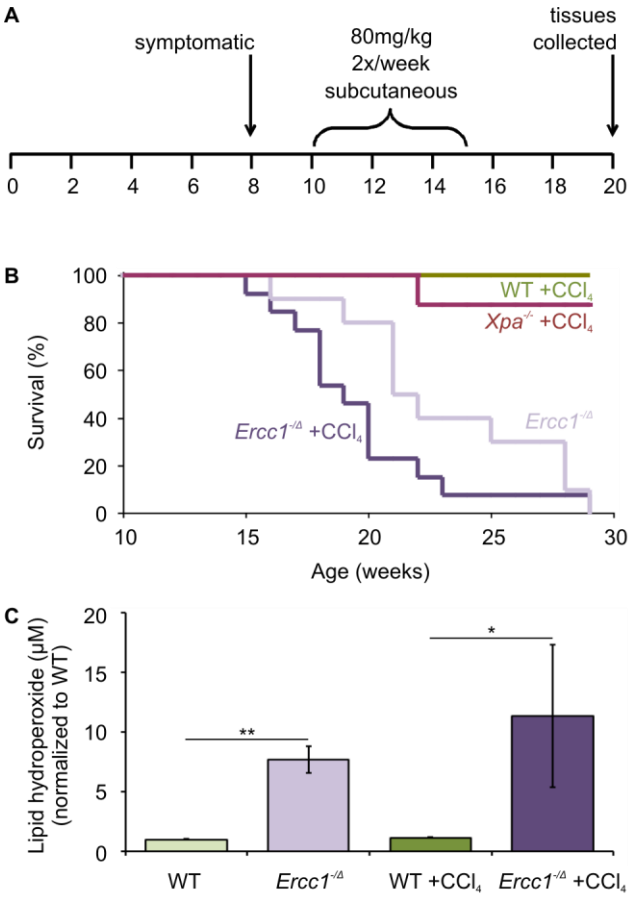

Figure 4.1: Chronic exposure to CCl_4 promotes lipid peroxidation and decreases lifespan of *Ercc1*$^{-/\Delta}$ mice

(**A**) CCl_4 was administered to WT, *Xpa*$^{-/-}$ and *Ercc1*$^{-/\Delta}$ mice by subcutaneous injection of 80mg/kg, twice a week for five weeks, beginning at 10 weeks of age. (**B**) Survival curve of the mice after treatment with CCl_4. Graphed are wild-type (WT) mice + CCl_4 (n=12; green), *Xpa*$^{-/-}$ mice + CCl_4 (n=8; red), untreated *Ercc1*$^{-/\Delta}$ mice (n=10; light purple), and *Ercc1*$^{-/\Delta}$ mice + CCl_4 (n=13; dark purple). (**C**) Lipid hydroperoxides (LOOH) measured by ELISA assay in liver tissue isolated from untreated WT (light green), untreated *Ercc1*$^{-/\Delta}$ (light purple), CCl_4-treated WT (dark green) and CCl_4-treated *Ercc1*$^{-/\Delta}$ mice (dark purple). Values indicate the mean for 3 mice per group ± S.E.M. '*', $p < 0.05$; '**' $p < 0.01$, one-tailed Student's *t*-test.

of *Ercc1*$^{-/\Delta}$ mice with CCl_4 conveyed a 1.5-fold induction in LOOH compared to untreated *Ercc1*$^{-/\Delta}$ mice (Figure 4.1C). There was no significant increase in LPO in WT mice with this dose of CCl_4.

4.2.2 CCl_4 accelerates the onset of age-related histopathologic changes

To determine to what extent CCl_4-induced lipid peroxidation affected the liver of WT and DNA repair-deficient mice, tissue sections were analyzed for histopathologic changes in a blinded fashion. Hepatocytes from WT mice treated with CCl_4 exhibited signs of increased nuclear size and focal necrosis, both changes associated with aging (Andrew, 1962; Chipchase *et al.*, 2003; Gregg *et al.*, 2012a). In addition, *Ercc1*$^{-/\Delta}$ liver samples contained hepatocytes that were extremely enlarged with dense eosinophilic cytoplasm (Figure 4.2A). There was significantly more hepatocellular necrosis and degeneration, but no inflammatory response in the ERCC1-deficient livers samples compared to CCl_4-treated WT mice. There were also foci of nodular regeneration evident in the *Ercc1*$^{-/\Delta}$ liver sections with frequent oval cell hyperplasia, often stemming from portal areas (Figure 4.2A).

The liver sections from WT and *Ercc1*$^{-/\Delta}$ littermate pairs treated with CCl_4 were stained with Masson's trichrome and periodic acid Schiff (PAS), to show fibrosis and glycogen deposition, respectively, which are both associated with advanced age (Gregg *et al.*, 2012a; Guarente and Kenyon, 2000; Guttman and Kohn, 1960; Jiang *et al.*, 2005; Lin *et al.*, 2001). Increased portal fibrosis was evident in the treated *Ercc1*$^{-/\Delta}$ mice compared to treated WT littermates by the dark blue staining with Masson's trichrome (Figure 4.2B). In addition, the CCl_4-treated *Ercc1*$^{-/\Delta}$ liver samples showed high levels of glycogen deposition (Figure 4.2C). These results indicate an increase in aging-related degeneration of the liver of mice treated with CCl_4.

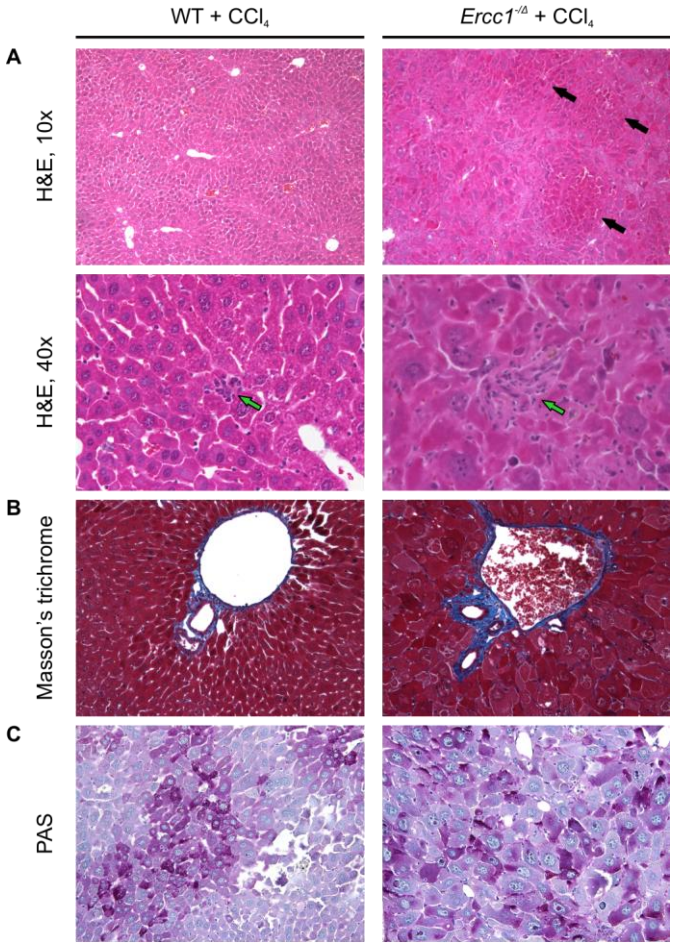

Figure 4.2: CCl_4 accelerates the onset of age-related histopathologic changes

(**A**) H&E stained liver sections from WT and *Ercc1*$^{-/\Delta}$ mice treated with CCl_4 (10x objective, top; 40x objective, bottom). Black arrows indicate areas of nodular regeneration, green arrows illustrates areas of necrosis. (**B**) Masson's trichrome stained liver sections from WT and *Ercc1*$^{-/\Delta}$ mice treated with CCl_4 (20x objective). Blue indicates areas of fibrosis. (**C**) Periodic acid Schiff (PAS) stained liver sections from WT and *Ercc1*$^{-/\Delta}$ mice (20x objective). The dark purple indicates areas of polysaccharide deposition.

4.2.3 Dietary PUFAs decrease lifespan of *Ercc1*$^{-/\Delta}$ mice

Mice were fed either a diet high in PUFAs (safflower oil) or an isocaloric, control diet, in which the PUFAs were replaced with saturated fats, starting at 21 days of age (at weaning) and continued throughout their entire lifespan. Mice were sacrificed when they were terminal, showing decreased spontaneous movement. Maximum lifespan was significantly reduced in PUFA-fed *Ercc1*$^{-/\Delta}$ mice compared to mice fed the control diet (Figure 4.3A & B; $p < 0.05$,

two-tailed Student's *t*-test). In addition, *Ercc1*$^{-/\Delta}$ mice that were fed the diet high in PUFAs exhibited increased aging-associated symptoms, including hind-limb muscle wasting, decreased grooming and increased osteoporotic changes (Figure 4.3C). Importantly, there was no difference in the weights of mice on the special diets compared to those fed normal mouse chow, indicating that the difference in lifespan could not be attributed to caloric restriction (Figure 4.4).

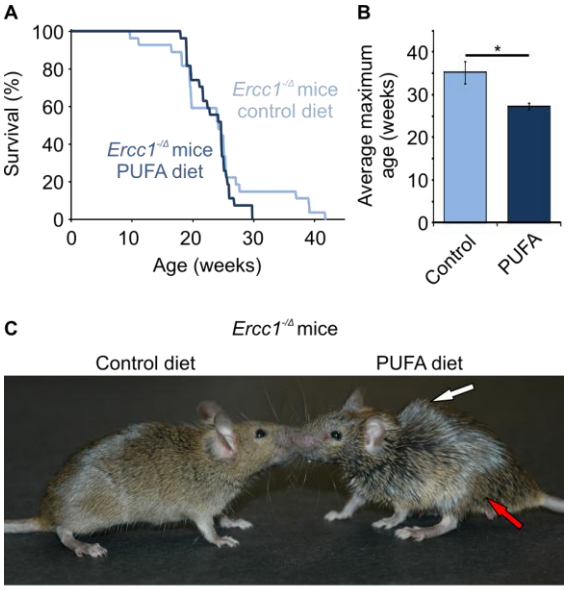

Figure 4.3: Dietary PUFAs decrease the lifespan of *Ercc1*$^{-/\Delta}$ mice

(**A**) The average maximum lifespan was calculated using the mean age of the oldest 20% of mice on each diet (Zhou *et al.*, 2012) (n = 6 per group; $p < 0.05$, two-tailed Student's *t*-test). (**B**) Photograph of control- or PUFA-fed *Ercc1*$^{-/\Delta}$ mice at 20 weeks of age. The white arrow illustrates kyphosis and the red arrow indicates hind-limb muscle wasting.

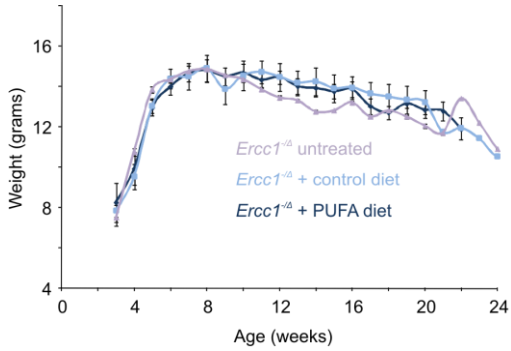

Figure 4.4: Weights of *Ercc1*$^{-/\Delta}$ mice

Weights in grams of untreated (light purple), control diet- (light blue), and PUFA diet-fed (dark blue) *Ercc1*$^{-/\Delta}$ mice starting at three weeks of age, when the mice were weaned onto the appropriate diet, until death

4.2.4 Dietary LPO promotes aging-related pathology in *Ercc1*$^{-/\Delta}$ mice

A veterinary pathologist, blinded to the treatment group, examined the tissue sections for histopathologic changes and scored the severity. Hematoxylin and eosin stained liver sections revealed portal fibrosis, necrosis and pyknotic nuclei in liver sections from *Ercc1*$^{-/\Delta}$ mice fed the PUFA diet compared to *Ercc1*$^{-/\Delta}$ mice fed the control diet (Figure 4.5A). Portal fibrosis was also evident by staining *Ercc1*$^{-/\Delta}$ livers with Masson's trichrome (Figure 4.5B). The severity of portal fibrosis was scored on average 30% higher (more severe) in ERCC1-deficient mice fed the diet high in PUFAs compared to mutant mice fed the control diet (Figure 4.5D). Additionally, *Ercc1*$^{-/\Delta}$ mice fed the diet high in PUFAs had an increase in the amount of PAS staining (glycogen storage) compared to *Ercc1*$^{-/\Delta}$ mice on the control diet (Figure 4.5C). The liver sections were also scored for portal fibrosis and hepatocellular abnormalities. Hepatocellular abnormalities were more severe in mutant mice fed the high PUFA diet compared to the control diet (Figure 4.5D). Taken together, these data indicate that dietary PUFA can promote aging-associate degenerative changes in the liver.

Kidneys from PUFA-fed *Ercc1*$^{-/\Delta}$ mice showed a loss of renal epithelial tubular cells and increased glomerulosclerosis compared to control-fed *Ercc1*$^{-/\Delta}$ mice (Figure 4.6A). However, Masson's trichrome stain of kidney cortex did not show differences in fibrosis between animals on the two diets (Figure 4.6B). In contrast PAS stain revealed an increase in extra-cellular matrix accumulation around the glomeruli in mutant mice fed the high PUFA diet (Figure 4.6C). When the kidney sections were scored for histopathology, there was an increase in both glomerular lesions and tubular abnormalities in the *Ercc1*$^{-/\Delta}$ mice fed a high PUFA diet compared to mice fed the control diet (Figure 4.6D). These data demonstrate that dietary PUFAs can promote aging-related degenerative changes in the kidney.

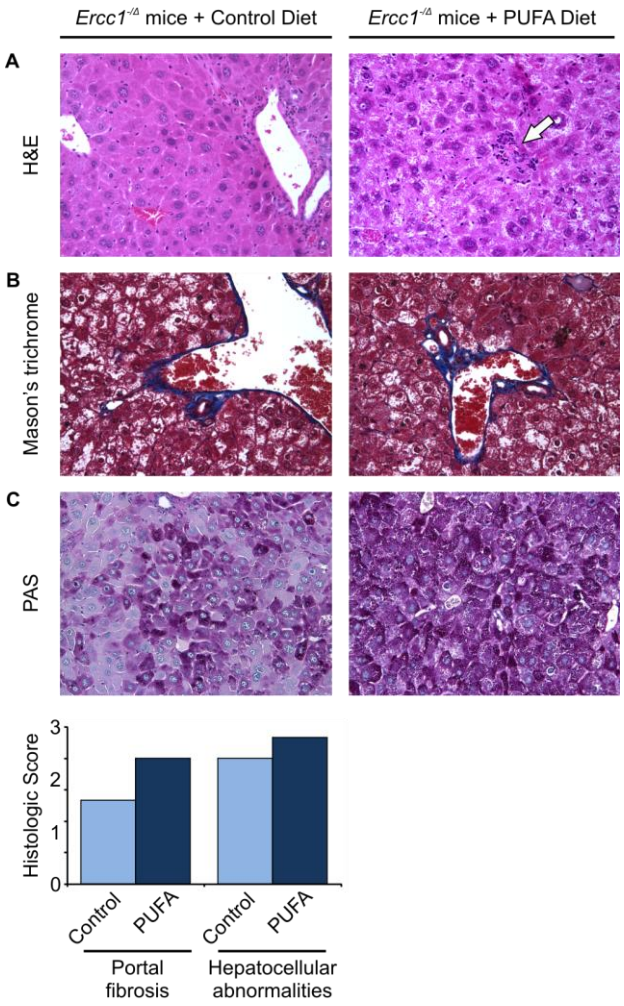

Figure 4.5: Dietary PUFAs accelerate the onset of aging-related histopathologic changes in the liver of *Ercc1*$^{-/\Delta}$ mice

(**A**) H&E stained liver sections from control- or PUFA-fed *Ercc1*$^{-/\Delta}$ mice (20x objective). White arrow illustrates necrosis. (**B**) Masson's trichrome stained liver sections from from control- or PUFA-fed *Ercc1*$^{-/\Delta}$ mice (20x objective). Blue indicates areas of fibrosis. (**C**) Periodic acid Schiff (PAS) stained liver sections from control- or PUFA-fed *Ercc1*$^{-/\Delta}$ mice (20x objective). Dark purple indicates areas of glycogen deposition. (**D**) Histogram indicating the average pathologic score assigned indicating the extent of portal fibrosis and hepatocellular changes in each group (n= 3 mice per group). The scores were assigned by a veterinary pathologist who was blinded as to the diet of the mice.

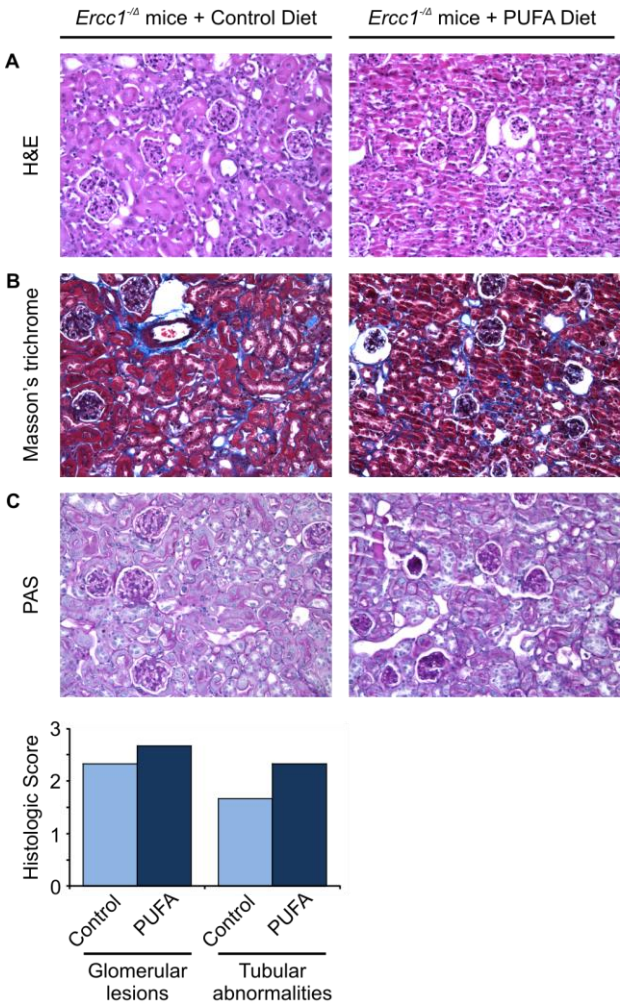

Figure 4.6: Dietary PUFAs accelerate the onset of aging-related histopathologic changes in the kidney of *Ercc1*$^{-/\Delta}$ mice

(**A**) H&E stained kidney sections from control- or high PUFA-fed *Ercc1*$^{-/\Delta}$ mice (20x objective). (**B**) Masson's trichrome stained kidney sections from control- or high PUFA-fed *Ercc1*$^{-/\Delta}$ mice (20x objective). (**C**) Periodic acid Schiff (PAS) stained kidney sections from control- or high PUFA-fed *Ercc1*$^{-/\Delta}$ mice (20x objective). (**D**) Histogram indicating the average pathologic score assigned indicating the extent of glomerulosclerosis and changes in the renal tubular epithelium for each group (n= 3 mice per group). The scores were assigned by a veterinary pathologist who was blinded as to the diet of the mice.

4.3 DISCUSSION AND FUTURE DIRECTIONS

Herein, we demonstrated that increased lipid peroxidation, whether through direct chemical induction or indirect dietary supplementation, can accelerate aging-associated histopathologies and affect the lifespan of mice. We used a cumulative dose of 800 mg/kg CCl_4, 10-fold lower than the lethal dose in mice (Faroon *et al.*, 2005), which resulted in extreme hepatotoxicity of *Ercc1*$^{-/\Delta}$ mice (Figure 4.2). Interestingly, the effects seen in the liver of WT animals treated with CCl_4, including increased nuclear size and focal necrosis (Figure 4.2A), have been shown to occur with normal age (Gregg *et al.*, 2012a; Ohtsubo and Nomaguchi, 1986), indicating that lipid peroxidation can promote aging-related changes in *Ercc1*$^{-/\Delta}$ and WT mice. Because CCl_4 can also lead to renal and neurological (purkinje cell damage) toxicitiy (1992), both the kidney and cerebellum from CCl_4-treated mice will also be evaluated for the effects of increased LPO in these tissues.

The Biomarkers of Oxidative Stress Studies (BOSS) have attempted to validate multiple non-invasive approaches to measure levels of oxidative stress in the plasma and urine of CCl_4-treated rats (Kadiiska *et al.*, 2000; Kadiiska *et al.*, 2005a; Kadiiska *et al.*, 2005b). The lipid hydroperoxide assay, one type of analysis evaluated in the BOSS project, represents a snapshot of LPO at one specific time point within a tissue (Kadiiska *et al.*, 2005a). This may account for the broad spectrum of measured lipid hydroperoxides in liver samples of *Ercc1*$^{-/\Delta}$ mice treated with CCl_4 (Figure 4.1C) as the samples were collected at end-of-life, which was, in itself, variable between treated mice. It would, therefore, be interesting in future studies to use more techniques (i.e. isoprostanes measured by immunoassay or GC-MS and malondialdehyde measured by GC-MS) developed in the BOSS projects to analyze LPO over time (Kadiiska *et al.*, 2005a). Additionally, using mass spectrometry analysis to identify types of DNA lesions

would also be beneficial to identifying whether LPO-induced DNA interstrand crosslinks are the lesions promoting age-related decline.

It is well-established that increased glycogen storage and lipofuscin deposition are biomarkers of aging in several organisms, including yeast, mouse, rat, and Chinese hamsters (Guarente and Kenyon, 2000; Guttman and Kohn, 1960; Jiang *et al.*, 2005; Lin *et al.*, 2001). PAS has been shown to stain not only glycogen, but also lipofuscin, the aging pigment, making PAS an indispensible tool for assessing aging in multiple tissues (Jung *et al.*, 2010; Kishi *et al.*, 2008). Therefore, our results, showing increased PAS staining in the liver and kidneys of *Ercc1*$^{-/\Delta}$ mice from either CCl_4 treatment, or a diet high in PUFAs, indicate an acceleration of aging compared to control animals (Figure 4.5 and Figure 4.6).

While CCl_4 resulted in exaggerated aging-associated pathologic phenotypes, similar changes, albeit to a much lesser extent, were observed in *Ercc1*$^{-/\Delta}$ mice fed a diet high in PUFAs, indicating that dietary intake can impact lipid peroxidation and aging. This identifies environmental and dietary factors that promote aging, providing potential targets for prevention. Future studies should focus on measuring lipid peroxidation after various chemical and dietary interventions. Ideally, these data will help us to provide better prevention strategies to eliminate environmental and dietary hazards, in order to improve the healthspan of humans.

4.4 MATERIALS AND METHODS

4.4.1 Mice

Ercc1$^{-/\Delta}$ mice were generated by breeding *Ercc1*$^{+/-}$ and *Ercc1*$^{+/\Delta}$ mice in inbred C57Bl/6J and FVB/n backgrounds, respectively, to create a cohort of mice that were in an f1 hybrid background yet genetically identical. The mice were genotyped by PCR as previously described (Ahmad *et al.*, 2008). All experiments were reviewed and approved by the University of Pittsburgh (Pittsburgh, PA) Institutional Animal Care and Use Committee and in accordance with the National Institutes of Health guidelines for the humane care of animals.

4.4.2 CCl_4 treatment of animals

WT, *Xpa*$^{-/-}$ and *Ercc1*$^{-/\Delta}$ mice were injected subcutaneously with 80 mg/kg CCl_4 twice a week for five weeks. Treatment began when the mice were 10 weeks of age. Animals were monitored daily and weighed twice a week. Mice were sacrificed when they were considered terminal or experienced reduced spontaneous activity. Tissues were isolated for histopathologic analysis.

4.4.3 Measuring lipid hydroperoxides

Lipid hydroperoxides were measured in fresh tissue homogenates using the Hydroperoxide Assay kit (#705003, Cayman Chemicals, Ann Arbor, MI) according to the manufacturer's instructions. Liver specimens were sonicated on ice in 1 mL of HPLC-grade water and used immediately after collection.

4.4.4 Food

Special diets were ordered from Harlan-Teklad. The chow pellets contained a standard formula of macronutrients (20.6% protein, 1.7% crude fiber, 3.5 kcal/g energy density and necessary micronutrients. The only difference was that the fat component of the diet was substituted with 12.4% polyunsaturated fats derived from safflower oil (PUFA diet). The control diet contained the same amount of saturated fat derived from coconut oil with a small component of polyunsaturated fat (<0.6% linoleic acid, which is essential for life).

4.4.5 Histological staining

Tissues were fixed in 10% formalin overnight, embedded in paraffin and sectioned using a microtome by standard procedures. Subsequently, sections were stained by standard procedures with hematoxylin and eosin (H&E), Masson's trichrome and periodic acid Schiff (PAS).

4.4.6 Scoring

Slides of liver, kidney and pancreas sections were scored by a veterinary pathologist who was blinded to the genotype and treatment of the animals. The scoring was based on a three point system with 0 being unaffected or no pathology and 3 being the most severe pathology.

5.0 NF-KB INHIBITION DELAYS DNA DAMAGE-INDUCED SENESCENCE AND AGING IN MICE

Adapted with permission from an accepted article in the *Journal of Clinical Investigation* (2012).

Tilstra, J.S.[1*], Robinson, A.R.[2,3*], Wang, J.[4*], Gregg, S.Q.[3,5*], Clauson, C.L.[1*], Reay, D.P.[6], Nasto, L.A.[7], St. Croix, C.M.[8], Usas, A.[7], Vo, N.[7], Huard, J.[1,7], Clemens, P.R.[6], Stolz, D.B.[5], Guttridge, D.C.[9], Watkins, S.C.[5], Garinis, G.A.[10], Wang, Y.[4], Niedernhofer, L.J.[1,3] and Robbins, P.D[1,7]. **(2012). IKK/NF-kB inhibition delays DNA damage-induced senescence and aging-related degenerative diseases. *J Clin Invest.* (accepted).**

[1]Department of Microbiology and Molecular Genetics, University of Pittsburgh School of Medicine, Pittsburgh PA, [2]Department of Human Genetics, University of Pittsburgh Graduate School of Public Health, Pittsburgh PA, [3]University of Pittsburgh Cancer Institute, Pittsburgh PA,[4]Department of Chemistry, University of California, Riverside, CA, [5]Department of Cell Biology, University of Pittsburgh School of Medicine, Pittsburgh PA, [6]Department of Neurology, University of Pittsburgh School of Medicine and Neurology Service, Department of Veterans Affairs Medical Center, Pittsburgh PA, and [7]Department of Orthopaedic Surgery, [8]Department of Environmental and Occupational Health, University of Pittsburgh School of Medicine, Pittsburgh PA; [9]Department of Molecular Virology, Immunology and Medical Genetics, Ohio State University, Columbus, Ohio and [10]Institute of Molecular Biology and Biotechnology, Heraklion, Crete, Greece

5.1 INTRODUCTION

Aging is characterized by the inability of tissues to maintain homeostasis (Kirkwood, 2005; Resnick and Marcantonio, 1997). This leads to an impaired response to stress and, as a consequence, an increased risk of morbidity and mortality (Kirkwood, 2005). The incidence of numerous debilitating chronic diseases such as cardiovascular disease, neurodegeneration, diabetes, arthritis and osteoporosis increases almost exponentially with age (Chung *et al.*, 2009). Aging is thought to be driven, at least in part, by the accumulation of stochastic damage in cells. This includes damage to proteins (Kirkwood, 2005), DNA, mitochondria (Green *et al.*, 2011) and telomeres (Liu *et al.*, 2002), which is driven by reactive oxygen species (Lee *et al.*, 1999; Packer and Fuehr, 1977; Trifunovic *et al.*, 2004) generated through chronic inflammation (Franceschi *et al.*, 2007; Gosselin and Abbadie, 2003) or aerobic respiration in mitochondria (Green *et al.*, 2011). However, the mechanism by which cellular damage drives aging is not known. The simplest model is that damage causes attrition of functional cells. But this is inadequate in light of emerging evidence that aging-related degenerative changes in old and damaged organisms can be delayed or reversed by circulating factors (Brack *et al.*, 2007; Conboy *et al.*, 2005; Lavasani *et al.*, 2012; Rando and Chang, 2012; Villeda *et al.*, 2011). These observations point instead towards the cellular response to damage being the key driver of aging.

The transcription factor NF-κB is a central component of the cellular response to damage, stress and inflammation (Hayden and Ghosh, 2008). In mammals, the NF-κB family consists of five subunits, p65/RelA, c-Rel, RelB, p50 and p52. NF-κB binds to DNA as a dimer, the most common being the p65p50 heterodimer (Hayden *et al.*, 2006). The p65p50 heterodimer is localized primarily in the cytoplasm, maintained in this inactive state via sequestration by IκB proteins (Hayden *et al.*, 2006). NF-κB activation via the canonical pathway is mediated by the

upstream IκB kinase (IKK), a heterotrimer consisting of two catalytic subunits, IKKα and IKKß, and a regulatory subunit termed IKKγ or NEMO (NF-κB Essential Modulator) (Hayden *et al.*, 2006). In response to a variety of factors, including pro-inflammatory cytokines, pathogens, oxidative stress and growth factors, IKK is activated and phosphorylates IκB, leading to its polyubiquitination and subsequent proteasomal degradation (Bubici *et al.*, 2006; Hayden and Ghosh, 2008; Ramana *et al.*, 2004; Wullaert *et al.*, 2006). IκB degradation allows NF-κB to translocate to the nucleus where it binds to its cognate DNA sequence as well as co-activators such as CBP/p300, to regulate gene expression (Furia *et al.*, 2002).

Numerous studies report increased NF-κB activity with aging. Human fibroblasts from aged individuals and Hutchinson-Gilford progeria syndrome (HGPS) patients have increased NF-κB activation (Adler, 2007; Kriete *et al.*, 2008). NF-κB DNA binding is increased in skin, liver, kidney, cerebellum, cardiac muscle, and gastric mucosa of old rodents compared to young (Bregegere *et al.*, 2006; Giardina and Hubbard, 2002; Helenius *et al.*, 1996; Korhonen *et al.*, 1997; Xiao and Majumdar, 2000). In addition, NF-κB was identified as the transcription factor most associated with mammalian aging, based on patterns of gene expression (Adler, 2007). Furthermore, chronic activation of NF-κB is observed in numerous age-related diseases (Tilstra *et al.*, 2011) including muscle atrophy (Cai *et al.*, 2004; Li *et al.*, 2008), multiple sclerosis (Ghosh *et al.*, 2007a), atherosclerosis (Cuaz-Perolin *et al.*, 2008), heart disease (Valen, 2004), both type I and II diabetes (Tilstra *et al.*, 2007), osteoarthritis (Berenbaum, 2004), dementia (Yamamoto and Gaynor, 2001), osteoporosis (Kim *et al.*, 2006), and cancer (Karin, 2006). However, these studies do not demonstrate a causal relationship between NF-κB activation and aging.

Genetic depletion of NF-κB in the skin of transgenic mice reversed age-related gene expression and histologic changes (Adler, 2007), providing support for NF-κB activation playing a causal role in skin aging. Similarly, haploinsufficiency of p65 leads to improved growth and extended lifespan of *Sirt6*$^{-/-}$ mice (Kawahara *et al.*, 2009). However, *Sirt6*$^{-/-}$ mice manifest severe colitis, suggesting that chronic inflammation may drive their degenerative phenotypes and that attenuating this inflammation through genetic depletion of NF-κB accounts for their improved lifespan (Mostoslavsky *et al.*, 2006; Natoli, 2009). Thus, it remains to be determined if NF-κB activation drives systemic aging and if NF-κB is a therapeutic target for attenuating and/or delaying aging-related degenerative changes.

To address these gaps in knowledge, we used a mouse model of XFE progeroid syndrome, a disease of accelerated aging caused by mutations in *XPF*, which encodes the catalytic subunit of the XPF-ERCC1 DNA repair endonuclease. The syndrome is characterized by accelerated aging of virtually all organ systems, all driven by failure to repair stochastic endogenous DNA damage. A murine model for XFE progeroid syndrome, *Ercc1*$^{-/\Delta}$ mice, which have about 10% of the normal amount of ERCC1 protein model, this disease and spontaneously develop progressive, degenerative changes that correlate strongly with natural aging (Goss *et al.*, 2011; Gregg *et al.*, 2012a; Niedernhofer *et al.*, 2006; Schumacher *et al.*, 2008; Vo *et al.*, 2010). Thus, the *Ercc1*$^{-/-}$ mice, which have a complete absence of ERCC1 protein, and *Ercc1*$^{-/\Delta}$ mice offer a unique opportunity to investigate the mechanism by which one type of cellular damage promotes aging and whether NF-κB plays a pivotal role.

We found that NF-κB is stochastically activated in a variety of cell types with normal and accelerated aging, and that genetic or pharmacologic inhibition of NF-κB activation delays the onset of numerous aging-related symptoms and pathologies. Inhibition of IKK/NF-κB activity

reduced cellular senescence and oxidative damage, including DNA and protein damage, revealing that cellular stress responses promote further cellular damage. Our findings strongly suggest that inhibitors of the IKK/NF-κB pathway may delay damage and extend healthspan in patients with accelerated aging and chronic degenerative diseases of old age.

5.2 RESULTS

5.2.1 NF-κB is activated during normal and accelerated aging

To examine the extent of NF-κB activation associated with aging, NF-κB^{EGFP} knock-in mice with the EGFP reporter under the control of NF-κB regulatory elements (NF-κB^{EGFP}) were used (Magness *et al.*, 2004). Kidney specimens from 3 month-old and 2 year-old NF-κB^{EGFP} reporter mice were compared (Figure 5.1A). The older wild-type (WT) mice had more cells expressing EGFP compared to young WT mice, indicative of increased NF-κB activation. EGFP expression was observed primarily in the glomeruli and was stochastic, with many cells showing strong expression while neighboring cells showed none. To determine if NF-κB is also upregulated in the progeroid mouse models, kidney specimens from *Ercc1*$^{-/\Delta}$NF-κB^{EGFP} mice (lifespan 7 months (Dollé *et al.*, 2011)) and WT NF-κB^{EGFP} littermates were isolated at 3 months of age (Figure 5.1B) and from *Ercc1*$^{-/-}$NF-κB^{EGFP} mice (lifespan 28 days (Niedernhofer *et al.*, 2006)) and WT NF-κB^{EGFP} littermates at 21 days (Figure 5.1C) to measure EGFP expression. Similar to natural aging, NF-κB activity was greater in the kidneys of ERCC1-deficient mice, particularly in the glomeruli, compared to WT littermates. In addition, EGFP+ cells were detected in the liver, pancreas, spleen and muscle of *Ercc1*$^{-/-}$NF-κB^{EGFP} mice (Figure 5.2). Amongst six littermate

pairs, we detected a significant increase in the fraction of EGFP+ cells in the progeroid mice: kidney (2.5-fold increase relative to WT littermates), pancreas (2.5-fold), muscle (1.7-fold), and liver (4-fold) (Figure 5.1D). In contrast, the percent of EGFP+ cells was 35% lower in the spleens of *Ercc1*$^{-/-}$NF-κB^{EGFP} mice than WT NF-κB^{EGFP} littermates, indicating that NF-κB activation is not exclusively driven by inflammation. These data support earlier reports (Adler, 2007; Kriete *et al.*, 2008) that there is increased NF-κB activation with mammalian aging, and extends this to include a murine model of XFE progeroid syndrome, which is driven by a DNA repair defect.

To confirm that NF-κB activity is increased in cells from progeroid *Ercc1*$^{-/-}$ mice, the levels of phosphorylated p65/RelA (p-p65) and IκB were measured by immunoblot in nuclear and cytoplasmic extracts from passage 5, congenic *Ercc1*$^{-/-}$ and WT primary MEFs. There was a >2-fold increase in nuclear p-p65 in *Ercc1*$^{-/-}$ MEFs compared to WT (Figure 5.1E), which correlated with an increase in the level of phosphorylated IκB (p-IκB) in the cytoplasm. Increased NF-κB binding activity was also detected in nuclear extracts from *Ercc1*$^{-/-}$ MEFs by electrophoretic mobility shift assay (EMSA, Figure 5.1F). Pretreatment of the nuclear lysates with anti-p50 and, in particular, anti-p65 antibodies reduced this DNA binding activity (Figure 5.3). These data establish increased NF-κB activity in DNA repair-deficient *Ercc1*$^{-/-}$ cells from progeroid mice and suggest that p65 is the predominant subunit contributing to this increased activity.

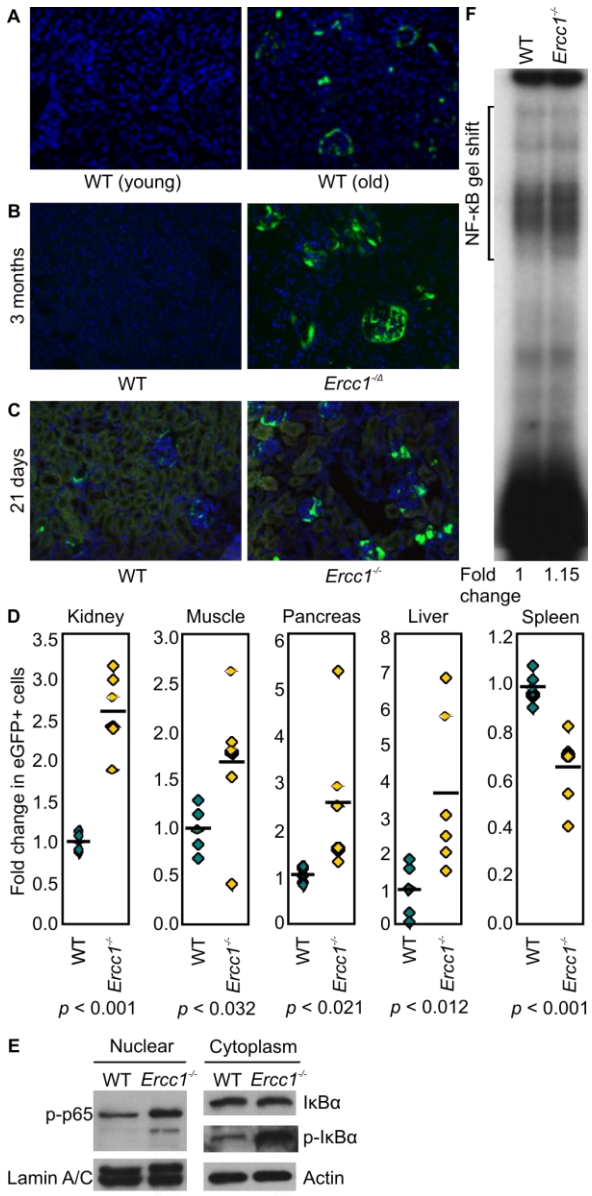

Figure 5.1: NF-κB activation is increased in tissues of old wild-type (WT) and progeroid, DNA repair-deficient mice

Kidney sections from NF-κB^{EGFP} mice were imaged using fluorescent microscopy to detect EGFP expression (green). Nuclei were counter-stained with Hoechst dye (blue; 20x objective). Comparisons include (**A**) Young adult (3 month-old) and old WT NF-κB^{EGFP} (2 year-old) mice, (**B**) *Ercc1*$^{-/\Delta}$NF-κB^{EGFP} and WT NF-κB^{EGFP} mice at 3 months of age, and (**C**) *Ercc1*$^{-/-}$NF-κB^{EGFP} and WT NF-κB^{EGFP} mice at 21 days of age. (**D**) Quantification of EGFP expression. The number of EGFP+ cells was counted in five random fields of tissue per mouse (n = 6 mice per group). Reported is the fold difference in the number of EGFP+ cells relative to the mean value (black bar) of the group. Diamond symbols represent individual mice (control in green and *Ercc1*$^{-/-}$NF-κB^{EGFP} in yellow). *P*-values were calculated using a Student's *t*-test. (**E**) *Ercc1*$^{-/-}$ and WT primary MEFs were passaged five times at 20% O_2 to promote the onset of senescence (Parrinello *et al.*, 2003a). The levels of p-p65, IκBα and p-IκBα in nuclear and cytoplasmic extracts were measured by immunoblot. (F) NF-κB EMSA was performed with a radiolabeled oligonucleotide containing an NF-κB binding site using nuclear extracts from *Ercc1*$^{-/-}$ and WT primary MEFs.

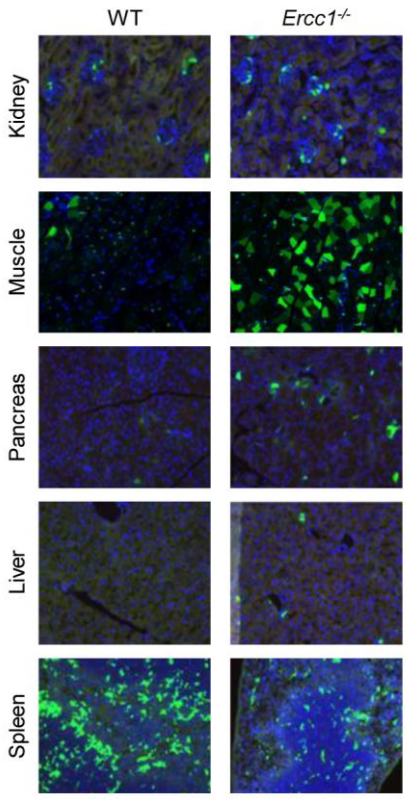

Figure 5.2: NF-κB is activated in DNA repair-deficient, progeroid *Ercc1*$^{-/\Delta}$ mice

Representative images of EGFP expression in tissue sections from 21 day-old progeroid *Ercc1*$^{-/-}$ mice and their normal littermates harboring the NF-κB^{EGFP} reporter knock-in contruct. Kidney, skeletal muscle, pancreas, liver, and spleen sections from *Ercc1*$^{-/-}$NF-κB^{EGFP} and WT NF-κB^{EGFP} mice were imaged using fluorescent microscopy to detect EGFP expression (green). Nuclei were counter-stained with Hoechst dye (blue; 20x objective).

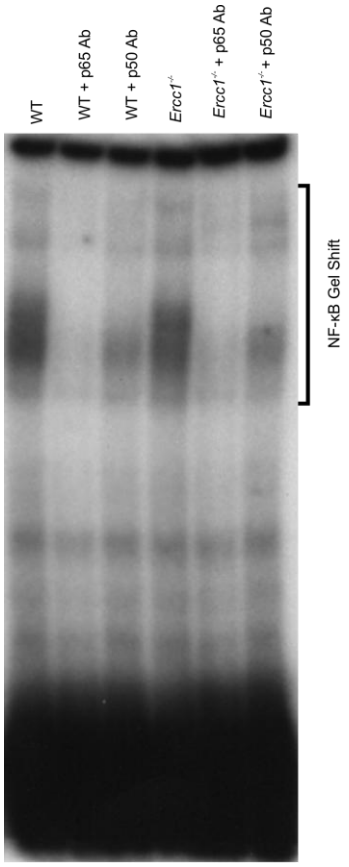

Figure 5.3: EMSA of NF-κB activity

EMSA was performed using nuclear extracts from WT and *Ercc1*$^{-/-}$ primary MEFs, passage 5 and a 5'-^{32}P end-labeled duplex oligonucleotide containing a centrally located NF-κB binding sequence. Some extracts were pre-incubated with antibodies against p65 and p50 to determine which NF-κB subunits are mediating NF-κB binding activity.

5.2.2 Genetic reduction of NF-κB delays the onset of progeroid symptoms in *Ercc1*$^{-/\Delta}$ mice

To determine if NF-κB activation drives age-related pathologies, *Ercc1*$^{-/\Delta}$ mice were bred to have a deletion of one allele of the NF-κB subunit, p65/RelA (*Ercc1*$^{-/\Delta}$*p65*$^{+/-}$). To determine if genetic depletion of p65 indeed resulted in reduced NF-κB DNA binding activity, EMSAs were performed using extracts from WT, *Ercc1*$^{-/-}$, *Ercc1*$^{-/-}$*p65*$^{+/-}$, and *Ercc1*$^{-/-}$*p65*$^{-/-}$ primary MEFs (Figure 5.4A). Heterozygosity of p65 resulted in a reduction in NF-κB binding activity, whereas homozygous deletion of p65 reduced NF-κB binding activity even further.

To examine the role of NF-κB/p65 in the aging process, *Ercc1*$^{-/\Delta}$ and *Ercc1*$^{-/\Delta}$*p65*$^{+/-}$ littermates were monitored biweekly for the onset of age-related symptoms. The onset of the majority of symptoms characteristic of *Ercc1*$^{-/\Delta}$ mice was delayed in *Ercc1*$^{-/\Delta}$*p65*$^{+/-}$ mice, including trembling, kyphosis, sarcopenia and urinary incontinence, all signs of neurodegeneration (Table 5.1). The aging score, representing the fraction of all aging-related symptoms that were delayed in *Ercc1*$^{-/\Delta}$*p65*$^{+/-}$ mice compared to littermate *Ercc1*$^{-/\Delta}$ mice, revealed a trend towards a delay in onset of aging pathologies (Figure 5.4B). Additionally, the overall physical appearance of the *Ercc1*$^{-/\Delta}$*p65*$^{+/-}$ mice was dramatically improved (Figure 5.4C). At 15 weeks of age, *Ercc1*$^{-/\Delta}$ mice exhibited ocular impairment, a wide-base stance (ataxia), sarcopenia, kyphosis and frailty, all of which were dramatically attenuated in *Ercc1*$^{-/\Delta}$*p65*$^{+/-}$ mice.

Table 5.1: Genetic depletion of the p65 subunit of NF-κB delays aging symptoms of progeroid *Ercc1*$^{-/\Delta}$ mice

Symptoms	Age at onset (weeks)		Change of onset (weeks)	Number of *Ercc1*$^{-/\Delta}$ mice (WT, *p65*$^{+/-}$)
	Ercc1$^{-/\Delta}$	*Ercc1*$^{-/\Delta}$ *p65*$^{+/-}$		
Dystonia	7.3	7.0	-0.3	7, 7
Trembling	7.0	7.1	0.1	7, 7
Kyphosis	9.8	11.1	1.3	7, 7
Ataxia	12.1	11.3	-0.8	7, 7
Sarcopenia	13.3	13.8	0.5	7, 7
Spontaneous activity	19.4	17.2	-2.2	5, 5
Urinary incontinence	15.9	19.3	3.4	4, 2

Ercc1$^{-/\Delta}$ and *Ercc1*$^{-/\Delta}$ *p65*$^{+/-}$ mice were evaluated biweekly for the onset of spontaneous symptoms associated with aging. Shown is the average age at onset of each symptom for each group and the difference between the group averages. Yellow shaded cells indicate symptoms delayed in the *p65* heterozygous mice.

In addition to assessing outward signs of aging, histologic analysis was performed. Mice were euthanized at 10 and 15 weeks of age and tissues collected for analysis of several hallmarks of age-related degeneration. Compared to *Ercc1*$^{-/\Delta}$ mice, *Ercc1*$^{-/\Delta}$*p65*$^{+/-}$ mice exhibited a marked reduction of steatosis (Figure 5.4D), a marker of aged liver (Farrell and Larter, 2006). Kidneys from *Ercc1*$^{-/\Delta}$ mice had increased proteinaceous renal tubular hyaline casts and glomerulosclerosis (Figure 5.4D), typical of aged kidneys (Remuzzi *et al.*, 2002; Rodriguez-Puyol, 1998), that was reduced in *Ercc1*$^{-/\Delta}$*p65*$^{+/-}$ mice. There also was a reduction in glial fibrillary acidic protein (GFAP) staining, a marker of neurodegeneration (Nichols *et al.*, 1993), in the cerebella of *Ercc1*$^{-/\Delta}$*p65*$^{+/-}$ mice compared to *Ercc1*$^{-/\Delta}$ littermates (Figure 5.4D). Finally, osteoporosis was significantly reduced in *Ercc1*$^{-/\Delta}$*p65*$^{+/-}$ mice (Figure 5.4D; Figure 5.5). Taken together, these results demonstrate that reducing NF-κB activity delays the onset of numerous age-related pathologies and extends healthspan.

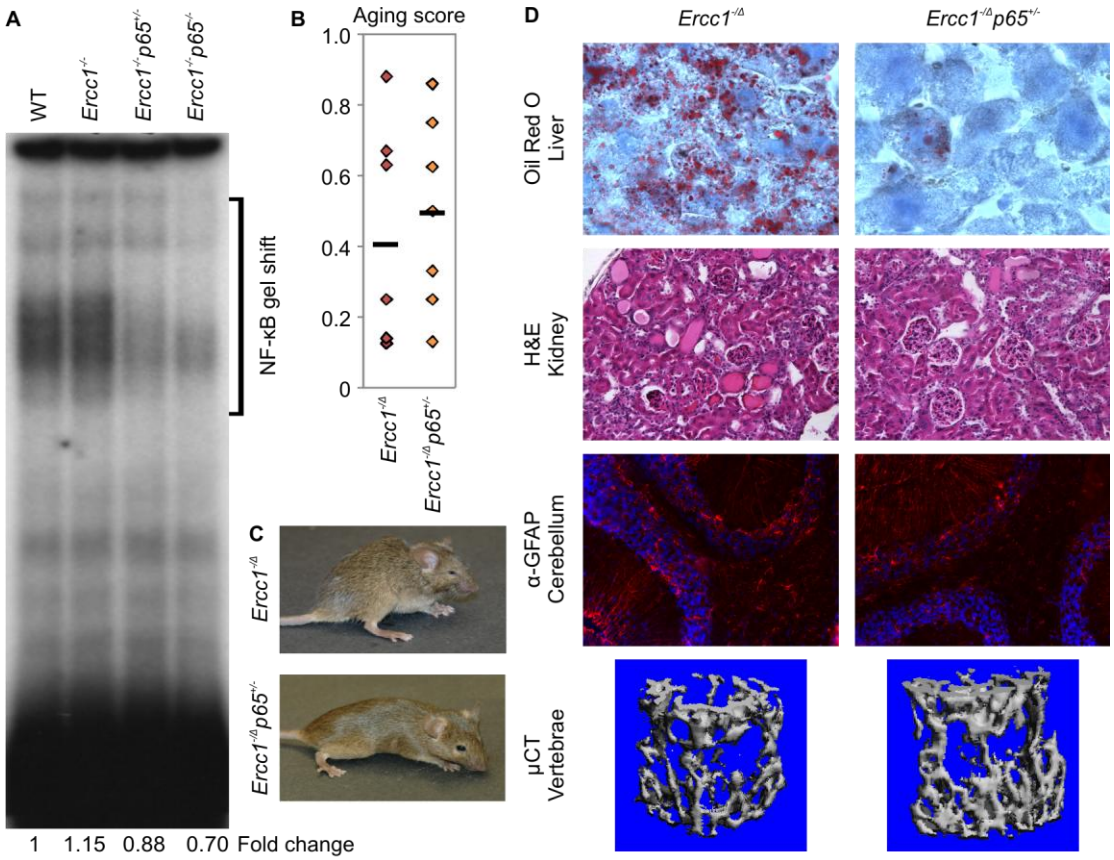

Figure 5.4: Genetic depletion of the p65 subunit of NF-κB delays aging symptoms and chronic diseases in progeroid *Ercc1*$^{-/\Delta}$ mice

(**A**) EMSA on nuclear extracts from passage 5 WT, *Ercc1*$^{-/-}$, *Ercc1*$^{-/-}$*p65*$^{+/-}$, *Ercc1*$^{-/-}$*p65*$^{-/-}$ MEFs grown at 20% O_2 to measure NF-κB activity after depletion of p65. (**B**) *Ercc1*$^{-/\Delta}$ and *Ercc1*$^{-/\Delta}$*p65*$^{+/-}$ mice were evaluated biweekly for the onset of spontaneous symptoms associated with aging. The aging score, which represents the fraction of aging symptoms delayed in a particular mouse compared to its sibling, for littermate pairs of *Ercc1*$^{-/\Delta}$ (red) and *Ercc1*$^{-/\Delta}$*p65*$^{+/-}$ (orange) mice and is a measure of healthspan (11). The mean aging score for each genotype is represented by a black bar. (**C**) Representative images of *Ercc1*$^{-/\Delta}$ and *Ercc1*$^{-/\Delta}$*p65*$^{+/-}$ sex-matched littermates at 15 weeks of age. (**D**) Histopathologic changes in *Ercc1*$^{-/\Delta}$*p65*$^{+/-}$ and *Ercc1*$^{-/\Delta}$ mice. Liver sections were stained with oil red O to detect neutral lipids in 10 week-old mice (hepatic steatosis; 100x objective). Kidney specimens from 15 week-old mice were stained with haematoxylin and eosin (H&E) to detect proteinaceous renal tubular hyaline casts and glomerulosclerosis (20x objective). Cerebellar sections were immunostained for glial fibrillary acidic protein (GFAP, red), a marker of neurodegeneration, in 10 week-old mice. Nuclei were counter-stained with DAPI (blue; 40x objective). Micro-computed tomography (μCT) of the vertebrae to assess bone porosity (quantification, Figure 5.5A).

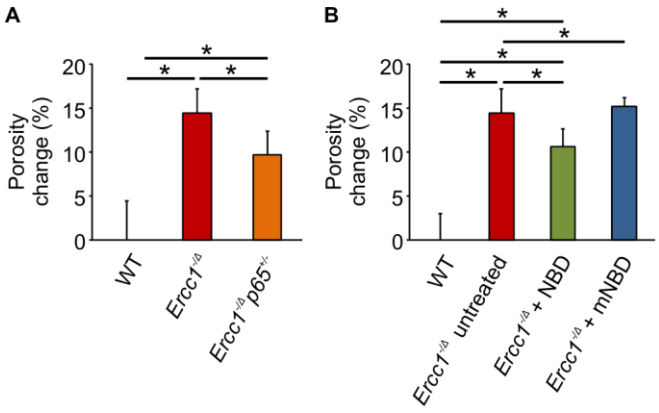

Figure 5.5: Quantitation of bone porosity (osteoporosis) in *Ercc1*$^{-/\Delta}$ mice following genetic or pharmacologic inhibition of NF-κB

Micro-computed tomography of spines isolated from mice using a VivaCT 40 (Scanco Medical) with 15 μm isotropic voxel size resolution, 55 kVp of energy and 145 μA of current. (A) The percent change in porosity in *Ercc1*$^{-/\Delta}$ and *Ercc1*$^{-/\Delta}$*p65*$^{+/-}$ mice compared to age-matched WT mice. '*', $p < 0.05$, Tukey-Kramer test. The values denote the mean ± S.D. of 9 mice per group. (B) The percent change in porosity in *Ercc1*$^{-/\Delta}$ mice treated with 8K-NBD or 8K-mNBD compared to age-matched WT mice. '*', $p < 0.05$, Tukey-Kramer test. The values denote the mean ± S.D. of 3 mice per group.

5.2.3 Pharmacologic inhibition of NF-κB delays the onset of progeroid symptoms in *Ercc1*$^{-/\Delta}$ mice

To determine if pharmacologic suppression of IKK/NF-κB signaling also results in an extension of healthspan, a peptide inhibitor of IKK, termed NBD, was used. The 11 amino acid NBD peptide, when fused to a protein transduction domain such as Antp or 8K, is efficacious for treating muscular dystrophy (Acharyya *et al.*, 2007), inflammatory bowel disease (Dave *et al.*, 2007), arthritis (Dai *et al.*, 2004), and Parkinson's disease (Ghosh *et al.*, 2007b) in mice. The activity of the peptide was tested *in vitro* by treating *Ercc1*$^{-/-}$ primary MEFs with 200 μM 8K-NBD. This led to a reduction in nuclear p-p65 (Figure 5.6A). *Ercc1*$^{-/\Delta}$ mice were chronically treated with 8K-NBD (10 mg/kg intraperitoneal, 3X per week) beginning at 5 wks of age, which is prior to the onset of their aging symptoms. Littermate mutant animals were treated with an

equivalent dose of an inactive, mutant peptide (8K-mNBD) used as a negative control. Investigators conducting the experiment were blinded as to the treatment group. Mice treated with 8K-NBD showed a delay in the onset of the majority of symptoms compared to siblings

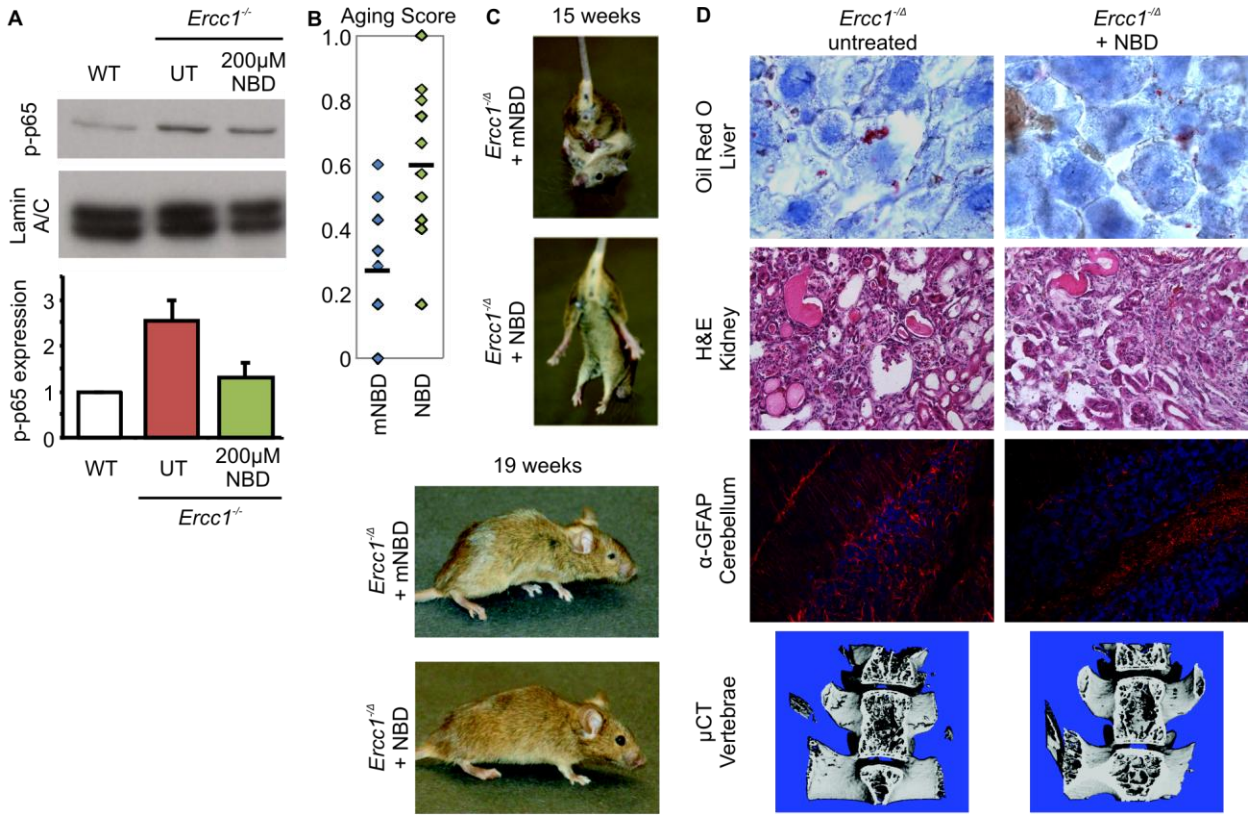

Figure 5.6: Pharmacologic inhibition of IKK/NF-κB activation delays aging symptoms and chronic diseases in progeroid *Ercc1*$^{-/\Delta}$ mice

Pharmacologic inhibition of IKK/NF-κB activation delays aging symptoms and chronic diseases in progeroid *Ercc1*$^{-/\Delta}$ mice. (**A**) Immunodetection of p-p65 in nuclear extracts of WT or *Ercc1*$^{-/-}$ primary MEFs treated with 200μM NBD or untreated (UT); Lamin A/C loading control. Histogram indicating the level of p-p65 normalized to untreated WT cells and corrected for loading. Values denote mean ± S.D. from three experiments. (**B**) Sibling, sex-matched pairs of *Ercc1*$^{-/\Delta}$ mice were treated with 8K-NBD or 8K-mNBD, 10mg/kg, i.p., 3X per week, beginning at 5 weeks of age. The aging score was calculated between *Ercc1*$^{-/\Delta}$ littermate pairs treated with 8K-mNBD (blue) or 8K-NBD (green). Mean aging score is represented by a black bar (p = 0.003, Student's t-test). (**C**) Representative images of *Ercc1*$^{-/\Delta}$ mice treated with 8K-NBD or 8K-mNBD peptide at 15 and 19 weeks of age. (**D**) Histopathologic changes analyzed in tissue sections from 18 week-old *Ercc1*$^{-/\Delta}$ mice treated with 8K-NBD or 8K-mNBD. Liver sections were stained with oil red O to detect neutral lipids (hepatic steatosis; 100x objective). Kidney specimens were stained with H&E to detect hyaline casts and glomerulosclerosis (20x objective). Cerebellar sections were immunostained for GFAP (red), a marker of neurodegeneration. Nuclei were counter-stained with DAPI (blue; 40x objective). μCT of vertebrae to measure bone porosity (quantification, Figure 5.5B).

treated with the mutant peptide (Table 5.2). Ataxia, sarcopenia and weight loss were significantly delayed (Table 5.2 and Table 5.3). In addition, the aging score revealed a highly significant difference between treatment groups (p = 0.003; Figure 5.6B). There also was a visible difference in the appearance of the mice treated with 8K-NBD compared to their siblings treated with the mutant peptide at 15 and 19 weeks of age (Figure 5.6C), including improved reflexes, gait, muscle and eyes.

Table 5.2: Pharmacologic suppression of IKK/NF-κB activation attenuates progeroid symptoms and pathologies of progeroid *Ercc1*$^{-/\Delta}$ mice

Symptoms	Age at onset (weeks)		Change of onset (weeks)	Number of *Ercc1*$^{-/\Delta}$ mice (mNBD, NBD)
	mNBD	NBD		
Dystonia	9.2	9.1	-0.1	12, 17
Trembling	10.7	9.8	-0.9	12, 17
Kyphosis	12.9	12.2	-0.7	11, 15
Ataxia*	14.5	16.2	1.7	10, 13
Sarcopenia*	15.1	17.2	2.1	8, 12
Spontaneous activity	20.4	10.7	0.3	3, 2
Urinary incontinence	17.5	19.7	2.2	5, 3

Sibling, sex-matched pairs of *Ercc1*$^{-/\Delta}$ mice were treated with 8K-NBD or 8K-mNBD, 10 mg/kg, i.p., 3X per week, beginning at 5 weeks of age and continuing throughout their lifespan. Shown is the average age at onset of characteristic progeroid symptoms in treated *Ercc1*$^{-/\Delta}$ mice and the difference between the group averages. Yellow shaded cells indicate symptoms delayed in mice treated with the NF-κB inhibitor 8K-NBD compared to 8K-mNBD. The asterisks indicate a significant delay ($p < 0.05$; Student's t-test).

Histologic analysis was performed on tissues of 19 week-old mice to determine if treatment with 8K-NBD reduced age-related pathology. Similar to the *Ercc1*$^{-/\Delta}$*p65*$^{+/-}$ mice, 8K-NBD treatment resulted in reduced liver steatosis and renal hyaline casts compared to control mice (Figure 5.6D). GFAP staining was also reduced, consistent with the delay in onset of symptoms caused by neurodegeneration (Figure 5.6D). μCT analysis revealed a significant reduction in bone porosity (osteoporosis) in mice treated with 8K-NBD compared to untreated *Ercc1*$^{-/\Delta}$ mice (Figure 5.6D and Figure 5.5B). Collectively these data demonstrate that pharmacological inhibition of IKK/NF-κB activation leads to attenuation of age-related pathologies.

Table 5.3: Chronic treatment of *Ercc1*$^{-/\Delta}$ mice with the NF-κB inhibitor 8K-NBD significantly delayed progeroid symptoms and pathologies

Symptoms	Age at onset (weeks)		Change of onset (weeks)	Number of *Ercc1*$^{-/\Delta}$ mice (Vehicle, NBD)
	Vehicle	NBD		
Dystonia	8.0	9.1	1.1	17, 17
Trembling*	7.8	9.8	2.0	17, 17
Kyphosis	11.3	12.1	0.8	17, 15
Ataxia**	13.9	16.4	2.5	17, 13
Sarcopenia***	14.0	16.9	2.9	16, 11
Spontaneous activity	17.8	18.4	0.6	8, 2
Urinary incontinence	13.6	18.5	4.9	5, 2

Ercc1$^{-/\Delta}$ mice were treated with 8KNBD,10 mg/kg, i.p., 3X per week, beginning at 5 weeks of age and continuing throughout their lifespan. Shown are the average age-at-onset of each symptom for mice treated with the peptide inhibitor or vehicle only (phosphate buffered saline) and the differences between the group averages. Yellow shaded cells indicate symptoms delayed in mice treated with the NF-κB inhibitor, 8K-NBD, versus vehicle-treated mice. *P*-values were determined using Student's *t*-test. '*', $p < 0.05$; '**', $p < 0.01$; '***', $p < 0.001$.

Unexpectedly, the age-at-onset of progeroid symptoms was delayed slightly in mutant animals treated with the mutant NBD peptide compared to untreated mutant animals (Table 5.2 vs. Table 5.1), suggesting that the mutant peptide has residual activity, which was confirmed in cell culture assays (data not shown). Therefore, we also compared the age-at-onset of symptoms in *Ercc1*$^{-/\Delta}$ mice treated with 8K-NBD to *Ercc1*$^{-/\Delta}$ mice treated with vehicle only (phosphate buffered saline) (Table 5.3). This comparison revealed a significant delay in the onset of even more symptoms in mice treated with 8K-NBD (trembling, ataxia, sarcopenia) and a more significant delay of all symptoms assessed. At 15 weeks of age *Ercc1*$^{-/\Delta}$ mice exhibited dystonia and cachexia, and by 19 weeks of age incontinence, ocular defects and sarcopenia were obvious (Figure 5.7). These symptoms were largely spared in *Ercc1*$^{-/\Delta}$ mice treated with 8K-NBD. These data demonstrate that pharmacologic inhibition of NF-κB activation can be used to simultaneously delay the onset of symptoms associated with multiple, common age-related chronic degenerative diseases.

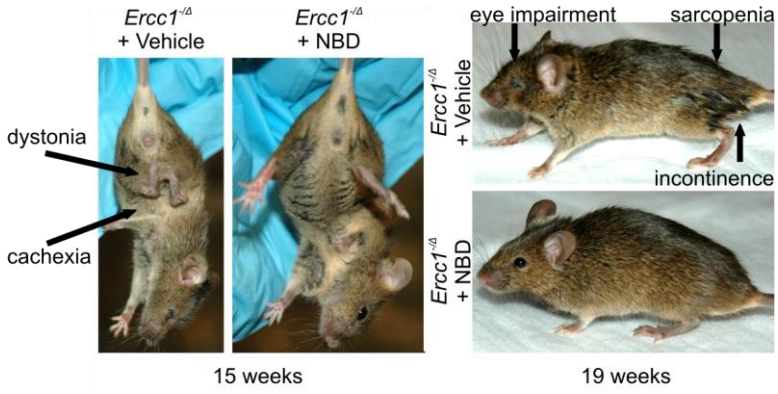

Figure 5.7: Chronic treatment of *Ercc1*$^{-/\Delta}$ mice with the NF-κB inhibitor, 8K-NBD, significantly delayed aging-related symptoms and chronic degenerative diseases

Ercc1$^{-/\Delta}$ mice were treated with 8K-NBD, 10 mg/kg, i.p., 3X per week, beginning at 5 weeks of age and continuing throughout their lifespan. Representative images of *Ercc1*$^{-/\Delta}$ mice treated with 8K-NBD or PBS at 15 and 19 weeks of age. Aging-related phenotypes are labeled with arrows.

5.2.4 8K-NBD alters NF-κB signaling *in vivo*

To determine if 8K-NBD indeed affects NF-κB-regulated gene expression *in vivo*, the gene expression profile from liver of 19 week-old *Ercc1*$^{-/\Delta}$ mice chronically exposed to 8K-NBD was compared to littermate mutant animals treated with the mutant peptide (8K-mNBD). A full mouse genome array revealed 1,269 genes (~5% of all genes) with significantly changed expression patterns between 8K-NBD-treated versus 8K-mNBD-treated mice ($p \leq 0.05$, 1.2-fold change up- or down-regulated). Of the 29 genes with known NF-κB regulatory elements that significantly differed between treatment groups, 26 were significantly down-regulated in mice treated with 8K-NBD (Table 5.4), demonstrating that 8K-NBD treatment reduces NF-κB activity *in vivo*.

All genes with significantly altered expression were grouped according to their known or predicted biological function into gene ontology (GO) categories. Significantly altered biological processes were identified as those with a disproportionate number of genes having altered expression relative to those printed on the Affymetrix chip. Five major biological processes were significantly suppressed in response to inhibition of NF-κB. These processes, ranked by their relative enrichment score, included immune responses, cell cycle regulation, apoptosis, stress and DNA damage responses, and growth hormone signaling (Figure 5.8A). Of note, NF-κB is known to regulate many of these processes and NF-κB activation was one of the GO categories identified as suppressed in tissues from mice chronically treated with 8K-NBD (Figure 5.8A). To validate the microarray data, the expression of a number of NF-κB target genes was measured using qRT-PCR, including *Apod*, *Gadd45b*, *Bcl2*, *Lamb2*, *Icam1*, *Plcd1* and *Sod1* (Figure 5.8B). Expression of the majority of these genes was confirmed to be reduced in mice treated with

Table 5.4: 8K-NBD inhibits NF-κB *in vivo* and corrects gene expression changes associated with aging

Gene symbol	Fold change	*p*
Csf3	1.8	0.001
Agt	1.2	0.02
Sod1	1.1	0.04
Ctsb	-1.1	0.02
Eng	-1.2	0.05
Il15ra	-1.2	0.001
Scarb1	-1.2	0.02
Prkcd	-1.2	0.01
Icam1	-1.3	0.01
Nfkbia	-1.3	0.02
Ccnd3	-1.3	0.03
Ccl19	-1.4	0.04
Tcrg	-1.4	0.01
App	-1.5	0.03
Bcl2	-1.5	0.007
Plcd1	-1.6	0.03
Ccnd2	-1.7	0.02
Cd48	-1.7	0.03
Sdc4	1.5	0.006
Abcb1a	-1.8	0.04
Cd80	-1.9	0.03
Upk1b	-1.9	0.03
Oas3	-2.0	0.03
Penk	-2.1	0.009
Ighg1	-2.4	0.03
Ptx3	-2.4	0.01
Lamb2	-2.5	0.009
Gadd45b	-3.5	0.02
Apod	-4.4	0.01

RNA was isolated from the liver of 18-19 week old *Ercc1*$^{-/\Delta}$ mice chronically treated with 8K-NBD or 8K-mNBD (n = 4 per group). Differences in gene expression were analyzed using total genome Affymetrix arrays. Shown are genes with known NF-κB regulatory elements that were significantly altered in *Ercc1*$^{-/\Delta}$ mice treated with 8K-NBD compared to 8K-mNBD. Green indicates genes implicated in inflammation; blue indicates genes implicated in cell survival and cell cycle control.

8K-NBD relative to littermates treated with the control peptide (n = 4 mice per group; Figure 5.8B).

The expression of key genes known to be altered in old WT mice was also evaluated by qRT-PCR (Schumacher *et al.*, 2008). The growth hormone/insulin-like growth factor 1 axis is

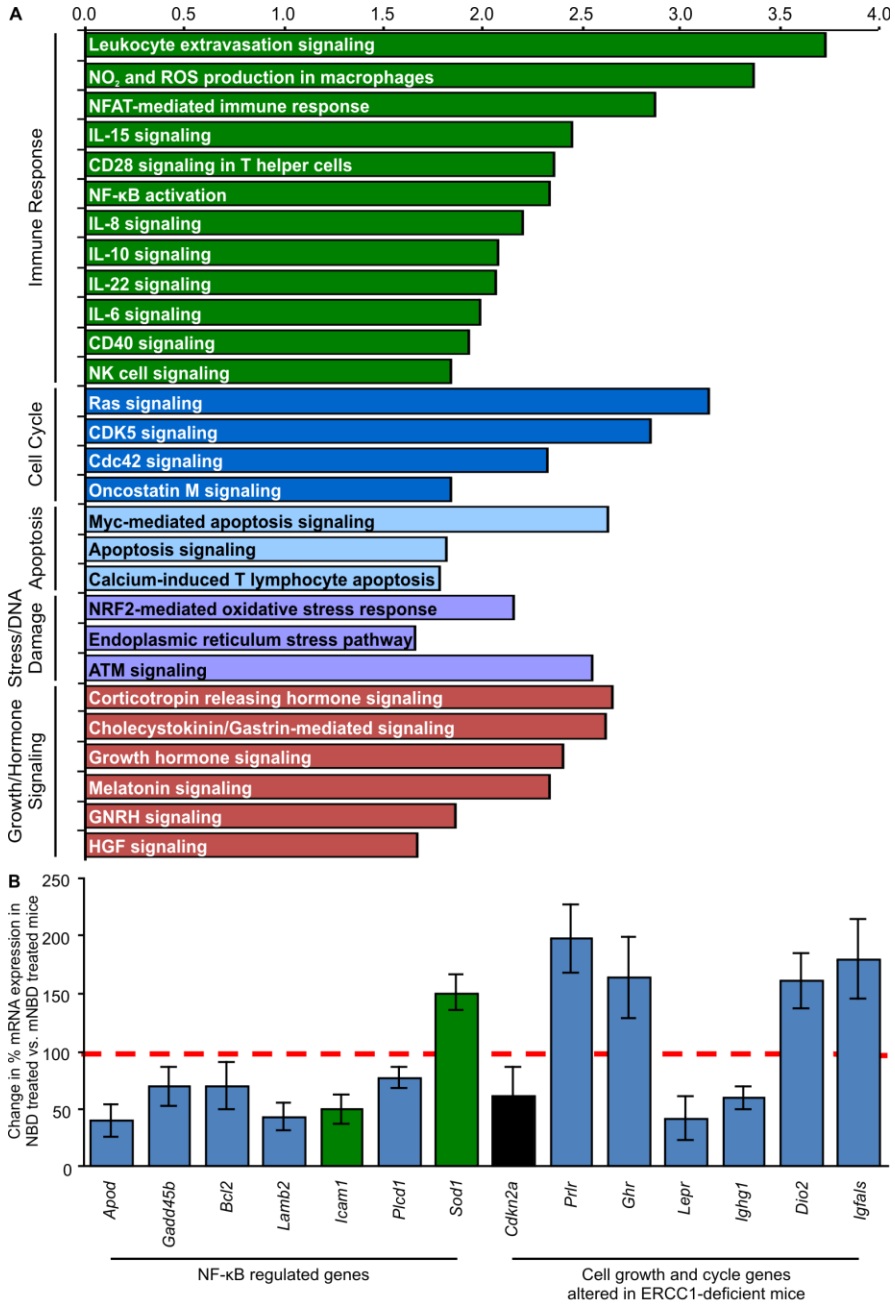

Figure 5.8: 8K-NBD inhibits NF-κB *in vivo* and corrects gene expression changes associated with aging

RNA was isolated from liver of 18-19 week-old *Ercc1*$^{-/\Delta}$ mice chronically treated with 8K-NBD or 8K-mNBD (n = 4 per group). Differences in gene expression were analyzed using total genome Affymetrix arrays. (**A**) Gene ontology enrichment analysis of the networks and pathways regulated by 8K-NBD. The biological processes most significantly affected by chronic inhibition of IKK/NF-κB are ranked by their relative enrichment score. (**B**) qRT-PCR of genes identified by microarray analysis to be significantly differentially expressed in *Ercc1*$^{-/\Delta}$ mice chronically treated with 8K-NBD relative to sibling mutant animals treated with 8K-mNBD. The dashed red line indicates mean expression in mice treated with the mutant peptide. The bars indicate the mean expression in mice treated with the NF-κB inhibitor 8K-NBD (n = 4 per treatment group) ± S.D. For the NF-κB regulated genes, green coloring indicates genes implicated in inflammation; blue indicates genes implicated in cell survival. In black is expression of *Cdkn2a* (the gene encoding p16^{INK4a}), a marker of cellular senescence.

downregulated in aged mice and progeroid ERCC1-deficient mice (Niedernhofer *et al.*, 2006). Interestingly, chronic treatment with 8K-NBD led to an increase in expression of many of these genes involved in these pathways including *Ghr, Prlr* and *Dio2* (Figure 5.8B).

5.2.5 Inhibition of NF-kB reduces senescence *in vitro* and *in vivo*

To examine the mechanism through which NF-κB inhibition extends healthspan, we examined the role of NF-κB in regulating cellular senescence *in vitro*. Primary mouse embryonic fibroblasts (MEFs) grown at atmospheric oxygen senesce prematurely due to oxidative stress (Parrinello *et al.*, 2003b). DNA repair-deficient *Ercc1*$^{-/-}$ MEFs senesce even earlier than congenic WT cells (Figure 5.9A). This corresponded with increased γH2AX foci (Figure 5.9B), a marker of cellular senescence (Rodier *et al.*, 2011). Deletion (*p65*$^{-/-}$) or p65 heterozygosity (*p65*$^{+/-}$) rescued proliferation and senescence to a large extent (Figure 5.9A and Figure 5.9B). Hepatocytes of *Ercc1*$^{-/\Delta}$ mice show profound cellular senescence (Gregg *et al.*, 2012a). Reduced expression of p65 resulted in a significant reduction in the number of senescent hepatocytes in *Ercc1*$^{-/\Delta}$ mice (Figure 5.9C). In addition, p16^{INK4a} expression was dramatically reduced in the livers of *Ercc1*$^{-/\Delta}$ mice chronically treated with 8K-NBD compared to untreated animals (Figure 5.9D), consistent with the qRT-PCR results (Figure 5.8B). Taken together, these results demonstrate that reducing NF-κB/p65 activity attenuates celluar senescence, at least under conditions of stress.

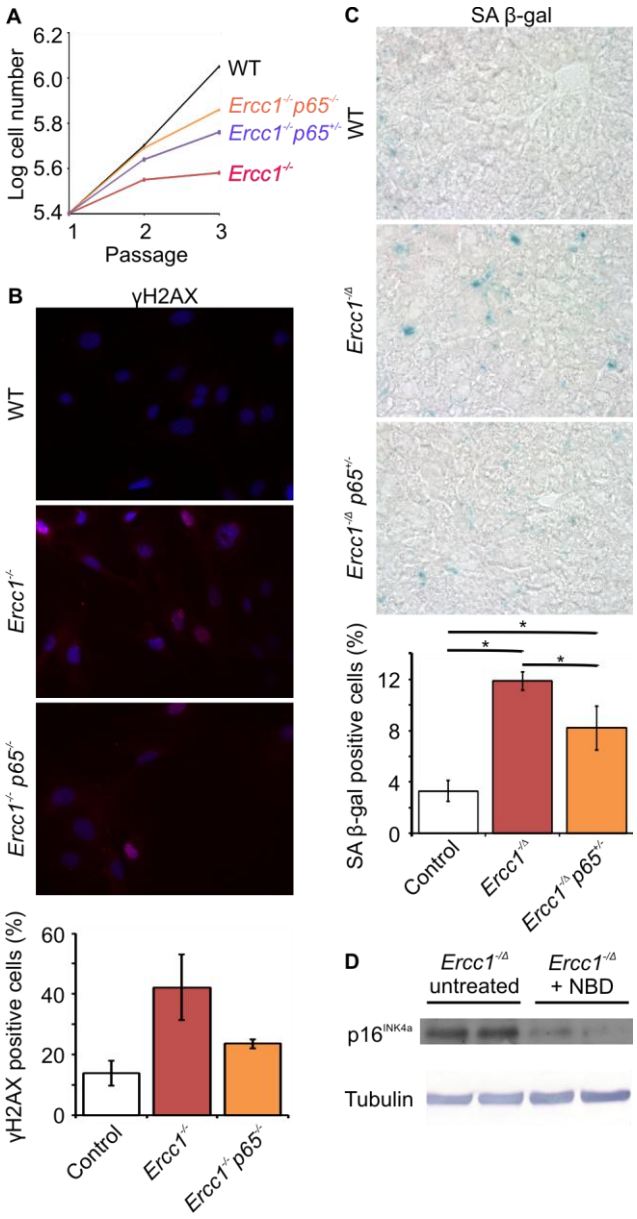

Figure 5.9: **Inhibition of NF-κB reduces cellular senescence *in vitro* and *in vivo***

(**A**) Proliferation of WT (black; n = 4), *Ercc1*$^{-/-}$ (red; n = 3), *Ercc1*$^{-/-}$*p65*$^{+/-}$ (purple; n = 1) and *Ercc1*$^{-/-}$*p65*$^{-/-}$ (orange; n = 3) congenic primary MEFs grown at 20% O_2 for several passages. *Ercc1*$^{-/-}$ MEFs grew slower than WT MEFs, while *Ercc1*$^{-/-}$*p65*$^{-/-}$ MEFs showed better growth compared to *Ercc1*$^{-/-}$ MEFs. (**B**) γH2AX staining (red) of passage 5 WT, *Ercc1*$^{-/-}$ and *Ercc1*$^{-/-}$*p65*$^{-/-}$ primary MEFs grown at 20% O_2. Nuclei were counter-stained with DAPI (blue; 20x objective). Histogram indicating the percent of cells positive for γH2AX foci. (**C**) SA β-gal staining of liver sections from 10 week-old control, *Ercc1*$^{-/\Delta}$ and *Ercc1*$^{-/\Delta}$*p65*$^{+/-}$ mice (40x objective). Histogram indicating the percent of SA β-gal positive cells from five images from at least nine mice per genotype. Values denote the mean ± S.E.M. '*', $p < 0.05$, Tukey-Kramer test. (**D**) Immunodetection of p16 in liver extracts of 19 week-old untreated *Ercc1*$^{-/\Delta}$ and NBD-treated *Ercc1*$^{-/\Delta}$ mice.

5.2.6 Inhibition of NF-κB reduces oxidative stress and damage *in vitro* and *in vivo*

A key driver of cellular senescence is genotoxic stress (Rodier and Campisi, 2011). Hence, we next asked if NF-κB activation in ERCC1-deficient cells regulates oxidative stress. *Ercc1*$^{-/-}$ and *Ercc1*$^{-/-}$*p65*$^{-/-}$ primary MEFs grown at 20% O_2 were stained with $DiOC_6$ (green) to identify mitochondria and MitoSOX (red) to measure superoxide anion in mitochondria. *Ercc1*$^{-/-}$*p65*$^{-/-}$ MEFs had reduced mitochondrial ROS compared to *Ercc1*$^{-/-}$ MEFs (Figure 5.10A). This was supported by the observation that *Ercc1*$^{-/\Delta}$*p65*$^{+/-}$ mice have less lipofuscin in their liver than *Ercc1*$^{-/\Delta}$ mice (Figure 5.10B). Lipofuscin is an accumulation of oxidized fatty acids associated with aging (Fletcher *et al.*, 1973; Siakotos and Koppang, 1973; Tappel, 1973; Taubold, 1975). We also examined the levels of a unique type of oxidatively induced DNA lesions, 8,5'-cyclopurine-2'-deoxynucleosides (cPu), which include 8,5'-cyclo-2'-deoxyadenosine (cdA) and 8,5'-cyclo-2'-deoxyguanosine (cdG). These lesions may serve as reliable biomarkers of oxidative DNA damage because they are rather stable and O_2 inhibits their formation, thus minimizing their artificial generation during DNA extraction and enzymatic digestion (Jaruga and Dizdaroglu, 2008). Levels of all four cPu lesions, i.e., *R*- and *S*-diastereomers of cdG and cdA, were significantly decreased in *Ercc1*$^{-/\Delta}$*p65*$^{+/-}$ mice compared to *Ercc1*$^{-/\Delta}$ littermates (Figure 5.10C). This was also true in *Ercc1*$^{-/\Delta}$ mice chronically treated with 8K-NBD compared to untreated mutant animals (Figure 5.10D) These data provide multiple lines of evidence supporting the conclusion that reduction in NF-κB activity leads to an attenuation of oxidative stress and damage.

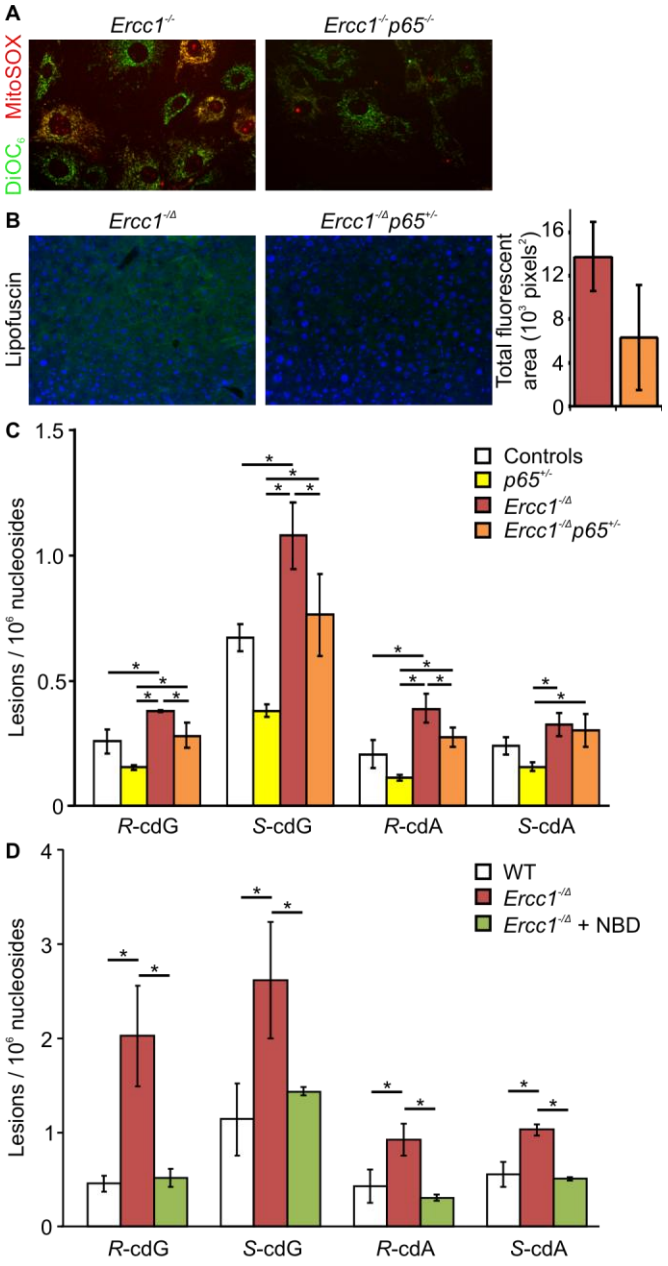

Figure 5.10: Inhibition of NF-κB reduces oxidative stress and damage *in vitro* and *in vivo*

(**A**) *Ercc1*$^{-/-}$ and *Ercc1*$^{-/-}$*p65*$^{-/-}$ passage 6 primary MEFs grown at 20% O_2 were stained with $DiOC_6$ (green) to mark mitochondria and MitoSOX (red) to detect mitochondrial superoxide anion (40x objective). (**B**) Liver sections from 10 week-old *Ercc1*$^{-/\Delta}$ and *Ercc1*$^{-/\Delta}$*p65*+/- mice imaged for lipofuscin fluorescence (20x objective). Histogram indicating the total fluorescent area for five images from three different mice per genotype calculated using MetaMorph software. (**C**) The levels of the (5'R) and (5'S) diastereomers of 8,5'-cyclo-2'-deoxyguanosine (cdG) and 8,5'-cyclo-2'-deoxyadenosine (cdA) in nuclear DNA isolated from the livers of 10 week-old control, *p65*$^{+/-}$, *Ercc1*$^{-/\Delta}$ and *Ercc1*$^{-/\Delta}$*p65*$^{+/-}$ mice. (**D**) The levels of cdG and cdA in nuclear DNA isolated from the livers of 19 week-old control, untreated *Ercc1*$^{-/\Delta}$and 8K-NBD-treated *Ercc1*$^{-/\Delta}$ mice. '*', $p < 0.05$, Tukey-Kramer test. Values denote the mean ± S.E.M. (n = 3 per group).

5.3 DISCUSSION

Time-dependent accumulation of damage to cells and macromolecules is thought to drive aging (Kirkwood, 2005). DNA damage is one type of damage implicated in aging based on the fact that mutations affecting a diverse array of DNA repair mechanisms lead to accelerated aging of one or more tissues (Hasty *et al.*, 2003a). However, what is not known is the mechanism by which, for instance, damage to the nuclear genome drives aging. The mechanism could be via loss of functional cells once a threshold of damage is reached. Alternatively, activation of conserved stress response pathways may promote aging. Herein, we used a well-defined murine system to decipher how damage drives aging: mice that spontaneously age rapidly as a consequence of failure to repair endogenous DNA damage (Dollé *et al.*, 2011; Gregg *et al.*, 2012a; Gregg *et al.*, 2011).

NF-κB is a family of transcription factors activated in response to a diverse array of cellular stressors (Miyamoto, 2011). NF-κB activity increases with chronologic age in a variety of tissues of mammals (Bregegere *et al.*, 2006; Giardina and Hubbard, 2002; Helenius *et al.*, 1996; Korhonen *et al.*, 1997; Xiao and Majumdar, 2000). Thus NF-κB activation could drive aging in response to time-dependent accumulation of cell damage. However, prior studies do not demonstrate a causal relationship between NF-κB activation and aging. Nor do they reveal what drives NF-κB activation with aging.

Using a knock-in NF-κB^{EGFP} reporter system, we discovered a significant increase in the percent of cells in which NF-κB is activated in old and DNA repair-deficient, progeroid mice relative to young WT mice. The progeroid mice had increased EGFP expression in kidney, skeletal muscle, pancreas and liver (Figure 5.1 and Figure 5.2). There was not significantly greater NF-κB activation in the spleen, suggesting that inflammatory cells are not the primary

driver of NF-κB activation. These data strongly support the conclusion that spontaneous, endogenous DNA damage is sufficient to drive NF-κB activation *in vivo*. The resolution afforded by the reporter construct revealed that age-related activation of NF-κB is stochastic, meaning that there is activation in one cell while none is detected in adjacent cells, rather than pan-activation throughout a tissue. This is consistent with the stochastic theory of aging, which posits that cellular damage occurs randomly in a fraction of cells (Kirkwood, 2005).

We also demonstrate a key causal role for NF-κB in driving multiple age-related pathologies. Inhibition of the IKK/NF-κB pathway, genetically through deletion of one copy of *p65* or pharmacologically using an IKK inhibitory peptide, delayed the onset and severity of aging-related pathologies in the musculoskeletal, hepatobiliary, renal, and nervous systems (Figure 5.4D and Figure 5.6D). Aging-related symptoms caused by these pathologies were also delayed or attenuated (Table 5.1 and Table 5.2). This provides strong experimental evidence that an increase of IKK/NF-κB activity plays a causal role in aging.

We further demonstrate that genetic reduction of NF-κB reduces the amount of mitochondrial-derived reactive oxygen species (Figure 5.10A). This could be mediated through upregulation of antioxidants. Expression of catalase and targets of NRF2 are significantly increased in mice chronically treated with the IKK inhibitor 8K-NBD (Figure 5.8) compared to an inactive mutant peptide. In further support of this, oxidative damage to lipids (lipofuscin; Figure 5.10B) and DNA (Figure 5.10C and Figure 5.10D) are significantly reduced in $Ercc1^{-/\Delta}p65^{+/-}$ mice and $Ercc1^{-/\Delta}$ mice chronically treated with the IKK inhibitor, 8K-NBD. This corresponded with a reduction in multiple markers of cellular senescence including reduced proliferation of primary cells, increased γH2AX foci and SA β-gal activity. These data support a mechanism by which accumulated cellular damage (in particular DNA damage) with aging leads

to activation of NF-κB. This in turn drives increased ROS production and even more cellular damage. Inhibiting NF-κB activation in response to stress is sufficient to attenuate damage and extend health a murine model of accelerated aging.

Interestingly, our data indicate that treating *Ercc1*$^{-/\Delta}$ mice with 8K-NBD beginning at five weeks of age has a greater beneficial effect than genetic depletion of p65 from conception. The delay in aging symptoms, the attenuation of osteoporosis, and the maintenance of weight were greater in mice in which NF-κB activity was inhibited pharmacologically compared to genetically. This could be because p65/NF-κB has a positive role during development and/or early in life. Also, *p65* was heterozygous in our mice, and therefore it is possible that the remaining copy of *p65* is sufficient to initiate a stress response. Alternatively, 8K-NBD may be more effective at inhibiting NF-κB in response to stress, possibly because inhibition of IKK would act upstream of p65 and could lead to the cytoplasmic sequestration of more than just the p65 subunit of NF-κB. Targeting IKK also may affect other pathways in addition to NF-κB. For example, IKK phosphorylates BCL10, CTNNB1, CCND1, FOXO3, TP53, ESR1, MTOR and HIF1A in addition to NF-κB (Li *et al.*, 2007; Lim *et al.*, 2009; Scheidereit, 2006; Shtutman *et al.*, 1999).

The magnitude of the effect on healthspan elicited by NF-κB inhibition has only been observed in outbred mice treated with rapamycin (Harrison *et al.*, 2009), which targets the mTOR pathway, or by genetic deletion of S6K1, a downstream target of mTOR (Selman *et al.*, 2009). Interestingly, mTOR has been shown to activate NF-κB via interaction with IKK (Dan *et al.*, 2008). In contrast to the results with rapamycin and our results with NBD, treatment with resveratrol and other SIRT agonists appear only able to extend healthspan and lifespan in mice on high fat diets (Baur *et al.*, 2006).

Interestingly, chronic inhibition of NF-κB with the 8K-NBD peptide caused a dramatic change in gene expression compared to *Ercc1*$^{-/\Delta}$ littermates treated with a less active control peptide. Expression of 5% of all genes was significantly altered. Based on ontology analysis of these genes, the biological process most significantly affected by NF-κB inhibition was the immune response, which was not surprisingly down-regulated. In addition, many processes previously demonstrated to be altered in progeroid or old WT mice, including suppression of the growth hormone/IGF-1 axis, inhibition of cell cycle progression, activation of pro-apoptotic mechanisms and DNA damage/stress response (Niedernhofer *et al.*, 2006), were at least partially corrected by NF-κB inhibition. This provides experimental evidence that NF-κB is indeed a master regulator of aging-related transcriptional reprogramming.

Gene expression analysis also confirmed the efficacy of inhibition of IKK/NF-κB by 8K-NBD, demonstrating decreased expression of numerous genes with known NF-κB promoter sequences including *Gadd45b*, *Ccnd*2, *Ccnd3*, *Bcl2*, *Apod* and *Prkcd* (Gilmore, 2009). The NF-κB regulated genes that were most down-regulated by 8K-NBD were *Apod* and *Gadd45*, both of which have been shown to have roles in cellular senescence and age-related disease (Jackson and Pereira-Smith, 2006; Provost *et al.*, 1991). Similarly, a number of cytokines and other pro-inflammatory genes, expressed by senescent cells (Coppe *et al.*, 2008a), are down-regulated in *Ercc1*$^{-/\Delta}$ mice chronically treated with 8K-NBD, notably *Il16*, *Il17ra*, *Il20*, *Il1r*, *Il15r*, *Il28ra*, *Ildr1* and *Il6st*. 8K-NBD treatment also reduced liver expression of p16 at both mRNA and protein level. Moreover, chronic 8K-NBD treatment significantly upregulated catalase, genes regulated by NRF2, and genes involved in mitochondrial respiration, all important in regulating ROS levels. These observations are consistent with the recent demonstration of a key role for p16-expressing, senescent cells in driving aging, suggesting that 8K-NBD treatment can reduce

senescence (Baker *et al.*, 2011). 8K-NBD treatment also suppressed expression of chemokines known to regulate the trafficking of immune cells during inflammation. Overall, the expression data demonstrate that inhibition of IKK/NF-κB leads to suppression of numerous processes that are known to modulate healthspan including inflammation and cellular senescence.

In conclusion, these studies demonstrate that spontaneous, endogenous DNA damage can activate NF-κB. Activation of NF-κB is stochastic, occurring only in a subset of cells. Chronic inhibition of IKK/NF-κB activation is sufficient to delay the onset of aging symptoms and chronic aging-related diseases that arise spontaneously in DNA repair–deficient *Ercc1*$^{-/\Delta}$ mice that model a human progeroid syndrome. Moreover, inhibiting NF-κB activation reduces ROS production and oxidative damage to lipids and DNA. This demonstrates a direct causal role for NF-κB in driving aging-related changes in response to cellular damage by promoting continued damage. Inhibition of NF-κB offers a novel strategy for simultaneously delaying and/or attenuating multiple chronic degenerative diseases in progeroid patients and potentially in old age.

5.4 MATERIALS AND METHODS

5.4.1 Mice

Ercc1$^{-/-}$ and *Ercc1*$^{-/\Delta}$ mice were generated in an f1 hybrid background by crossing heterozygous *Ercc1*$^{+/-}$ and *Ercc1*$^{+/\Delta}$ mice from two different inbred C57Bl/6J and FVB/n backgrounds, to obtain genetically identical mice without strain-specific pathology. The mice were genotyped using PCR as previously described (Ahmad *et al.*, 2008). *Ercc1*$^{-/-}$NF-κB^{EGFP} mice were generated by crossing *Ercc1*$^{+/-}$ C57Bl/6J mice with NF-κB^{EGFP} mice (provided by Christian Jobin, UNC Chapel Hill) (Karrasch *et al.*, 2007). These mice were then bred with *Ercc1*$^{+/-}$ FVB/n to generate *Ercc1*$^{-/-}$NF-κB^{EGFP} mice. *p65*$^{+/-}$ mice were bred with *Ercc1*$^{+/-}$ C57Bl/6J mice. These were then bred with *Ercc1*$^{+/\Delta}$ FVB/n to generate *Ercc1*$^{-/\Delta}$*p65*$^{+/-}$ mice.

5.4.2 Isolation and treatment of mouse embryonic fibroblasts

Double heterozygous mice were bred to yield WT, *Ercc1*$^{-/-}$, *Ercc1*$^{-/-}$*p65*$^{+/-}$ and *Ercc1*$^{-/-}$*p65*$^{-/-}$ pups for isolation of primary mouse embryonic fibroblasts (MEFs) as previously described (Niedernhofer *et al.*, 2006). The cells were grown in 1:1 DMEM:Ham's F10 supplemented with 10% FBS, 1%, penicillin and streptomycin and 1% non-essential amino acids. They were passaged 5 times at 20% oxygen prior to fractionation using the NE-PER Cytoplasmic and Nuclear Extraction Reagent Kit (ThermoFisher Scientific, Rockford, IL) for Western blot analysis or EMSA. For 8K-NBD treatment, cells were incubated with 200μM 8K-NBD for 3 hours prior to collection and immunoblotting for p-p65.

5.4.3 Nuclear extracts and Western blotting

Immunodetection of activated NF-κB and IκB in nuclear and cytoplasmic cell fractions was performed as previously described (Xiong *et al.*, 2004) using anti-p-p65 (93H1), anti-p-IκBα (5A5) (Cell Signaling, Danvers, MA) and anti-IκBα (sc371; Santa Cruz Biotechnology, Santa Cruz, CA). Anti-lamin A/C (sc20681; Santa Cruz Biotechnology, Santa Cruz, CA) and anti-β-actin (Abcam, Cambridge, MA) antibodies were used as loading controls for the nuclear and cytoplasmic fractions, respectively. Immunodetection of $p16^{INK4a}$ from liver extracts was performed using anti-$p16^{INK4a}$ antibody (sc1207; Santa Cruz Biotechnology, Santa Cruz, CA) with anti-tubulin (ab4074, Abcam, Cambridge, MA) as a loading control. All primary antibodies were used at a 1:1000 dilution and an overnight incubation at 4°C.

5.4.4 Electrophoretic mobility shift assay (EMSA)

EMSA was completed based on a modified protocol described in (Reay *et al.*, 2011). Briefly, nuclear cellular fractions were extracted from MEFs using NE-PER Cytoplasmic and Nuclear Extraction Reagent Kit (ThermoFisher Scientific, Rockford, IL). 5 µg of each extract was mixed with 2 µL of 5X Gel Shift Binding Buffer (Promega, Madison, WI) and nuclease-free distilled water in a 9 µL final volume. This was followed by incubation with an α-^{32}P-deoxycytodine triphosphate radiolabeled DNA probe containing the NF-κB binding domain (MP Biomedicals, Solon, OH). The design of the NF-κB probe was described previously (Guttridge *et al.*, 1999). The oligonucleotide sequences are as follows, with the DNA binding sequence underlined: NF-κB template: 5′-CAGGGCTGGGGATTCCCCATCTCCACAGTTTCACTTC-3′; NF-κB annealing: 5′-GAAGTGAAACTGTGG-3′ (Integrated DNA Technologies, Inc., Coralville, IA).

dNTPs used to fill the overhangs were added using DNA Polymerase I, Large (Klenow) Fragment (Invitrogen, Carlsbad, CA) and the reaction was purified using illustra MicroSpin G50 columns (GE Healthcare, Piscataway, NJ). Probes were added at a count per minute (cpm) of ~150,000 in 1 μL, followed by separation on a 6% non-denaturing polyacrylamide gel. For competition assays 2 μl of 100 μg/ml antibodies against p65/RelA and p50 were added to nuclear extracts and incubated for 20 minutes, prior to the addition of the duplex oligonucleotide.

5.4.5 Fluorescence microscopy

To quantify NF-κB activity, EGFP expression was measured in tissues, using Metamorph software (MDS Analytical Technologies, Sunnyvale, CA). Five 20X images were taken of each tissue analyzed for each mouse (n=6 per genotype, age) and the percent of cells expressing EGFP was quantified based on tissue area. This was reported as the fold increase in the number of EGFP+ cells above the average value for controls. Anti-GFAP (13-0300; Invitrogen, Carlsbad, CA) was used at a 1:250 dilution and incubated overnight at 4°C. Anti-p-H2AX (05-636 Millipore, Billerica, MA) was used at a 1:500 dilution and incubated overnight at 4˚C. For lipofuscin analysis, five 40X images were taken of liver sections from control, *Ercc1*$^{-/\Delta}$ and *Ercc1*$^{-/\Delta}$*p65*$^{+/-}$ mice sacrificed at 10 weeks of age (n=3 per genotype). To quantify lipofuscin, the total green fluorescent area was quantified using Metamorph software. This was then reported as the average total area between the mice in the group.

5.4.6 Cell proliferation measurement

Proliferation was assessed as previously described (Ahmad *et al.*, 2008). Briefly, WT and mutant MEFs were plated at a density of 0.25 x 10^6 per 6cm dish. Cells were trypsinized at confluence, counted, and replated at the same density until mutant cells stopped growing. The total number of cells at each passage was calculated as follows: [(no. of cells at previous passage/no. of cells plated) x no. of cells at current passage]. The total cell number was plotted as the log cell number.

5.4.7 Senescence-associated β-galactosidase

Fixed liver sections from control, *Ercc1*$^{-/\Delta}$ and *Ercc1*$^{-/\Delta}$*p65*$^{+/-}$ mice sacrificed at 10 weeks of age (n>9 per genotype) were stained for senescence-associated β-galactosidase as described previously (Debacq-Chainiaux *et al.*, 2009). Five 40X images per mouse were taken on brightfield (SA β-gal) and DAPI staining was use to count total cell number per section. The percent of cells that were senescent for each animal was averaged and plotted using standard error of the mean for error calculation.

5.4.8 Measurement of reactive oxygen species *in vitro*

To measure superoxide anion levels, *Ercc1*$^{-/-}$*p65*$^{-/-}$ and *Ercc1*$^{-/-}$ MEFs were grown to 80-90% confluency and rinsed with PBS. Media was replaced with serum-free media containing 5μM MitoSOX™ reagent (M36008, Invitrogen, Carlsbad, CA) and 2.5μM $DiOC_6$ (D273, Invitrogen,

Carlsbad, CA). Cells were incubated for 25 minutes at 37°C. They were then washed twice with PBS, replaced with media containing serum, and imaged immediately.

5.4.9 Measurement of 8,5'-cyclopurine-2'-deoxynucleosides in nuclear DNA of mouse livers

Nuclear DNA was isolated from mouse livers using a high-salt method (Miller *et al.*, 1988b) and analyzed for DNA damage as described previously (Wang *et al.*, 2011a). In brief, nuclear DNA was digested using a four-enzyme cocktail, and to the digestion mixture was added uniformly ^{15}N-labeled cdA and cdG. The resulting nucleoside mixture was subjected to off-line high performance liquid chromatography (HPLC) separation for the enrichment of the lesions under study, following previously described procedures (Wang *et al.*, 2011a). The LC-MS/MS/MS experiments were conducted using an LTQ linear ion trap mass spectrometer using recently described conditions (Wang *et al.*, 2011a).

5.4.10 Peptides

8K-NBD (KKKKKKKKGGTALDWSWLQTE) and inactive 8K-mutant NBD (8K-mNBD) (KKKKKKKKGGTALDASALQTE) were synthesized at the University of Pittsburgh Peptide facility. Peptides were dissolved in DMSO at 40μM and stored at -80°C until dilution in PBS directly before use.

5.4.11 NBD treatment of animals

Sibling pairs of *Ercc1*$^{-/\Delta}$ mice housed in a single cage were treated with 8K-NBD or 8K-mNBD 10mg/kg three times per week intraperitoneally by an investigator blinded as to the treatment group. Treatment began at 5 weeks of age before the animals were symptomatic and continued throughout their lifespan. Mice were euthanized via CO_2 inhalation at 12 or 18-20 weeks of age and tissues isolated for histopathological analysis.

5.4.12 Phenotype and weight measurements

Mice were weighed biweekly and assessed for the onset of characteristic progeroid symptoms including kyphosis, dystonia, trembling, ataxia, and urinary incontinence due to neurodegeneration, muscle wasting and reduced spontaneous activity due to frailty. The aging score is an overall measurement of the quality of life or healthspan and reflects the fraction of symptoms that occurred later in mice with reduced IKK/NF-κB activity. The aging score was determined as follows. For each symptom, the mouse in which the symptom was delayed received a score of +1 and the control littermate a score of 0. If the symptoms occurred simultaneously in both mice, both mice received score of 0. The sum of score for each animal was divided by the number of symptoms measured to determine the fraction of symptoms delayed. This number was plotted for each animal as well as average determined for each treatment group to give an overall aging score.

5.4.13 Immunohistochemistry

Tissues were fixed in 10% formalin overnight, embedded in paraffin and sectioned using a microtome by standard procedures. Haematoxylin and eosin staining was done according to standard procedures. Fixed frozen sections of liver were stained for oil red O by the following procedure. Slides were rinsed in running tap water for 10 min, rinsed with 60% isopropanol, stained with oil red O for 15 min, rinsed with 60% isopropanol, counterstained by dipping 15 times in haematoxylin, rinsed with distilled water and mounted with gelvatol.

5.4.14 Micro-computed tomography

Micro-computed tomography of the spines isolated from WT and *Ercc1*$^{-/\Delta}$ mice littermates were acquired using a VivaCT 40 (Scanco USA, Inc, Wayne, PA) with 15 μm isotropic voxel size resolution, 55 kVp of energy and 145 μA of current. After the acquisition of transverse two-dimensional image slices, three-dimensional reconstruction of the lumbar vertebrae was performed using a constant threshold value of 235, which was selected manually for the bone voxels by visually matching the threshold areas to the gray-scale images.

5.4.15 Microarray

Genome-wide expression was measured in mice treated with 8K-NBD or 8K-mNBD, as previously described (Niedernhofer *et al.*, 2006). All significant gene entries were subjected to GO classification (http://www.geneontology.org). Significant overrepresentation of pathways and gene networks was determined by DAVID (http://david.abcc.ncifcrf.gov/summary.jsp;

through BBID, BIOCARTA and KEGG annotations), as well as by means of the ingenuity pathway analysis software (IPA) (www.ingenuity.com). Microarray data is available on ArrayExpress (E-MEXP-3615).

5.4.16 Statistics overview

To determine significance a two-tailed Student's *t*-test was used with *p*-values of less than 0.05 considered significant. In addition, higher levels of significance ($p < 0.01$; $p < 0.001$) are indicated in a Table 5.3. For analysis of experiments involving more than two groups, ANOVA with a post-hoc Tukey-Kramer test was performed to determine significance (McDonald, 2009; Schumacher *et al.*, 2008). For the microarray data, significant overrepresentation of pathways and gene networks was determined by DAVID (http://david.abcc.ncifcrf.gov/summary.jsp; through BBID, BIOCARTA and KEGG annotations), as well as by means of the ingenuity pathway analysis software (IPA) (www.ingenuity.com).

5.4.17 Study approval

Experiments involving mice were reviewed and approved by the University of Pittsburgh (Pittsburgh, PA) Institutional Animal Care and Use Committee and in accord with the National Institutes of Health guidelines for the humane care of animals.

6.0 OVERALL CONCLUSIONS AND FUTURE DIRECTIONS

The overarching goal of my dissertation was to address the contribution that DNA interstrand crosslinks have on aging. In order to address this problem, I took a genetic approach using a mouse model deficient in the DNA repair endonuclease, ERCC1-XPF. Mutations in this protein complex result in premature aging of mice and men (de Waard *et al.*, 2010; Goss *et al.*, 2011; Gregg *et al.*, 2012a; Jaspers *et al.*, 2007; Niedernhofer *et al.*, 2006; Vo *et al.*, 2010). One advantage to using this mouse model was the elimination of genetic and environmental variables that can complicate analyses and produce confounding results. The only difference between the mice used in these studies was the mutation in the alleles of *Ercc1*. Therefore, differences that were observed can be directly attributed to the effects of DNA damage.

ERCC1-deficient mice have been shown to mimic natural aging in multiple organ systems (de Waard *et al.*, 2010; Goss *et al.*, 2011; Gregg *et al.*, 2012a; Vo *et al.*, 2010). Therefore, because they rapidly, but predictably, age over the course of seven months (de Waard *et al.*, 2010), rather than the normal murine lifespan of three years, ERCC1-deficient mice present a valuable tool to study the acceleration or delay of aging symptoms in a shortened timeframe.

Data presented herein demonstrate that DNA interstrand crosslinks can promote age-related degeneration and that amelioration of endogenous sources of DNA damage can result in improved healthspan. Chapter 2.0 addressed whether DNA interstrand crosslinks could promote

age-related degeneration *in vitro* and *in vivo*. This demonstrates for the first time that cytostasis (senescence), rather than cytotoxicity (cell death), promotes age-related decline in the liver, kidney and brain, and presents a mechanism by which cancer survivors experience symptoms of accelerated aging years after chemotherapeutic treatment. The results show that increased DNA damage and senescence can be induced by a crosslinking agent, while a monoadducting, structurally similar compound, promotes cell death through apoptosis. Additionally, age-related symptoms of ERCC1-deficient mice can be accelerated by treatment with a crosslinking agent. Taken together, these data indicate that long-term side effects of premature aging can occur as a result of cytostasis induced by the crosslinking compound.

This study on the cytostatic nature of crosslinking agents raises an important issue of whether cancer treatment could be applied with the goal of inducing cytostasis, rather than cytotoxicity. Recent studies have shown that senescent cells secrete cytokines, chemokines, growth factors, cell surface molecules, and survival factors that promote senescence in surrounding cells (Coppe *et al.*, 2008b). Human tumor cells are able to senesce, *in vitro* and *in vivo*, in response to genotoxic chemotherapeutic agents (Coppe *et al.*, 2008b). A study of prostate cancer biopsies before and after treatment with the DNA crosslinking agent, mitoxantrone, confirmed that the senescence-associated secretory phenotype (SASP) can be induced by crosslinking chemotherapy (Coppe *et al.*, 2008b). Therefore, the SASP could be promoting the accelerated aging symptoms that result from treatment with crosslinking agents. An interesting study would be to cross ERCC1-deficient mice with INK-ATTAC mice (mice that clear $p16^{INK4a}$ expressing cells) (Baker *et al.*, 2011). $P16^{INK4a}$ is a tumor suppressor involved in cell cycle regulation. Increased expression of $p16^{INK4a}$ results in reduced proliferative capacity and senescence (Kim and Sharpless, 2006). Crossing INK-ATTAC mice to ERCC1-deficient mice

would eliminate $p16^{INK4a}$-positive senescent cells and is proposed to slow the progression of the accelerated aging of these mice. In addition, the combined mutant mice could then be treated with crosslinking agents and the progression of their aging symptoms could be monitored. It is proposed that the elimination of the $p16^{INK4a}$-positive cells would considerably slow the premature aging of *Ercc1*$^{-/\Delta}$ mice.

Chapter 3.0 addressed whether mitochondrial-produced reactive oxygen species (ROS) are an endogenous source of DNA ICLs. The amount of DNA damage and resulting genetic mutations found in the nuclear genome increases with age in a variety of tissues in aged organisms (Dolle *et al.*, 2002; Hamilton *et al.*, 2001; Mecocci *et al.*, 1999; Wang *et al.*, 2012). In addition, mitochondria are the main source of ROS, due to normal cellular respiration (Doig *et al.*, 2006; Tronche *et al.*, 2002), some of which can diffuse throughout the cell damaging lipids, DNA, RNA and proteins (Chakravarti and Chakravarti, 2007; Cooke *et al.*, 2003; Cui *et al.*, 2012; Mandavilli *et al.*, 2002). We found that targeting a radical scavenger directly to the mitochondria reduced the amount of nuclear oxidative DNA damage. In fact, we found that not only was DNA damage reduced by treatment with XJB, but aging-associated symptoms and pathologies in *Ercc1*$^{-/\Delta}$ mice were also delayed supporting the hypothesis that ROS-induced crosslinks are a potential source of endogenous DNA damage that drives aging.

Future plans should include directly measuring ROS through spin trap assays and 2',7'-dichlorofluorescein diacetate (DCFDA) fresh tissue assays. Preliminary DCFDA data show that there is a significant increase of ROS in liver extracts of *Ercc1*$^{-/\Delta}$ mice. Measuring ROS in tissues from mice treated with XJB would directly show that the radical scavenger can deplete harmful ROS in various tissues throughout the organism. In addition, ERCC1-deficient mice could be crossed with mice that overexpress superoxide dismutase to genetically deplete ROS.

As we found a delay of neurodegenerative phenotypes in the ERCC1-deficient mice treated with XJB, previous studies have indicated that superoxide dismutase overexpressing mice can rescue neurodegenerative phenotypes (Massaad *et al.*, 2009).

Chapter 4.0 of my dissertation investigated lipid peroxidation (LPO) as a potential endogenous source of DNA ICLs. To induce LPO, mice were treated with a sub-lethal dose of CCl_4 or a diet high in polyunsaturated fatty acids (PUFAs). Lipid hydroperoxides, one byproduct of LPO, are increased in both normally and prematurely aged mice (Tokumaru *et al.*, 1996). In fact, CCl_4 treatment of *Ercc1*$^{-/\Delta}$ mice resulted in a further increase of lipid hydroperoxide. This coincided with extreme exaggeration of aging-associated liver pathologies. Similar changes, though to a much lesser extent were observed in the liver of *Ercc1*$^{-/\Delta}$ mice fed a diet high in PUFAs. Analysis of kidneys from the ERCC1-deficient mice fed the high PUFA diet also showed aging-related histopathological changes.

As previously discussed, future studies will include analyzing additional tissues from these mice. Furthermore, tissues should also be analyzed for the mechanism that leads to the acceleration of the *Ercc1*$^{-/\Delta}$ aging phenotype. TUNEL and cleaved caspase-3 staining can be completed to identify whether apoptosis plays a role. However, based on data from the mechlorethamine study, cellular senescence is likely the cause. Unfortunately, senescence markers require either fixed frozen or snap frozen tissues, which are unavailable from these mice. Therefore, repeating CCl_4 treatment of the mice would be beneficial, not only to obtain samples for senescence analyses, but this would also allow for LPO to be measured overtime to determine if there is a critical level of lipid peroxidation that the mice must pass before they exhibit increased pathologies and symptoms associated with aging. If this is the case, additional interventional studies could be completed, to investigate whether treating mice at later

timepoints, before the threshold is hit, would rescue or delay the acceleration of age-associated symptoms and pathologies.

Finally, chapter 5.0 in my dissertation investigated the role in NF-κB and aging. We found that NF-κB is increased in both normal and prematurely aged mice. In addition, DNA damage activates NF-κB, which promotes aging. Futhermore, by both genetic and pharmacologic inhibition of NF-κB, we were able to delay symptoms and pathologies associated with advanced age in the *Ercc1*$^{-/\Delta}$ mice.

Because NF-κB was found to only be activated in a subset of cells in a stochastic manner within various tissues, additional studies are underway to pinpoint the individual cell types in which NF-κB is activated. Future studies should focus on treating NF-κB^{EGFP} reporter mice with XJB to determine if a reduction in ROS can also attenuate NF-κB activation. This would help to reveal the order of events during the process of senescence.

My studies have revealed a cytostatic mechanism of premature aging in relation to increased DNA damage. In addition, we have shown that viable therapeutic approaches exist that could present novel methods to delay and attenuate the symptoms of aging, thereby increasing the quality of life in old age.

7.0 PUBLIC HEALTH PERSPECTIVE

Between 2000 and 2030, as a result of the aging "baby boom" generation, the number of older Americans (age 65 and over) is expected to double and comprise nearly 20% of the total population (Greenberg, 2011; Gregg *et al.*, 2012a). In addition, the biggest risk factor for a number of diseases including cancer, heart disease, arthritis, and dementia is advanced age (Resnick and Dosa, 2004). In light of the projected increase in the population of older Americans, the cost of healthcare will skyrocket and is projected to reach $4.6 trillion by 2020, a two-fold increase since 2008 (2012b). Consequently, identifying the causes of aging and strategies to ameliorate aging-related diseases, while preserving tissue homeostasis, is a pressing public health issue.

Furthermore, because early clinical chemotherapy trials were started in the late 1970s and early 1980s, only now has long-term toxicity become evident in cancer survivors (Maccormick, 2006). Patients have suffered from a number of health problems that are typically associated with advanced age, including neurodegenerative, musculoskeletal and osteoporotic symptoms, as well as skin changes and fatigue. Therefore, chemotherapies have been identified as a possible source of premature aging in long-term cancer survivors (Grillari *et al.*, 2007; Maccormick, 2006). Our studies, utilizing DNA-repair deficient mice that age rapidly address both of these needs, enabling us to test hypotheses about the causes of aging, how DNA damage contributes to aging,

and also to identify things in our environment (exposures and diets) that lead to DNA damage, which if avoided could promote improved health in old age.

APPENDIX

PUBLICATIONS

Robinson, A.R.*, Tilstra, J.S.*, Wang, J.*, Gregg, S.Q.*, Clauson, C.L.*, Reay, D., Nasto, L.A., St. Croix, C., Usas, A., Vo, N., Huard, J. Clemens, P., Stoltz, D.B., Gutteridge, D.C., Watkins, S.C., Garinis, G.A., Wang, Y., Niedernhofer, L.J., and P.D. Robbins, P.D. (2012) Inhibition of NF-κB transcriptional activation delays the onset of age-related degenerative disease. *Journal of Clinical Investigation* (accepted).

Nasto, L.A., Seo, H.Y., **Robinson, A.R.,** Tilstra, J.S., Clauson, C.L., Sowa, G.A., Ngo, K., Dong, Q., Pola, E., Lee, J.Y., Niedernhofer, L.J., Kang, J.D., Robbins, P.D., and N. Vo. (2012) Inhibition of NF-κB activity ameliorates age-associated disc degeneration in a mouse model of accelerated aging. *Spine* (accepted). PMID: 22343279

Smith, S.C., **Robinson, A.R.,** Niedernhofer, L.J. and M. Hetman (2012) Down-regulation of cholesterol biosynthesis in forebrains of ERCC1-deficient mice. *Neurobiology of Disease.* 45, 1136-1144. PMID: 22245387.

Lavasani, M., **Robinson, A.R.,** Lu, A., Song, M., Feduska, J.M., Ahani, B., Tilstra, J.S., Feldman, C.H., Robbins, P.D., Niedernhofer, L.J.*, J. Huard* (2012) Muscle-derived stem/progenitor cell dysfunction limits healthspan and lifespan in a murine progeria model. *Nature Communications.* 3, 608. PMID: 22215083.

Gregg, S.Q., Gutierrez, V., **Robinson, A.R.,** Woodell, T., Nakao, A., Ross, M., Michalopolous, G., Rigatti, L., Rothermel, C.E., Stolz, D.B. and L.J. Niedernhofer. (2011). A mouse model of accelerated liver aging due to a defect in DNA repair. *Hepatology* 55, 609-621. PMID: 21953681.

Gregg, S.Q., **Robinson, A.R.** and L.J. Niedernhofer. (2011). Physiological consequences of defects in ERCC1-XPF DNA repair endonuclease. *DNA Repair (Amst)* 10, 781-791. PMID: 21612988.

Goss, J.R., Stolz, D.B., **Robinson, A.R.,** Zhang, M., Arbujas, N., Robbins, P.D., Glorioso, J.C. and L.J. Niedernhofer. (2011). Premature aging –related peripheral neuropathy in a mouse model of progeria. *Mechanisms of Ageing and Development.* PMID: 21596054.

Matoka, D.J., Yao, V., Harya, D.S., Gregg, J.L., **Robinson, A.R.,** Niedernhofer, L.J., Parwani, A., Maier, C., and D.J. Bacich (2011) Deficiency of DNA repair nuclease ERCC1-XPF promotes prostate cancer progression in a tissue recombination model. *The Prostate*. PMID: 22212909.

Vo, N., Seo, H.Y., **Robinson, A.,** Sowa, G., Bentley, D., Taylor, L., Studer, R., Usas, A., Huard, J., Alber, S., Watkins, S.C., Lee, J., Coehlo, P., Wang, D., Loppini, M., Robbins, P.D., Niedernhofer, L.J. and J. Kang. (2010). Accelerated aging of intervertebral discs in a mouse model of progeria. *Journal of Orthopaedic Research.* 28, 1600-1607. PMID: 20973062.

Schumacher, B., van der Pluijm, I., Moorhouse, M.J., Kosteas, T., **Robinson, A.R.,** Suh, Y., Breit, T.M., van Steeg, H., Niedernhofer, L.J., van Ijcken, W., Bartke, A., Spindler, S.R., Hoeijmakers, J.H., van der Horst, G.T. and G.A.Garinis. (2008). Delayed and accelerated aging share common longevity assurance mechanisms. *PLoS Genetics*. 4, e1000161. PMID: 18704162.

Ahmad, A., **Robinson, A.R.,** Duensing, A., van Drunen, E., Beverloo, H.B., Weisberg, D.B., Hasty, P., Hoeijmakers, J.H. and L.J. Niedernhofer. (2008). ERCC1-XPF endonuclease facilitates DNA double-strand break repair. *Molecular and Cellular Biology.* 28: 5082-5092. PMID: 18541667.

Jaspers, N.G.J., Raams, A., Silengo, M.C., Wijgers, N., Niedernhofer, L.J., **Robinson, A.R.,** Giglia,-Mari, G., Hoogstraten, D., Hoeijmakers, J.H.J, and W. Vermeulen (2007) First case of human ERCC1 deficiency displays a mild defect in nucleotide excision repair but severe developmental failure. *American Journal of Human Genetics.* 80(3):457-66. PMID: 17273966.

Niedernhofer, L.J., Garinis, G.A., Raams, A., Lalai, A.S., **Robinson, A.R.,** Appeldoorn, E., Lalai, A., Odijk, H., Oostendorp, R., Ahmad, A., van Leeuwen, W., Theil, A.F., van der Horst, G.T.J., Vermeulen, W., Meinecke, P., Kleijer, W.J., Vijg, J., Jaspers, N.G.J., and J.H.J. Hoeijmakers (2006) A novel progeroid syndrome reveals that genotoxic stress suppresses the somatotroph axis. *Nature.* 444(7122):1038-43. PMID: 17183314.

BIBLIOGRAPHY

(1992). Carbon Tetrachloride. In Technology Transfer Network (U.S. Environmental Protection Agency).

(2001a). Summary of the toxicity assessment of carbon tetrachloride, S.A.B.o.T.A. Pollutants, ed. (Raleigh, NC).

(2001b). World Population Ageing: 1950-2050, D.o.E.a.S. Affairs, ed. (New York, NY)).

(2009). Cadmium Compounds. Hazardous Substances Data Bank *TOXNET*, http://toxnet.nlm.nih.gov/. Accessed 5/4/2012.

(2011a). Healthy Aging: Fact Sheet, N.C.o. Aging, ed. (Washington, D.C.).

(2011b). USDA National Nutrient Database for Standard Reference (USDA, Agricultural Research Service)).

(2012a). Melphalan. In MedlinePlus (Bethesda, MD, U.S. National Library of Medicine).

(2012b). National Health Expenditure Projections 2010-2020, C.f.M.M. Services, ed. (Baltimore, MD, Office of the Actuary).

Acharyya, S., Villalta, S.A., Bakkar, N., Bupha-Intr, T., Janssen, P.M., Carathers, M., Li, Z.W., Beg, A.A., Ghosh, S., Sahenk, Z., *et al.* (2007). Interplay of IKK/NF-kappaB signaling in macrophages and myofibers promotes muscle degeneration in Duchenne muscular dystrophy. J Clin Invest *117*, 889-901.

Adair, G.M., Rolig, R.L., Moore-Faver, D., Zabelshansky, M., Wilson, J.H., and Nairn, R.S. (2000). Role of ERCC1 in removal of long non-homologous tails during targeted homologous recombination. EMBO J *19*, 5552-5561.

Adler, A., Sinha, S., Kawahara, TLA., Zhang, JY., Segal, E., Chang, HY. (2007). Motif module map reveals enforcement of aging by continual NF-kB activity. Genes Dev *21*.

Ahmad, A., Enzlin, J.H., Bhagwat, N.R., Wijgers, N., Raams, A., Appledoorn, E., Theil, A.F., JH, J.H., Vermeulen, W., NG, J.J., *et al.* (2010). Mislocalization of XPF-ERCC1 nuclease contributes to reduced DNA repair in XP-F patients. PLoS Genet *6*, e1000871.

Ahmad, A., Robinson, A.R., Duensing, A., van Drunen, E., Beverloo, H.B., Weisberg, D.B., Hasty, P., Hoeijmakers, J.H., and Niedernhofer, L.J. (2008). ERCC1-XPF endonuclease facilitates DNA double-strand break repair. Mol Cell Biol *28*, 5082-5092.

Al-Minawi, A.Z., Saleh-Gohari, N., and Helleday, T. (2008). The ERCC1/XPF endonuclease is required for efficient single-strand annealing and gene conversion in mammalian cells. Nucleic Acids Res *36*, 1-9.

Ames, B.N. (1989). Endogenous DNA damage as related to cancer and aging. Mutat Res *214*, 41-46.

Andersen, S.L., Bergstralh, D.T., Kohl, K.P., LaRocque, J.R., Moore, C.B., and Sekelsky, J. (2009). Drosophila MUS312 and the vertebrate ortholog BTBD12 interact with DNA structure-specific endonucleases in DNA repair and recombination. Mol Cell *35*, 128-135.

Anderson, S.K., and Walker, E.B. Medicinal Chemistry. In Anticancer Drugs.

Andrew, W. (1962). An electron microscope study of age changes in the liver of the mouse. Am J Anat *110*, 1-18.

Arase, S., Kozuka, T., Tanaka, K., Ikenaga, M., and Takebe, H. (1979). A sixth complementation group in xeroderma pigmentosum. Mutat Res *59*, 143-146.

Astorg, P., Arnault, N., Czernichow, S., Noisette, N., Galan, P., and Hercberg, S. (2004). Dietary intakes and food sources of n-6 and n-3 PUFA in French adult men and women. Lipids *39*, 527-535.

Auerbach, A.D. (2009). Fanconi anemia and its diagnosis. Mutat Res *668*, 4-10.

Axelrad, J.E., Louis, E.D., Honig, L.S., Flores, I., Ross, G.W., Pahwa, R., Lyons, K.E., Faust, P.L., and Vonsattel, J.P. (2008). Reduced Purkinje cell number in essential tremor: a postmortem study. Arch Neurol *65*, 101-107.

Bae, Y.S., Oh, H., Rhee, S.G., and Yoo, Y.D. (2011). Regulation of reactive oxygen species generation in cell signaling. Mol Cells *32*, 491-509.

Baker, B.S., Carpenter, A.T., and Ripoll, P. (1978). The Utilization during Mitotic Cell Division of Loci Controlling Meiotic Recombination and Disjunction in DROSOPHILA MELANOGASTER. Genetics *90*, 531-578.

Baker, D.J., Wijshake, T., Tchkonia, T., LeBrasseur, N.K., Childs, B.G., van de Sluis, B., Kirkland, J.L., and van Deursen, J.M. (2011). Clearance of p16Ink4a-positive senescent cells delays ageing-associated disorders. Nature *479*, 232-236.

Balaban, R.S., Nemoto, S., and Finkel, T. (2005). Mitochondria, oxidants, and aging. Cell *120*, 483-495.

Bardwell, A.J., Bardwell, L., Tomkinson, A.E., and Friedberg, E.C. (1994). Specific cleavage of model recombination and repair intermediates by the yeast Rad1-Rad10 DNA endonuclease. Science *265*, 2082-2085.

Baur, J.A., Pearson, K.J., Price, N.L., Jamieson, H.A., Lerin, C., Kalra, A., Prabhu, V.V., Allard, J.S., Lopez-Lluch, G., Lewis, K.*, et al.* (2006). Resveratrol improves health and survival of mice on a high-calorie diet. Nature *444*, 337-342.

Behl, C. (1999). Alzheimer's disease and oxidative stress: implications for novel therapeutic approaches. Prog Neurobiol *57*, 301-323.

Berenbaum, F. (2004). Signaling transduction: target in osteoarthritis. Curr Opin Rheumatol *16*, 616-622.

Berger, F., Paulmurugan, R., Bhaumik, S., and Gambhir, S.S. (2008). Uptake kinetics and biodistribution of 14C-D-luciferin--a radiolabeled substrate for the firefly luciferase catalyzed bioluminescence reaction: impact on bioluminescence based reporter gene imaging. Eur J Nucl Med Mol Imaging *35*, 2275-2285.

Berneburg, M., Clingen, P.H., Harcourt, S.A., Lowe, J.E., Taylor, E.M., Green, M.H., Krutmann, J., Arlett, C.F., and Lehmann, A.R. (2000). The cancer-free phenotype in trichothiodystrophy is unrelated to its repair defect. Cancer Res *60*, 431-438.

Bhagwat, N., Olsen, A.L., Wang, A.T., Hanada, K., Stuckert, P., Kanaar, R., D'Andrea, A., Niedernhofer, L.J., and McHugh, P.J. (2009). XPF-ERCC1 participates in the Fanconi anemia pathway of cross-link repair. Mol Cell Biol *29*, 6427-6437.

Bosma, P.T., van Eert, S.J., Jaspers, N.G., Stoter, G., and Nooter, K. (2003). Functional cloning of drug resistance genes from retroviral cDNA libraries. Biochem Biophys Res Commun *309*, 605-611.

Brack, A.S., Conboy, M.J., Roy, S., Lee, M., Kuo, C.J., Keller, C., and Rando, T.A. (2007). Increased Wnt Signaling During Aging Alters Muscle Stem Cell Fate and Increases Fibrosis. Science *317*, 807-810.

Bregegere, F., Milner, Y., and Friguet, B. (2006). The ubiquitin-proteasome system at the crossroads of stress-response and ageing pathways: a handle for skin care? Ageing Res Rev *5*, 60-90.

Brookman, K.W., Lamerdin, J.E., Thelen, M.P., Hwang, M., Reardon, J.T., Sancar, A., Zhou, Z.Q., Walter, C.A., Parris, C.N., and Thompson, L.H. (1996). ERCC4 (XPF) encodes a human nucleotide excision repair protein with eukaryotic recombination homologs. Mol Cell Biol *16*, 6553-6562.

Brooks, P.J. (2007). The case for 8,5'-cyclopurine-2'-deoxynucleosides as endogenous DNA lesions that cause neurodegeneration in xeroderma pigmentosum. Neuroscience *145*, 1407-1417.

Brooks, P.J., Wise, D.S., Berry, D.A., Kosmoski, J.V., Smerdon, M.J., Somers, R.L., Mackie, H., Spoonde, A.Y., Ackerman, E.J., Coleman, K.*, et al.* (2000). The oxidative DNA lesion 8,5'-(S)-cyclo-2'-deoxyadenosine is repaired by the nucleotide excision repair pathway and blocks gene expression in mammalian cells. J Biol Chem *275*, 22355-22362.

Bubici, C., Papa, S., Dean, K., and Franzoso, G. (2006). Mutual cross-talk between reactive oxygen species and nuclear factor-kappa B: molecular basis and biological significance. Oncogene *25*, 6731-6748.

Buege, J.A., and Aust, S.D. (1978). Microsomal lipid peroxidation. Methods Enzymol *52*, 302-310.

Busch, D.B., van Vuuren, H., de Wit, J., Collins, A., Zdzienicka, M.Z., Mitchell, D.L., Brookman, K.W., Stefanini, M., Riboni, R., Thompson, L.H.*, et al.* (1997). Phenotypic heterogeneity in nucleotide excision repair mutants of rodent complementation groups 1 and 4. Mutat Res *383*, 91-106.

Cai, D., Frantz, J.D., Tawa, N.E., Jr., Melendez, P.A., Oh, B.C., Lidov, H.G., Hasselgren, P.O., Frontera, W.R., Lee, J., Glass, D.J.*, et al.* (2004). IKKbeta/NF-kappaB activation causes severe muscle wasting in mice. Cell *119*, 285-298.

Carlsen, H., Moskaug, J.O., Fromm, S.H., and Blomhoff, R. (2002). In vivo imaging of NF-kappa B activity. J Immunol *168*, 1441-1446.

Caruso, L.B., and Silliman, R.A. (2006). Geriatric Medicine, 17 edn (New York, McGraw Hill).

Chakravarti, B., and Chakravarti, D.N. (2007). Oxidative modification of proteins: age-related changes. Gerontology *53*, 128-139.

Chance, B., Sies, H., and Boveris, A. (1979). Hydroperoxide metabolism in mammalian organs. Physiol Rev *59*, 527-605.

Charloux, C., Paul, M., Loisance, D., and Astier, A. (1995). Inhibition of hydroxyl radical production by lactobionate, adenine, and tempol. Free Radic Biol Med *19*, 699-704.

Chipchase, M.D., O'Neill, M., and Melton, D.W. (2003). Characterization of premature liver polyploidy in DNA repair (Ercc1)-deficient mice. Hepatology *38*, 958-966.

Christakis, P. (2011). The birth of chemotherapy at Yale. Bicentennial lecture series: Surgery Grand Round. Yale J Biol Med *84*, 169-172.

Chung, H.Y., Cesari, M., Anton, S., Marzetti, E., Giovannini, S., Seo, A.Y., Carter, C., Yu, B.P., and Leeuwenburgh, C. (2009). Molecular inflammation: underpinnings of aging and age-related diseases. Ageing Res Rev *8*, 18-30.

Conboy, I.M., Conboy, M.J., Wagers, A.J., Girma, E.R., Weissman, I.L., and Rando, T.A. (2005). Rejuvenation of aged progenitor cells by exposure to a young systemic environment. Nature *433*, 760-764.

Cooke, M.S., Evans, M.D., Dizdaroglu, M., and Lunec, J. (2003). Oxidative DNA damage: mechanisms, mutation, and disease. FASEB J *17*, 1195-1214.

Coppe, J.P., Patil, C.K., Rodier, F., Sun, Y., Munoz, D.P., Goldstein, J., Nelson, P.S., Desprez, P.Y., and Campisi, J. (2008a). Senescence-associated secretory phenotypes reveal cell-nonautonomous functions of oncogenic RAS and the p53 tumor suppressor. PLoS Biol *6*, 2853-2868.

Coppe, J.P., Patil, C.K., Rodier, F., Sun, Y., Munoz, D.P., Goldstein, J., Nelson, P.S., Desprez, P.Y., and Campisi, J. (2008b). Senescence-associated secretory phenotypes reveal cell-nonautonomous functions of oncogenic RAS and the p53 tumor suppressor. PLoS Biol *6*, 2853-2868.

Crossan, G.P., van der Weyden, L., Rosado, I.V., Langevin, F., Gaillard, P.H., McIntyre, R.E., Gallagher, F., Kettunen, M.I., Lewis, D.Y., Brindle, K.*, et al.* (2011). Disruption of mouse Slx4, a regulator of structure-specific nucleases, phenocopies Fanconi anemia. Nat Genet *43*, 147-152.

Cuaz-Perolin, C., Billiet, L., Bauge, E., Copin, C., Scott-Algara, D., Genze, F., Buchele, B., Syrovets, T., Simmet, T., and Rouis, M. (2008). Antiinflammatory and antiatherogenic effects of the NF-kappaB inhibitor acetyl-11-keto-beta-boswellic acid in LPS-challenged ApoE-/- mice. Arterioscler Thromb Vasc Biol *28*, 272-277.

Cui, H., Kong, Y., and Zhang, H. (2012). Oxidative stress, mitochondrial dysfunction, and aging. J Signal Transduct *2012*, 646354.

Dai, S., Hirayama, T., Abbas, S., and Abu-Amer, Y. (2004). The IkappaB kinase (IKK) inhibitor, NEMO-binding domain peptide, blocks osteoclastogenesis and bone erosion in inflammatory arthritis. J Biol Chem *279*, 37219-37222.

Dan, H.C., Cooper, M.J., Cogswell, P.C., Duncan, J.A., Ting, J.P., and Baldwin, A.S. (2008). Akt-dependent regulation of NF-{kappa}B is controlled by mTOR and Raptor in association with IKK. Genes Dev *22*, 1490-1500.

Dave, S.H., Tilstra, J.S., Matsuoka, K., Li, F., Karrasch, T., Uno, J.K., Sepulveda, A.R., Jobin, C., Baldwin, A.S., Robbins, P.D.*, et al.* (2007). Amelioration of chronic murine colitis by peptide-mediated transduction of the IkappaB kinase inhibitor NEMO binding domain peptide. J Immunol *179*, 7852-7859.

de Boer, J., Andressoo, J.O., de Wit, J., Huijmans, J., Beems, R.B., van Steeg, H., Weeda, G., van der Horst, G.T., van Leeuwen, W., Themmen, A.P., *et al.* (2002). Premature aging in mice deficient in DNA repair and transcription. Science *296*, 1276-1279.

de Laat, W.L., Jaspers, N.G., and Hoeijmakers, J.H. (1999). Molecular mechanism of nucleotide excision repair. Genes Dev *13*, 768-785.

de Laat, W.L., Sijbers, A.M., Odijk, H., Jaspers, N.G., and Hoeijmakers, J.H. (1998). Mapping of interaction domains between human repair proteins ERCC1 and XPF. Nucleic Acids Res *26*, 4146-4152.

De Silva, I.U., McHugh, P.J., Clingen, P.H., and Hartley, J.A. (2000). Defining the roles of nucleotide excision repair and recombination in the repair of DNA interstrand cross-links in mammalian cells. Mol Cell Biol *20*, 7980-7990.

de Vries, A., van Oostrom, C.T., Hofhuis, F.M., Dortant, P.M., Berg, R.J., de Gruijl, F.R., Wester, P.W., van Kreijl, C.F., Capel, P.J., van Steeg, H., *et al.* (1995). Increased susceptibility to ultraviolet-B and carcinogens of mice lacking the DNA excision repair gene XPA. Nature *377*, 169-173.

de Waard, M.C., van der Pluijm, I., Zuiderveen Borgesius, N., Comley, L.H., Haasdijk, E.D., Rijksen, Y., Ridwan, Y., Zondag, G., Hoeijmakers, J.H., Elgersma, Y., *et al.* (2010). Age-related motor neuron degeneration in DNA repair-deficient Ercc1 mice. Acta Neuropathol *120*, 461-475.

Debacq-Chainiaux, F., Erusalimsky, J.D., Campisi, J., and Toussaint, O. (2009). Protocols to detect senescence-associated beta-galactosidase (SA-betagal) activity, a biomarker of senescent cells in culture and in vivo. Nat Protoc *4*, 1798-1806.

Diderich, K., Alanazi, M., and Hoeijmakers, J.H. (2011). Premature aging and cancer in nucleotide excision repair-disorders. DNA Repair (Amst) *10*, 772-780.

Dimri, G.P., Lee, X., Basile, G., Acosta, M., Scott, G., Roskelley, C., Medrano, E.E., Linskens, M., Rubelj, I., Pereira-Smith, O., *et al.* (1995). A biomarker that identifies senescent human cells in culture and in aging skin in vivo. Proc Natl Acad Sci U S A *92*, 9363-9367.

Ding, L., Kuhne, W.W., Hinton, D.E., Song, J., and Dynan, W.S. (2010). Quantifiable biomarkers of normal aging in the Japanese medaka fish (Oryzias latipes). PLoS One *5*, e13287.

Doig, J., Anderson, C., Lawrence, N.J., Selfridge, J., Brownstein, D.G., and Melton, D.W. (2006). Mice with skin-specific DNA repair gene (Ercc1) inactivation are hypersensitive to ultraviolet irradiation-induced skin cancer and show more rapid actinic progression. Oncogene *25*, 6229-6238.

Dollé, M., Kuiper, R., Roodbergen, M., Robinson, J., Vlugt, S., Wijnhoven, S., Beems, R., Fonteyne, L., With, P., Pluijm, I., *et al.* (2011). Broad segmental progeroid changes in short-lived *Ercc1*$^{-/\Delta 7}$ mice. In Pathobiology of Aging & Age-related Diseases.

Dolle, M.E., Busuttil, R.A., Garcia, A.M., Wijnhoven, S., van Drunen, E., Niedernhofer, L.J., van der Horst, G., Hoeijmakers, J.H., van Steeg, H., and Vijg, J. (2006). Increased genomic instability is not a prerequisite for shortened lifespan in DNA repair deficient mice. Mutat Res *596*, 22-35.

Dolle, M.E., Snyder, W.K., Dunson, D.B., and Vijg, J. (2002). Mutational fingerprints of aging. Nucleic Acids Res *30*, 545-549.

Dronkert, M.L., and Kanaar, R. (2001). Repair of DNA interstrand cross-links. Mutat Res *486*, 217-247.

Ellis, N.A., Ciocci, S., and German, J. (2001). Back mutation can produce phenotype reversion in Bloom syndrome somatic cells. Hum Genet *108*, 167-173.

Enzlin, J.H., and Scharer, O.D. (2002). The active site of the DNA repair endonuclease XPF-ERCC1 forms a highly conserved nuclease motif. EMBO J *21*, 2045-2053.

Fagbemi, A.F., Orelli, B., and Scharer, O.D. (2011). Regulation of endonuclease activity in human nucleotide excision repair. DNA Repair (Amst) *10*, 722-729.

Fan, L., Fuss, J.O., Cheng, Q.J., Arvai, A.S., Hammel, M., Roberts, V.A., Cooper, P.K., and Tainer, J.A. (2008). XPD helicase structures and activities: insights into the cancer and aging phenotypes from XPD mutations. Cell *133*, 789-800.

Faroon, O., Taylor, J., Roney, N., Fransen, M.E., Bogaczyk, S., and Diamond, G. (2005). Toxicological profile for carbon tetrachloride, U.S.D.o.H.a.H. Services, ed. (Atlanta, GA, Agency for Toxic Substances and Disease Registry).

Farrell, G.C., and Larter, C.Z. (2006). Nonalcoholic fatty liver disease: from steatosis to cirrhosis. Hepatology *43*, S99-S112.

Fawell, J.K., and Mascarenhas, R. (2004). Carbon tetrachloride in drinking-water, W. Water Sanitation and Health Programme, ed. (World Health Organization).

Fekairi, S., Scaglione, S., Chahwan, C., Taylor, E.R., Tissier, A., Coulon, S., Dong, M.Q., Ruse, C., Yates, J.R., 3rd, Russell, P., *et al.* (2009). Human SLX4 is a Holliday junction resolvase subunit that binds multiple DNA repair/recombination endonucleases. Cell *138*, 78-89.

Fink, M.P., Macias, C.A., Xiao, J., Tyurina, Y.Y., Jiang, J., Belikova, N., Delude, R.L., Greenberger, J.S., Kagan, V.E., and Wipf, P. (2007). Hemigramicidin-TEMPO conjugates: novel mitochondria-targeted anti-oxidants. Biochem Pharmacol *74*, 801-809.

Fishman-Lobell, J., and Haber, J.E. (1992). Removal of nonhomologous DNA ends in double-strand break recombination: the role of the yeast ultraviolet repair gene RAD1. Science *258*, 480-484.

Fletcher, B.L., Dillard, C.J., and Tappel, A.L. (1973). Measurement of fluorescent lipid peroxidation products in biological systems and tissues. Anal Biochem *52*, 1-9.

Franceschi, C., Capri, M., Monti, D., Giunta, S., Olivieri, F., Sevini, F., Panourgia, M.P., Invidia, L., Celani, L., Scurti, M.*, et al.* (2007). Inflammaging and anti-inflammaging: a systemic perspective on aging and longevity emerged from studies in humans. Mech Ageing Dev *128*, 92-105.

Frantz, M.C., and Wipf, P. (2010). Mitochondria as a target in treatment. Environ Mol Mutagen *51*, 462-475.

Friedberg, E.C., Walker, G.C., Siede, W., Wood, R.D., Schultz, R.A., and Ellenberger, T. (2006). DNA Repair and Mutagenesis, 2nd ed. edn (Washington, D.C., ASM Press).

Fujiwara, Y., Ichihashi, M., Uehara, Y., Matsumoto, A., Yamamoto, Y., Kano, Y., and Tanakura, Y. (1985a). Xeroderma pigmentosum groups C and F: additional assignments and a review of the subjects in Japan. J Radiat Res *26*, 443-449.

Fujiwara, Y., Uehara, Y., Ichihashi, M., and Nishioka, K. (1985b). Xeroderma pigmentosum complementation group F: more assignments and repair characteristics. Photochem Photobiol *41*, 629-634.

Furia, B., Deng, L., Wu, K., Baylor, S., Kehn, K., Li, H., Donnelly, R., Coleman, T., and Kashanchi, F. (2002). Enhancement of nuclear factor-kappa B acetylation by coactivator p300 and HIV-1 Tat proteins. J Biol Chem *277*, 4973-4980.

Gane, E.J., Weilert, F., Orr, D.W., Keogh, G.F., Gibson, M., Lockhart, M.M., Frampton, C.M., Taylor, K.M., Smith, R.A., and Murphy, M.P. (2010). The mitochondria-targeted anti-oxidant mitoquinone decreases liver damage in a phase II study of hepatitis C patients. Liver Int *30*, 1019-1026.

Geleziunas, R., McQuillan, A., Malapetsa, A., Hutchinson, M., Kopriva, D., Wainberg, M.A., Hiscott, J., Bramson, J., and Panasci, L. (1991). Increased DNA synthesis and repair-enzyme expression in lymphocytes from patients with chronic lymphocytic leukemia resistant to nitrogen mustards. J Natl Cancer Inst *83*, 557-564.

Ghosh, A., Roy, A., Liu, X., Kordower, J.H., Mufson, E.J., Hartley, D.M., Ghosh, S., Mosley, R.L., Gendelman, H.E., and Pahan, K. (2007a). Selective inhibition of NF-kappaB

activation prevents dopaminergic neuronal loss in a mouse model of Parkinson's disease. Proc Natl Acad Sci U S A *104*, 18754-18759.

Ghosh, A., Roy, A., Liu, X., Kordower, J.H., Mufson, E.J., Hartley, D.M., Ghosh, S., Mosley, R.L., Gendelman, H.E., and Pahan, K. (2007b). Selective inhibition of NF-kappaB activation prevents dopaminergic neuronal loss in a mouse model of Parkinson's disease. Proc Natl Acad Sci U S A *104*, 18754-18759.

Giardina, C., and Hubbard, A.K. (2002). Growing old with nuclear factor-kappaB. Cell Stress Chaperones *7*, 207-212.

Gilman, A. (1963). The initial clinical trial of nitrogen mustard. Am J Surg *105*, 574-578.

Gilmore, T. (2009). Rel/NF-kB Transcription Factors. In wwwnf-kborg.

Goldstein, S., Merenyi, G., Russo, A., and Samuni, A. (2003). The role of oxoammonium cation in the SOD-mimic activity of cyclic nitroxides. J Am Chem Soc *125*, 789-795.

Goss, J.R., Stolz, D.B., Robinson, A.R., Zhang, M., Arbujas, N., Robbins, P.D., Glorioso, J.C., and Niedernhofer, L.J. (2011). Premature aging-related peripheral neuropathy in a mouse model of progeria. Mech Ageing Dev *132*, 437-442.

Gosselin, K., and Abbadie, C. (2003). Involvement of Rel/NF-kappa B transcription factors in senescence. Exp Gerontol *38*, 1271-1283.

Graham, J.M., Jr., Anyane-Yeboa, K., Raams, A., Appeldoorn, E., Kleijer, W.J., Garritsen, V.H., Busch, D., Edersheim, T.G., and Jaspers, N.G. (2001). Cerebro-oculo-facio-skeletal syndrome with a nucleotide excision-repair defect and a mutated XPD gene, with prenatal diagnosis in a triplet pregnancy. Am J Hum Genet *69*, 291-300.

Green, D.R., Galluzzi, L., and Kroemer, G. (2011). Mitochondria and the autophagy-inflammation-cell death axis in organismal aging. Science *333*, 1109-1112.

Greenberg, S. (2011). A Profile of Older Americans: 2011, U.S.D.o.H.a.H. Services, ed. (Washington, D.C., Administration on Aging)).

Gregg, S.Q., Gutierrez, V., Robinson, A.R., Woodell, T., Nakao, A., Ross, M.A., Michalopoulos, G.K., Rigatti, L., Rothermel, C.E., Kamileri, I.*, et al.* (2012a). A mouse model of accelerated liver aging caused by a defect in DNA repair. Hepatology *55*, 609-621.

Gregg, S.Q., Robinson, A.R., and Niedernhofer, L.J. (2011). Physiological consequences of defects in ERCC1-XPF DNA repair endonuclease. DNA Repair *10*, 781-791.

Gregg, S.Q., Wang, J., Frantz, M.C., Maniar, S., Guerrero, C., Skoda, E.M., St. Croix, C.M., Stolz, D.B., Robbins, P.D., Wang, Y.*, et al.* (2012b). Endogenous oxidative DNA lesions drive cellular senescence. submitted.

Grillari, J., Katinger, H., and Voglauer, R. (2007). Contributions of DNA interstrand cross-links to aging of cells and organisms. Nucleic Acids Res *35*, 7566-7576.

Guarente, L., and Kenyon, C. (2000). Genetic pathways that regulate ageing in model organisms. Nature *408*, 255-262.

Guttman, P.H., and Kohn, H.I. (1960). Progressive intercapillary glomerulosclerosis in the mouse, rat, and Chinese hamster, associated with aging and x-ray exposure. Am J Pathol *37*, 293-307.

Guttridge, D.C., Albanese, C., Reuther, J.Y., Pestell, R.G., and Baldwin, A.S., Jr. (1999). NF-kappaB controls cell growth and differentiation through transcriptional regulation of cyclin D1. Mol Cell Biol *19*, 5785-5799.

Hagelstrom, R.T., Blagoev, K.B., Niedernhofer, L.J., Goodwin, E.H., and Bailey, S.M. (2010). Hyper telomere recombination accelerates replicative senescence and may promote premature aging. Proc Natl Acad Sci U S A *107*, 15768-15773.

Hamel, B.C., Raams, A., Schuitema-Dijkstra, A.R., Simons, P., van der Burgt, I., Jaspers, N.G., and Kleijer, W.J. (1996). Xeroderma pigmentosum--Cockayne syndrome complex: a further case. J Med Genet *33*, 607-610.

Hamilton, M.L., Van Remmen, H., Drake, J.A., Yang, H., Guo, Z.M., Kewitt, K., Walter, C.A., and Richardson, A. (2001). Does oxidative damage to DNA increase with age? Proc Natl Acad Sci U S A *98*, 10469-10474.

Hansson, J., Lewensohn, R., Ringborg, U., and Nilsson, B. (1987). Formation and removal of DNA cross-links induced by melphalan and nitrogen mustard in relation to drug-induced cytotoxicity in human melanoma cells. Cancer Res *47*, 2631-2637.

Harman, D. (1956). Aging: a theory based on free radical and radiation chemistry. J Gerontol *11*, 298-300.

Harman, D. (1992a). Free radical theory of aging. Mutat Res *275*, 257-266.

Harman, D. (1992b). Free radical theory of aging: history. EXS *62*, 1-10.

Harper, J.M. (2008). Wild-derived mouse stocks: an underappreciated tool for aging research. Age (Dordr) *30*, 135-145.

Harrison, D.E., Strong, R., Sharp, Z.D., Nelson, J.F., Astle, C.M., Flurkey, K., Nadon, N.L., Wilkinson, J.E., Frenkel, K., Carter, C.S.*, et al.* (2009). Rapamycin fed late in life extends lifespan in genetically heterogeneous mice. Nature *460*, 392-395.

Hartley, J.A., Berardini, M.D., and Souhami, R.L. (1991). An agarose gel method for the determination of DNA interstrand crosslinking applicable to the measurement of the rate of total and "second-arm" crosslink reactions. Anal Biochem *193*, 131-134.

Hasty, P., Campisi, J., Hoeijmakers, J., van Steeg, H., and Vijg, J. (2003a). Aging and Genome Maintenance: Lessons from the Mouse? Science *299*, 1355-1359.

Hasty, P., Campisi, J., Hoeijmakers, J., van Steeg, H., and Vijg, J. (2003b). Aging and genome maintenance: lessons from the mouse? Science *299*, 1355-1359.

Hayden, M.S., and Ghosh, S. (2008). Shared principles in NF-kappaB signaling. Cell *132*, 344-362.

Hayden, M.S., West, A.P., and Ghosh, S. (2006). NF-kappaB and the immune response. Oncogene *25*, 6758-6780.

Hefner, E., Preuss, S.B., and Britt, A.B. (2003). Arabidopsis mutants sensitive to gamma radiation include the homologue of the human repair gene ERCC1. J Exp Bot *54*, 669-680.

Helenius, M., Hanninen, M., Lehtinen, S.K., and Salminen, A. (1996). Changes associated with aging and replicative senescence in the regulation of transcription factor nuclear factor-kappa B. Biochem J *318 (Pt 2)*, 603-608.

Heston, W.E. (1950). Carcinogenic action of the mustards. J Natl Cancer Inst *11*, 415-423.

Hirschhorn, R. (2003). In vivo reversion to normal of inherited mutations in humans. J Med Genet *40*, 721-728.

Hoeijmakers, J.H. (2001). Genome maintenance mechanisms for preventing cancer. Nature *411*, 366-374.

Hoffman, C., and Rice, D.P. (1996). Chronic Care in America: A 21st Century Challenge (San Francisco, CA).

Hoy, C.A., Thompson, L.H., Mooney, C.L., and Salazar, E.P. (1985). Defective DNA cross-link removal in Chinese hamster cell mutants hypersensitive to bifunctional alkylating agents. Cancer Res *45*, 1737-1743.

Hsia, K.T., Millar, M.R., King, S., Selfridge, J., Redhead, N.J., Melton, D.W., and Saunders, P.T. (2003). DNA repair gene Ercc1 is essential for normal spermatogenesis and oogenesis and for functional integrity of germ cell DNA in the mouse. Development *130*, 369-378.

Imoto, K., Boyle, J., Oh, K., Khan, S., Ueda, T., Nadem, C., Slor, H., Orgal, S., Gadoth, N., Busch, D.*, et al.* (2007). Patients with defects in the interacting nucleotide excision repair

proteins ERCC1 or XPF show xeroderma pigmentosum with late onset severe neurological degeneration. J Invest Dermatol *127*.

Itoh, T., Linn, S., Ono, T., and Yamaizumi, M. (2000). Reinvestigation of the classification of five cell strains of xeroderma pigmentosum group E with reclassification of three of them. J Invest Dermatol *114*, 1022-1029.

Ivanov, E.L., and Haber, J.E. (1995). RAD1 and RAD10, but not other excision repair genes, are required for double-strand break-induced recombination in Saccharomyces cerevisiae. Mol Cell Biol *15*, 2245-2251.

Jackson, J.G., and Pereira-Smith, O.M. (2006). p53 is preferentially recruited to the promoters of growth arrest genes p21 and GADD45 during replicative senescence of normal human fibroblasts. Cancer Res *66*, 8356-8360.

Jang, Y.C., and Remmen, V.H. (2009). The mitochondrial theory of aging: insight from transgenic and knockout mouse models. Exp Gerontol *44*, 256-260.

Jaruga, P., and Dizdaroglu, M. (2008). 8,5'-Cyclopurine-2'-deoxynucleosides in DNA: Mechanisms of formation, measurement, repair and biological effects. DNA Repair *7*, 1413-1425.

Jaspers, N.G., Raams, A., Silengo, M.C., Wijgers, N., Niedernhofer, L.J., Robinson, A.R., Giglia-Mari, G., Hoogstraten, D., Kleijer, W.J., Hoeijmakers, J.H.*, et al.* (2007). First reported patient with human ERCC1 deficiency has cerebro-oculo-facio-skeletal syndrome with a mild defect in nucleotide excision repair and severe developmental failure. Am J Hum Genet *80*, 457-466.

Jendrach, M., Pohl, S., Voth, M., Kowald, A., Hammerstein, P., and Bereiter-Hahn, J. (2005). Morpho-dynamic changes of mitochondria during ageing of human endothelial cells. Mech Ageing Dev *126*, 813-821.

Jiang, J., Kurnikov, I., Belikova, N.A., Xiao, J., Zhao, Q., Amoscato, A.A., Braslau, R., Studer, A., Fink, M.P., Greenberger, J.S.*, et al.* (2007). Structural requirements for optimized delivery, inhibition of oxidative stress, and antiapoptotic activity of targeted nitroxides. J Pharmacol Exp Ther *320*, 1050-1060.

Jiang, T., Liebman, S.E., Lucia, M.S., Li, J., and Levi, M. (2005). Role of altered renal lipid metabolism and the sterol regulatory element binding proteins in the pathogenesis of age-related renal disease. Kidney Int *68*, 2608-2620.

Jump, D.B. (2002). The biochemistry of n-3 polyunsaturated fatty acids. J Biol Chem *277*, 8755-8758.

Jung, T., Hohn, A., and Grune, T. (2010). Lipofuscin: Detection and Quantification by Microscopic Techniques. In Advanced Protocols in Oxidative Stress II, Methods in Molecular Biology, D. Armstrong, ed. (Humana Press).

Kadiiska, M.B., Gladen, B.C., Baird, D.D., Dikalova, A.E., Sohal, R.S., Hatch, G.E., Jones, D.P., Mason, R.P., and Barrett, J.C. (2000). Biomarkers of oxidative stress study: are plasma antioxidants markers of CCl(4) poisoning? Free Radic Biol Med *28*, 838-845.

Kadiiska, M.B., Gladen, B.C., Baird, D.D., Germolec, D., Graham, L.B., Parker, C.E., Nyska, A., Wachsman, J.T., Ames, B.N., Basu, S.*, et al.* (2005a). Biomarkers of oxidative stress study II: are oxidation products of lipids, proteins, and DNA markers of CCl4 poisoning? Free Radic Biol Med *38*, 698-710.

Kadiiska, M.B., Gladen, B.C., Baird, D.D., Graham, L.B., Parker, C.E., Ames, B.N., Basu, S., Fitzgerald, G.A., Lawson, J.A., Marnett, L.J.*, et al.* (2005b). Biomarkers of oxidative stress study III. Effects of the nonsteroidal anti-inflammatory agents indomethacin and meclofenamic acid on measurements of oxidative products of lipids in CCl4 poisoning. Free Radic Biol Med *38*, 711-718.

Kagan, V.E., Wipf, P., Stoyanovsky, D., Greenberger, J.S., Borisenko, G., Belikova, N.A., Yanamala, N., Samhan Arias, A.K., Tungekar, M.A., Jiang, J.*, et al.* (2009). Mitochondrial targeting of electron scavenging antioxidants: Regulation of selective oxidation vs random chain reactions. Adv Drug Deliv Rev *61*, 1375-1385.

Karin, M. (2006). Nuclear factor-kappaB in cancer development and progression. Nature *441*, 431-436.

Karrasch, T., Kim, J.S., Muhlbauer, M., Magness, S.T., and Jobin, C. (2007). Gnotobiotic IL-10-/-;NF-kappa B(EGFP) mice reveal the critical role of TLR/NF-kappa B signaling in commensal bacteria-induced colitis. J Immunol *178*, 6522-6532.

Kawahara, T.L., Michishita, E., Adler, A.S., Damian, M., Berber, E., Lin, M., McCord, R.A., Ongaigui, K.C., Boxer, L.D., Chang, H.Y.*, et al.* (2009). SIRT6 links histone H3 lysine 9 deacetylation to NF-kappaB-dependent gene expression and organismal life span. Cell *136*, 62-74.

Kelso, G.F., Porteous, C.M., Coulter, C.V., Hughes, G., Porteous, W.K., Ledgerwood, E.C., Smith, R.A., and Murphy, M.P. (2001). Selective targeting of a redox-active ubiquinone to mitochondria within cells: antioxidant and antiapoptotic properties. J Biol Chem *276*, 4588-4596.

Kim, H.J., Chang, E.J., Kim, H.M., Lee, S.B., Kim, H.D., Su Kim, G., and Kim, H.H. (2006). Antioxidant alpha-lipoic acid inhibits osteoclast differentiation by reducing nuclear factor-kappaB DNA binding and prevents in vivo bone resorption induced by receptor activator of nuclear factor-kappaB ligand and tumor necrosis factor-alpha. Free Radic Biol Med *40*, 1483-1493.

Kim, W.Y., and Sharpless, N.E. (2006). The regulation of INK4/ARF in cancer and aging. Cell *127*, 265-275.

Kim, Y., Lach, F.P., Desetty, R., Hanenberg, H., Auerbach, A.D., and Smogorzewska, A. (2011). Mutations of the SLX4 gene in Fanconi anemia. Nat Genet *43*, 142-146.

Kirkwood, T.B. (2005). Understanding the odd science of aging. Cell *120*, 437-447.

Kishi, S., Bayliss, P.E., Uchiyama, J., Koshimizu, E., Qi, J., Nanjappa, P., Imamura, S., Islam, A., Neuberg, D., Amsterdam, A.*, et al.* (2008). The identification of zebrafish mutants showing alterations in senescence-associated biomarkers. PLoS Genet *4*, e1000152.

Klein, H.L. (1988). Different types of recombination events are controlled by the RAD1 and RAD52 genes of Saccharomyces cerevisiae. Genetics *120*, 367-377.

Knipscheer, P., Raschle, M., Smogorzewska, A., Enoiu, M., Ho, T.V., Scharer, O.D., Elledge, S.J., and Walter, J.C. (2009). The Fanconi anemia pathway promotes replication-dependent DNA interstrand cross-link repair. Science *326*, 1698-1701.

Kondo, S., Mamada, A., Miyamoto, C., Keong, C.H., Satoh, Y., and Fujiwara, Y. (1989). Late onset of skin cancers in 2 xeroderma pigmentosum group F siblings and a review of 30 Japanese xeroderma pigmentosum patients in groups D, E and F. Photodermatol *6*, 89-95.

Korhonen, P., Helenius, M., and Salminen, A. (1997). Age-related changes in the regulation of transcription factor NF-kappa B in rat brain. Neurosci Lett *225*, 61-64.

Kotnis, A., Du, L., Liu, C., Popov, S.W., and Pan-Hammarstrom, Q. (2009). Non-homologous end joining in class switch recombination: the beginning of the end. Philos Trans R Soc Lond B Biol Sci *364*, 653-665.

Kraemer, K.H., Lee, M.M., and Scotto, J. (1987). Xeroderma pigmentosum. Cutaneous, ocular, and neurologic abnormalities in 830 published cases. Arch Dermatol *123*, 241-250.

Kraemer, K.H., Levy, D.D., Parris, C.N., Gozukara, E.M., Moriwaki, S., Adelberg, S., and Seidman, M.M. (1994). Xeroderma pigmentosum and related disorders: examining the linkage between defective DNA repair and cancer. J Invest Dermatol *103*, 96S-101S.

Kriete, A., Mayo, K.L., Yalamanchili, N., Beggs, W., Bender, P., Kari, C., and Rodeck, U. (2008). Cell autonomous expression of inflammatory genes in biologically aged fibroblasts associated with elevated NF-kappaB activity. Immun Ageing *5*, 5.

Krishna, M.C., Samuni, A., Taira, J., Goldstein, S., Mitchell, J.B., and Russo, A. (1996). Stimulation by nitroxides of catalase-like activity of hemeproteins. Kinetics and mechanism. J Biol Chem *271*, 26018-26025.

Kuraoka, I., Kobertz, W.R., Ariza, R.R., Biggerstaff, M., Essigmann, J.M., and Wood, R.D. (2000). Repair of an interstrand DNA cross-link initiated by ERCC1-XPF repair/recombination nuclease. J Biol Chem *275*, 26632-26636.

Lackner, C., Gogg-Kamerer, M., Zatloukal, K., Stumptner, C., Brunt, E.M., and Denk, H. (2008). Ballooned hepatocytes in steatohepatitis: the value of keratin immunohistochemistry for diagnosis. J Hepatol *48*, 821-828.

Lavasani, M., Robinson, A.R., Lu, A., Song, M., Feduska, J.M., Ahani, B., Tilstra, J.S., Feldman, C.H., Robbins, P.D., Niedernhofer, L.J., *et al.* (2012). Muscle-derived stem/progenitor cell dysfunction limits healthspan and lifespan in a murine progeria model. Nat Commun *3*, 608.

Lawrence, N.J., Sacco, J.J., Brownstein, D.G., Gillingwater, T.H., and Melton, D.W. (2008). A neurological phenotype in mice with DNA repair gene Ercc1 deficiency. DNA Repair (Amst) *7*, 281-291.

Lawrence, N.J., Song, L., Doig, J., Ritchie, A.M., Brownstein, D.G., and Melton, D.W. (2009). Topical thymidine dinucleotide application protects against UVB-induced skin cancer in mice with DNA repair gene (Ercc1)-deficient skin. DNA Repair (Amst) *8*, 664-671.

Le May, N., Mota-Fernandes, D., Velez-Cruz, R., Iltis, I., Biard, D., and Egly, J.M. (2010). NER factors are recruited to active promoters and facilitate chromatin modification for transcription in the absence of exogenous genotoxic attack. Mol Cell *38*, 54-66.

Lee, A.C., Fenster, B.E., Ito, H., Takeda, K., Bae, N.S., Hirai, T., Yu, Z.X., Ferrans, V.J., Howard, B.H., and Finkel, T. (1999). Ras proteins induce senescence by altering the intracellular levels of reactive oxygen species. J Biol Chem *274*, 7936-7940.

Li, H., Malhotra, S., and Kumar, A. (2008). Nuclear factor-kappa B signaling in skeletal muscle atrophy. J Mol Med (Berl) *86*, 1113-1126.

Li, L., Elledge, S.J., Peterson, C.A., Bales, E.S., and Legerski, R.J. (1994). Specific association between the human DNA repair proteins XPA and ERCC1. Proc Natl Acad Sci U S A *91*, 5012-5016.

Li, X.L., Shen, S.R., Wang, S., Ouyang, H.H., and Li, G.C. (2002). Restoration of T cell-specific V(D)J recombination in DNA-PKcs(-/-) mice by ionizing radiation: The effects on survival, development, and tumorigenesis. Sheng Wu Hua Xue Yu Sheng Wu Wu Li Xue Bao (Shanghai) *34*, 149-157.

Li, Y., Wang, Z., Kong, D., Murthy, S., Dou, Q.P., Sheng, S., Reddy, G.P., and Sarkar, F.H. (2007). Regulation of FOXO3a/beta-catenin/GSK-3beta signaling by 3,3'-diindolylmethane contributes to inhibition of cell proliferation and induction of apoptosis in prostate cancer cells. J Biol Chem *282*, 21542-21550.

Lim, W., Cho, J., Kwon, H.Y., Park, Y., Rhyu, M.R., and Lee, Y. (2009). Hypoxia-inducible factor 1 alpha activates and is inhibited by unoccupied estrogen receptor beta. FEBS Lett *583*, 1314-1318.

Lin, S.S., Manchester, J.K., and Gordon, J.I. (2001). Enhanced gluconeogenesis and increased energy storage as hallmarks of aging in Saccharomyces cerevisiae. J Biol Chem *276*, 36000-36007.

Lindahl, T., and Barnes, D.E. (2000). Repair of endogenous DNA damage. Cold Spring Harb Symp Quant Biol *65*, 127-133.

Liu, L., Trimarchi, J.R., Smith, P.J., and Keefe, D.L. (2002). Mitochondrial dysfunction leads to telomere attrition and genomic instability. Aging Cell *1*, 40-46.

Lowry, R.B., MacLean, R., McLean, D.M., and Tischler, B. (1971). Cataracts, microcephaly, kyphosis, and limited joint movement in two siblings: a new syndrome. J Pediatr *79*, 282-284.

Ma, J.L., Kim, E.M., Haber, J.E., and Lee, S.E. (2003). Yeast Mre11 and Rad1 proteins define a Ku-independent mechanism to repair double-strand breaks lacking overlapping end sequences. Mol Cell Biol *23*, 8820-8828.

Maccormick, R.E. (2006). Possible acceleration of aging by adjuvant chemotherapy: a cause of early onset frailty? Med Hypotheses *67*, 212-215.

Macias, C.A., Chiao, J.W., Xiao, J., Arora, D.S., Tyurina, Y.Y., Delude, R.L., Wipf, P., Kagan, V.E., and Fink, M.P. (2007). Treatment with a novel hemigramicidin-TEMPO conjugate prolongs survival in a rat model of lethal hemorrhagic shock. Ann Surg *245*, 305-314.

Magness, S.T., Jijon, H., Van Houten Fisher, N., Sharpless, N.E., Brenner, D.A., and Jobin, C. (2004). In vivo pattern of lipopolysaccharide and anti-CD3-induced NF-kappa B activation using a novel gene-targeted enhanced GFP reporter gene mouse. J Immunol *173*, 1561-1570.

Mandavilli, B.S., Santos, J.H., and Van Houten, B. (2002). Mitochondrial DNA repair and aging. Mutat Res *509*, 127-151.

Massaad, C.A., Washington, T.M., Pautler, R.G., and Klann, E. (2009). Overexpression of SOD-2 reduces hippocampal superoxide and prevents memory deficits in a mouse model of Alzheimer's disease. Proc Natl Acad Sci U S A *106*, 13576-13581.

Matsumura, Y., Nishigori, C., Yagi, T., Imamura, S., and Takebe, H. (1998). Characterization of molecular defects in xeroderma pigmentosum group F in relation to its clinically mild symptoms. Hum Mol Genet *7*, 969-974.

Maynard, S., Schurman, S.H., Harboe, C., de Souza-Pinto, N.C., and Bohr, V.A. (2009). Base excision repair of oxidative DNA damage and association with cancer and aging. Carcinogenesis *30*, 2-10.

Mayne, L.V., and Lehmann, A.R. (1982). Failure of RNA synthesis to recover after UV irradiation: an early defect in cells from individuals with Cockayne's syndrome and xeroderma pigmentosum. Cancer Res *42*, 1473-1478.

McDonald, J.H. (2009). Handbook of Biological Statistics, 2nd ed edn ((2nd ed.). Baltimore, Maryland, Sparky House Publishing).

McHugh, P.J., Spanswick, V.J., and Hartley, J.A. (2001). Repair of DNA interstrand crosslinks: molecular mechanisms and clinical relevance. Lancet Oncol *2*, 483-490.

McVey, M., and Lee, S.E. (2008). MMEJ repair of double-strand breaks (director's cut): deleted sequences and alternative endings. Trends Genet *24*, 529-538.

McWhir, J., Selfridge, J., Harrison, D.J., Squires, S., and Melton, D.W. (1993). Mice with DNA repair gene (ERCC-1) deficiency have elevated levels of p53, liver nuclear abnormalities and die before weaning. Nat Genet *5*, 217-224.

Mecocci, P., Fano, G., Fulle, S., MacGarvey, U., Shinobu, L., Polidori, M.C., Cherubini, A., Vecchiet, J., Senin, U., and Beal, M.F. (1999). Age-dependent increases in oxidative damage to DNA, lipids, and proteins in human skeletal muscle. Free Radic Biol Med *26*, 303-308.

Meira, L.B., Graham, J.M., Jr., Greenberg, C.R., Busch, D.B., Doughty, A.T., Ziffer, D.W., Coleman, D.M., Savre-Train, I., and Friedberg, E.C. (2000). Manitoba aboriginal kindred with original cerebro-oculo- facio-skeletal syndrome has a mutation in the Cockayne syndrome group B (CSB) gene. Am J Hum Genet *66*, 1221-1228.

Melis, J.P., Wijnhoven, S.W., Beems, R.B., Roodbergen, M., van den Berg, J., Moon, H., Friedberg, E., van der Horst, G.T., Hoeijmakers, J.H., Vijg, J.*, et al.* (2008). Mouse models for xeroderma pigmentosum group A and group C show divergent cancer phenotypes. Cancer Res *68*, 1347-1353.

Metz, J.M., Smith, D., Mick, R., Lustig, R., Mitchell, J., Cherakuri, M., Glatstein, E., and Hahn, S.M. (2004). A phase I study of topical Tempol for the prevention of alopecia induced by whole brain radiotherapy. Clin Cancer Res *10*, 6411-6417.

Michaelson-Richie, E.D., Ming, X., Codreanu, S.G., Loeber, R.L., Liebler, D.C., Campbell, C., and Tretyakova, N.Y. (2011). Mechlorethamine-induced DNA-protein cross-linking in human fibrosarcoma (HT1080) cells. J Proteome Res *10*, 2785-2796.

Millard, J.T., Raucher, S., and Hopkins, P.B. (1990). Mechlorethamine cross-links deoxyguanosine residues at 5'-GNC sequences in duplex DNA fragments. J Am Chem Soc *112*, 2459-2460.

Miller, E.R., 3rd, Pastor-Barriuso, R., Dalal, D., Riemersma, R.A., Appel, L.J., and Guallar, E. (2005). Meta-analysis: high-dosage vitamin E supplementation may increase all-cause mortality. Ann Intern Med *142*, 37-46.

Miller, S.A., Dykes, D.D., and Polesky, H.F. (1988a). A simple salting out procedure for extracting DNA from human nucleated cells. Nucleic Acids Res *16*, 1215.

Miller, S.A., Dykes, D.D., and Polesky, H.F. (1988b). A simple salting out procedure for extracting DNA from human nucleated cells. Nucleic Acids Research *16*, 1215.

Mitchell, J.B., Russo, A., Kuppusamy, P., and Krishna, M.C. (2000). Radiation, radicals, and images. Ann N Y Acad Sci *899*, 28-43.

Miyamoto, S. (2011). Nuclear initiated NF-[kappa]B signaling: NEMO and ATM take center stage. Cell Res *21*, 116-130.

Moriwaki, S., Nishigori, C., Imamura, S., Yagi, T., Takahashi, C., Fujimoto, N., and Takebe, H. (1993). A case of xeroderma pigmentosum complementation group F with neurological abnormalities. Br J Dermatol *128*, 91-94.

Mostoslavsky, R., Chua, K.F., Lombard, D.B., Pang, W.W., Fischer, M.R., Gellon, L., Liu, P., Mostoslavsky, G., Franco, S., Murphy, M.M.*, et al.* (2006). Genomic instability and aging-like phenotype in the absence of mammalian SIRT6. Cell *124*, 315-329.

Muller, F.L., Lustgarten, M.S., Jang, Y., Richardson, A., and Van Remmen, H. (2007). Trends in oxidative aging theories. Free Radic Biol Med *43*, 477-503.

Munoz, I.M., Hain, K., Declais, A.C., Gardiner, M., Toh, G.W., Sanchez-Pulido, L., Heuckmann, J.M., Toth, R., Macartney, T., Eppink, B.*, et al.* (2009a). Coordination of structure-specific nucleases by human SLX4/BTBD12 is required for DNA repair. Mol Cell *35*, 116-127.

Munoz, P., Blanco, R., de Carcer, G., Schoeftner, S., Benetti, R., Flores, J.M., Malumbres, M., and Blasco, M.A. (2009b). TRF1 controls telomere length and mitotic fidelity in epithelial homeostasis. Mol Cell Biol *29*, 1608-1625.

Munoz, P., Blanco, R., Flores, J.M., and Blasco, M.A. (2005). XPF nuclease-dependent telomere loss and increased DNA damage in mice overexpressing TRF2 result in premature aging and cancer. Nat Genet *37*, 1063-1071.

Murakami, S. (2006). Stress resistance in long-lived mouse models. Exp Gerontol *41*, 1014-1019.

Nakane, H., Takeuchi, S., Yuba, S., Saijo, M., Nakatsu, Y., Murai, H., Nakatsuru, Y., Ishikawa, T., Hirota, S., Kitamura, Y., *et al.* (1995). High incidence of ultraviolet-B-or chemical-carcinogen-induced skin tumours in mice lacking the xeroderma pigmentosum group A gene. Nature *377*, 165-168.

Natoli, G. (2009). When sirtuins and NF-kappaB collide. Cell *136*, 19-21.

Nevedomskaya, E., Meissner, A., Goraler, S., de Waard, M., Ridwan, Y., Zondag, G., van der Pluijm, I., Deelder, A.M., and Mayboroda, O.A. (2010). Metabolic profiling of accelerated aging ERCC1 d/- mice. J Proteome Res *9*, 3680-3687.

Nichols, N.R., Day, J.R., Laping, N.J., Johnson, S.A., and Finch, C.E. (1993). GFAP mRNA increases with age in rat and human brain. Neurobiol Aging *14*, 421-429.

Niedernhofer, L.J., Daniels, J.S., Rouzer, C.A., Greene, R.E., and Marnett, L.J. (2003). Malondialdehyde, a product of lipid peroxidation, is mutagenic in human cells. J Biol Chem *278*, 31426-31433.

Niedernhofer, L.J., Essers, J., Weeda, G., Beverloo, B., de Wit, J., Muijtjens, M., Odijk, H., Hoeijmakers, J.H., and Kanaar, R. (2001). The structure-specific endonuclease Ercc1-Xpf is required for targeted gene replacement in embryonic stem cells. EMBO J *20*, 6540-6549.

Niedernhofer, L.J., Garinis, G.A., Raams, A., Lalai, A.S., Robinson, A.R., Appeldoorn, E., Odijk, H., Oostendorp, R., Ahmad, A., van Leeuwen, W., *et al.* (2006). A new progeroid syndrome reveals that genotoxic stress suppresses the somatotroph axis. Nature *444*, 1038-1043.

Niedernhofer, L.J., Odijk, H., Budzowska, M., van Drunen, E., Maas, A., Theil, A.F., de Wit, J., Jaspers, N.G., Beverloo, H.B., Hoeijmakers, J.H., *et al.* (2004). The structure-specific endonuclease Ercc1-Xpf is required to resolve DNA interstrand cross-link-induced double-strand breaks. Mol Cell Biol *24*, 5776-5787.

Nishigori, C., Ishizaki, K., Takebe, H., Imamura, S., and Hayakawa, M. (1986). A case of xeroderma pigmentosum group F with late onset of clinical symptoms. Arch Dermatol *122*, 510-511.

Norris, P.G., Hawk, J.L., Avery, J.A., and Giannelli, F. (1988). Xeroderma pigmentosum complementation group F in a non-Japanese patient. J Am Acad Dermatol *18*, 1185-1188.

Nouspikel, T., Lalle, P., Leadon, S.A., Cooper, P.K., and Clarkson, S.G. (1997). A common mutational pattern in Cockayne syndrome patients from xeroderma pigmentosum group G: implications for a second XPG function. Proc Natl Acad Sci U S A *94*, 3116-3121.

Nunez, F., Chipchase, M.D., Clarke, A.R., and Melton, D.W. (2000). Nucleotide excision repair gene (ERCC1) deficiency causes G(2) arrest in hepatocytes and a reduction in liver binucleation: the role of p53 and p21. FASEB J *14*, 1073-1082.

Ohtsubo, K., and Nomaguchi, T.A. (1986). A flow cytofluorometric study on age-dependent ploidy class changes in mouse hepatocyte nuclei. Mech Ageing Dev *36*, 125-131.

Ojwang, J.O., Grueneberg, D.A., and Loechler, E.L. (1989). Synthesis of a duplex oligonucleotide containing a nitrogen mustard interstrand DNA-DNA cross-link. Cancer Res *49*, 6529-6537.

Osawa, T., Davies, D., and Hartley, J.A. (2011). Mechanism of cell death resulting from DNA interstrand cross-linking in mammalian cells. Cell Death Dis *2*, e187.

Packer, L., and Fuehr, K. (1977). Low oxygen concentration extends the lifespan of cultured human diploid cells. Nature *267*, 423-425.

Paques, F., and Haber, J.E. (1997). Two pathways for removal of nonhomologous DNA ends during double-strand break repair in Saccharomyces cerevisiae. Mol Cell Biol *17*, 6765-6771.

Park, C.H., Bessho, T., Matsunaga, T., and Sancar, A. (1995). Purification and characterization of the XPF-ERCC1 complex of human DNA repair excision nuclease. J Biol Chem *270*, 22657-22660.

Parmar, K., D'Andrea, A., and Niedernhofer, L.J. (2009). Mouse models of Fanconi anemia. Mutat Res *668*, 133-140.

Parrinello, S., Samper, E., Krtolica, A., Goldstein, J., Melov, S., and Campisi, J. (2003a). Oxygen sensitivity severely limits the replicative lifespan of murine fibroblasts. Nat Cell Biol *5*, 741-747.

Parrinello, S., Samper, E., Krtolica, A., Goldstein, J., Melov, S., and Campisi, J. (2003b). Oxygen sensitivity severely limits the replicative lifespan of murine fibroblasts. Nat Cell Biol *5*, 741-747.

Paul, C., Povey, J.E., Lawrence, N.J., Selfridge, J., Melton, D.W., and Saunders, P.T. (2007). Deletion of genes implicated in protecting the integrity of male germ cells has differential effects on the incidence of DNA breaks and germ cell loss. PLoS One *2*, e989.

Pena, S.D., and Shokeir, M.H. (1974). Autosomal recessive cerebro-oculo-facio-skeletal (COFS) syndrome. Clin Genet *5*, 285-293.

Petit, C., and Sancar, A. (1999). Nucleotide excision repair: from E. coli to man. Biochimie *81*, 15-25.

Podmore, I.D., Griffiths, H.R., Herbert, K.E., Mistry, N., Mistry, P., and Lunec, J. (1998). Vitamin C exhibits pro-oxidant properties. Nature *392*, 559.

Pooranaperundevi, M., Sumiyabanu, M.S., Viswanathan, P., Sundarapandiyan, R., and Anuradha, C.V. (2010). Insulin resistance induced by high-fructose diet potentiates carbon tetrachloride hepatotoxicity. Toxicol Ind Health *26*, 89-104.

Prado, F., and Aguilera, A. (1995). Role of reciprocal exchange, one-ended invasion crossover and single-strand annealing on inverted and direct repeat recombination in yeast: different requirements for the RAD1, RAD10, and RAD52 genes. Genetics *139*, 109-123.

Prasher, J.M., Lalai, A.S., Heijmans-Antonissen, C., Ploemacher, R.E., Hoeijmakers, J.H., Touw, I.P., and Niedernhofer, L.J. (2005). Reduced hematopoietic reserves in DNA interstrand crosslink repair-deficient Ercc1-/- mice. EMBO J *24*, 861-871.

Provost, P.R., Marcel, Y.L., Milne, R.W., Weech, P.K., and Rassart, E. (1991). Apolipoprotein D transcription occurs specifically in nonproliferating quiescent and senescent fibroblast cultures. FEBS Lett *290*, 139-141.

Qin, L., and Crews, F.T. (2012). NADPH oxidase and reactive oxygen species contribute to alcohol-induced microglial activation and neurodegeneration. J Neuroinflammation *9*, 5.

Ramana, K.V., Friedrich, B., Srivastava, S., Bhatnagar, A., and Srivastava, S.K. (2004). Activation of nuclear factor-kappaB by hyperglycemia in vascular smooth muscle cells is regulated by aldose reductase. Diabetes *53*, 2910-2920.

Rando, ThomasÂ A., and Chang, HowardÂ Y. (2012). Aging, Rejuvenation, and Epigenetic Reprogramming: Resetting the Aging Clock. Cell *148*, 46-57.

Raschle, M., Knipscheer, P., Enoiu, M., Angelov, T., Sun, J., Griffith, J.D., Ellenberger, T.E., Scharer, O.D., and Walter, J.C. (2008). Mechanism of replication-coupled DNA interstrand crosslink repair. Cell *134*, 969-980.

Rashid, M., Kotwani, A., and Fahim, M. (2011). Long-acting phosphodiesterase 5 inhibitor, tadalafil, and superoxide dismutase mimetic, tempol, protect against acute hypoxia-induced pulmonary hypertension in rats. Hum Exp Toxicol.

Reay, D.P., Yang, M., Watchko, J.F., Daood, M., O'Day, T.L., Rehman, K.K., Guttridge, D.C., Robbins, P.D., and Clemens, P.R. (2011). Systemic delivery of NEMO binding domain/IKKgamma inhibitory peptide to young mdx mice improves dystrophic skeletal muscle histopathology. Neurobiol Dis.

Remuzzi, A., Gagliardini, E., Donadoni, C., Fassi, A., Sangalli, F., Lepre, M.S., Remuzzi, G., and Benigni, A. (2002). Effect of angiotensin II antagonism on the regression of kidney disease in the rat. Kidney Int *62*, 885-894.

Resnick, N.M., and Dosa, D. (2004). Harrison's Principles of Internal Medicine, 15 edn (Montreal, McGraw-Hill).

Resnick, N.M., and Marcantonio, E.R. (1997). How should clinical care of the aged differ? Lancet *350*, 1157-1158.

Rikans, L.E., and Hornbrook, K.R. (1997). Lipid peroxidation, antioxidant protection and aging. Biochim Biophys Acta *1362*, 116-127.

Rink, S.M., Solomon, M.S., Taylor, M.J., Rajur, S.B.-N., McLaughlin, L.W., and Hopkins, P.B. (1993). Covalent structure of a nitrogen mustard-induced DNA interstrand cross-link: an N7-to-N7 linkage of deoxyguanosine residues at the duplex sequence 5'-d(GNC). J Am Chem Soc *115*, 2551-2557.

Robinson, I., de Serna, D.G., Gutierrez, A., and Schade, D.S. (2006). Vitamin E in humans: an explanation of clinical trial failure. Endocr Pract *12*, 576-582.

Rodier, F., and Campisi, J. (2011). Four faces of cellular senescence. J Cell Biol *192*, 547-556.

Rodier, F., Coppe, J.P., Patil, C.K., Hoeijmakers, W.A., Munoz, D.P., Raza, S.R., Freund, A., Campeau, E., Davalos, A.R., and Campisi, J. (2009). Persistent DNA damage signalling triggers senescence-associated inflammatory cytokine secretion. Nat Cell Biol *11*, 973-979.

Rodier, F., Munoz, D.P., Teachenor, R., Chu, V., Le, O., Bhaumik, D., Coppe, J.P., Campeau, E., Beausejour, C.M., Kim, S.H.*, et al.* (2011). DNA-SCARS: distinct nuclear structures that sustain damage-induced senescence growth arrest and inflammatory cytokine secretion. J Cell Sci *124*, 68-81.

Rodriguez-Puyol, D. (1998). The aging kidney. Kidney Int *54*, 2247-2265.

Romieu, A., Gasparutto, D., and Cadet, J. (1999). Synthesis and characterization of oligonucleotides containing 5',8-cyclopurine 2'-deoxyribonucleosides: (5'R)-5',8-cyclo-2'-deoxyadenosine, (5'S)-5',8-cyclo-2'-deoxyguanosine, and (5'R)-5',8-cyclo-2'-deoxyguanosine. Chem Res Toxicol *12*, 412-421.

Ross, W.E., Ewig, R.A., and Kohn, K.W. (1978). Differences between melphalan and nitrogen mustard in the formation and removal of DNA cross-links. Cancer Res *38*, 1502-1506.

Roughley, P.J. (2004). Biology of intervertebral disc aging and degeneration: involvement of the extracellular matrix. Spine (Phila Pa 1976) *29*, 2691-2699.

Roughley, P.J., Alini, M., and Antoniou, J. (2002). The role of proteoglycans in aging, degeneration and repair of the intervertebral disc. Biochem Soc Trans *30*, 869-874.

Salmon, A.B., Richardson, A., and Perez, V.I. (2010). Update on the oxidative stress theory of aging: does oxidative stress play a role in aging or healthy aging? Free Radic Biol Med *48*, 642-655.

Sargent, R.G., Brenneman, M.A., and Wilson, J.H. (1997a). Repair of site-specific double-strand breaks in a mammalian chromosome by homologous and illegitimate recombination. Mol Cell Biol *17*, 267-277.

Sargent, R.G., Meservy, J.L., Perkins, B.D., Kilburn, A.E., Intody, Z., Adair, G.M., Nairn, R.S., and Wilson, J.H. (2000). Role of the nucleotide excision repair gene ERCC1 in formation of recombination-dependent rearrangements in mammalian cells. Nucleic Acids Res *28*, 3771-3778.

Sargent, R.G., Rolig, R.L., Kilburn, A.E., Adair, G.M., Wilson, J.H., and Nairn, R.S. (1997b). Recombination-dependent deletion formation in mammalian cells deficient in the nucleotide excision repair gene ERCC1. Proc Natl Acad Sci U S A *94*, 13122-13127.

Satoh, H., Hiyama, K., Takeda, M., Awaya, Y., Watanabe, K., Ihara, Y., Maeda, H., Ishioka, S., and Yamakido, M. (1996). Telomere shortening in peripheral blood cells was related with aging but not with white blood cell count. Jpn J Hum Genet *41*, 413-417.

Scheidereit, C. (2006). IkappaB kinase complexes: gateways to NF-kappaB activation and transcription. Oncogene *25*, 6685-6705.

Schiestl, R.H., and Prakash, S. (1990). RAD10, an excision repair gene of Saccharomyces cerevisiae, is involved in the RAD1 pathway of mitotic recombination. Mol Cell Biol *10*, 2485-2491.

Schlake, C., Ostermann, K., Schmidt, H., and Gutz, H. (1993). Analysis of DNA repair pathways of Schizosaccharomyces pombe by means of swi-rad double mutants. Mutat Res *294*, 59-67.

Schrader, C.E., Vardo, J., Linehan, E., Twarog, M.Z., Niedernhofer, L.J., Hoeijmakers, J.H., and Stavnezer, J. (2004). Deletion of the nucleotide excision repair gene Ercc1 reduces immunoglobulin class switching and alters mutations near switch recombination junctions. J Exp Med *200*, 321-330.

Schumacher, B., van der Pluijm, I., Moorhouse, M.J., Kosteas, T., Robinson, A.R., Suh, Y., Breit, T.M., van Steeg, H., Niedernhofer, L.J., van Ijcken, W.*, et al.* (2008). Delayed and accelerated aging share common longevity assurance mechanisms. PloS Genet *4*, e1000161.

Sekelsky, J.J., McKim, K.S., Chin, G.M., and Hawley, R.S. (1995). The Drosophila meiotic recombination gene mei-9 encodes a homologue of the yeast excision repair protein Rad1. Genetics *141*, 619-627.

Selfridge, J., Hsia, K.T., Redhead, N.J., and Melton, D.W. (2001). Correction of liver dysfunction in DNA repair-deficient mice with an ERCC1 transgene. Nucleic Acids Res *29*, 4541-4550.

Selfridge, J., Song, L., Brownstein, D.G., and Melton, D.W. (2010). Mice with DNA repair gene Ercc1 deficiency in a neural crest lineage are a model for late-onset Hirschsprung disease. DNA Repair (Amst) *9*, 653-660.

Selman, C., Tullet, J.M., Wieser, D., Irvine, E., Lingard, S.J., Choudhury, A.I., Claret, M., Al-Qassab, H., Carmignac, D., Ramadani, F.*, et al.* (2009). Ribosomal protein S6 kinase 1 signaling regulates mammalian life span. Science *326*, 140-144.

Shtutman, M., Zhurinsky, J., Simcha, I., Albanese, C., D'Amico, M., Pestell, R., and Ben-Ze'ev, A. (1999). The cyclin D1 gene is a target of the beta-catenin/LEF-1 pathway. Proc Natl Acad Sci U S A *96*, 5522-5527.

Siakotos, A.N., and Koppang, N. (1973). Procedures for the isolation of lipopigments from brain, heart and liver, and their properties: A review. Mech Ageing Dev *2*, 177-200.

Sijbers, A.M., de Laat, W.L., Ariza, R.R., Biggerstaff, M., Wei, Y.F., Moggs, J.G., Carter, K.C., Shell, B.K., Evans, E., de Jong, M.C.*, et al.* (1996a). Xeroderma pigmentosum group F caused by a defect in a structure-specific DNA repair endonuclease. Cell *86*, 811-822.

Sijbers, A.M., van der Spek, P.J., Odijk, H., van den Berg, J., van Duin, M., Westerveld, A., Jaspers, N.G., Bootsma, D., and Hoeijmakers, J.H. (1996b). Mutational analysis of the human nucleotide excision repair gene ERCC1. Nucleic Acids Res *24*, 3370-3380.

Sijbers, A.M., van Voorst Vader, P.C., Snoek, J.W., Raams, A., Jaspers, N.G., and Kleijer, W.J. (1998). Homozygous R788W point mutation in the XPF gene of a patient with xeroderma pigmentosum and late-onset neurologic disease. J Invest Dermatol *110*, 832-836.

Silva, F.G. (2005). The aging kidney: a review -- part I. Int Urol Nephrol *37*, 185-205.

Smith, R.A., Hartley, R.C., and Murphy, M.P. (2011). Mitochondria-targeted small molecule therapeutics and probes. Antioxid Redox Signal *15*, 3021-3038.

Smith, R.A., Porteous, C.M., Coulter, C.V., and Murphy, M.P. (1999). Selective targeting of an antioxidant to mitochondria. Eur J Biochem *263*, 709-716.

Smogorzewska, A., van Steensel, B., Bianchi, A., Oelmann, S., Schaefer, M.R., Schnapp, G., and de Lange, T. (2000). Control of human telomere length by TRF1 and TRF2. Mol Cell Biol *20*, 1659-1668.

Snow, B.J., Rolfe, F.L., Lockhart, M.M., Frampton, C.M., O'Sullivan, J.D., Fung, V., Smith, R.A., Murphy, M.P., and Taylor, K.M. (2010). A double-blind, placebo-controlled study

to assess the mitochondria-targeted antioxidant MitoQ as a disease-modifying therapy in Parkinson's disease. Mov Disord *25*, 1670-1674.

Sonoda, E., Sasaki, M.S., Morrison, C., Yamaguchi-Iwai, Y., Takata, M., and Takeda, S. (1999). Sister chromatid exchanges are mediated by homologous recombination in vertebrate cells. Mol Cell Biol *19*, 5166-5169.

Soule, B.P., Hyodo, F., Matsumoto, K., Simone, N.L., Cook, J.A., Krishna, M.C., and Mitchell, J.B. (2007). Therapeutic and clinical applications of nitroxide compounds. Antioxid Redox Signal *9*, 1731-1743.

Stoepker, C., Hain, K., Schuster, B., Hilhorst-Hofstee, Y., Rooimans, M.A., Steltenpool, J., Oostra, A.B., Eirich, K., Korthof, E.T., Nieuwint, A.W.*, et al.* (2011). SLX4, a coordinator of structure-specific endonucleases, is mutated in a new Fanconi anemia subtype. Nat Genet *43*, 138-141.

Stone, M.P., Cho, Y.J., Huang, H., Kim, H.Y., Kozekov, I.D., Kozekova, A., Wang, H., Minko, I.G., Lloyd, R.S., Harris, T.M.*, et al.* (2008). Interstrand DNA cross-links induced by alpha,beta-unsaturated aldehydes derived from lipid peroxidation and environmental sources. Acc Chem Res *41*, 793-804.

Svendsen, J.M., Smogorzewska, A., Sowa, M.E., O'Connell, B.C., Gygi, S.P., Elledge, S.J., and Harper, J.W. (2009). Mammalian BTBD12/SLX4 assembles a Holliday junction resolvase and is required for DNA repair. Cell *138*, 63-77.

Tapias, A., Auriol, J., Forget, D., Enzlin, J.H., Scharer, O.D., Coin, F., Coulombe, B., and Egly, J.M. (2004). Ordered conformational changes in damaged DNA induced by nucleotide excision repair factors. J Biol Chem *279*, 19074-19083.

Tappel, A.L. (1973). Lipid peroxidation damage to cell components. Federation proceedings *32*, 1870-1874.

Taubold, R.D. (1975). Studies on chemical nature of lipofusion (age pigment) isolated from normal human brain. Lipids *10*, 383-390.

Thielmann, H.W., Popanda, O., Edler, L., and Jung, E.G. (1991). Clinical symptoms and DNA repair characteristics of xeroderma pigmentosum patients from Germany. Cancer Res *51*, 3456-3470.

Thorel, F., Constantinou, A., Dunand-Sauthier, I., Nouspikel, T., Lalle, P., Raams, A., Jaspers, N.G., Vermeulen, W., Shivji, M.K., Wood, R.D.*, et al.* (2004). Definition of a short region of XPG necessary for TFIIH interaction and stable recruitment to sites of UV damage. Mol Cell Biol *24*, 10670-10680.

Tian, M., Shinkura, R., Shinkura, N., and Alt, F.W. (2004). Growth retardation, early death, and DNA repair defects in mice deficient for the nucleotide excision repair enzyme XPF. Mol Cell Biol *24*, 1200-1205.

Tilstra, J., Rehman, K.K., Hennon, T., Plevy, S.E., Clemens, P., and Robbins, P.D. (2007). Protein transduction: identification, characterization and optimization. Biochem Soc Trans *35*, 811-815.

Tilstra, J.S., Clauson, C.L., Niedernhofer, L.J., and Robbins, P.D. (2011). NF-κB in aging and disease. Aging and Disease *2*, 449-465.

Tokuda, K., and Bodell, W.J. (1987). Cytotoxicity and sister chromatid exchanges in 9L cells treated with monofunctional and bifunctional nitrogen mustards. Carcinogenesis *8*, 1697-1701.

Tokumaru, S., Iguchi, H., and Kojo, S. (1996). Change of the lipid hydroperoxide level in mouse organs on ageing. Mech Ageing Dev *86*, 67-74.

Trifunovic, A., Wredenberg, A., Falkenberg, M., Spelbrink, J.N., Rovio, A.T., Bruder, C.E., Bohlooly, Y.M., Gidlof, S., Oldfors, A., Wibom, R.*, et al.* (2004). Premature ageing in mice expressing defective mitochondrial DNA polymerase. Nature *429*, 417-423.

Tripsianes, K., Folkers, G., Ab, E., Das, D., Odijk, H., Jaspers, N.G., Hoeijmakers, J.H., Kaptein, R., and Boelens, R. (2005). The structure of the human ERCC1/XPF interaction domains reveals a complementary role for the two proteins in nucleotide excision repair. Structure *13*, 1849-1858.

Tronche, F., Casanova, E., Turiault, M., Sahly, I., and Kellendonk, C. (2002). When reverse genetics meets physiology: the use of site-specific recombinases in mice. FEBS Lett *529*, 116-121.

Tsodikov, O.V., Enzlin, J.H., Scharer, O.D., and Ellenberger, T. (2005). Crystal structure and DNA binding functions of ERCC1, a subunit of the DNA structure-specific endonuclease XPF-ERCC1. Proc Natl Acad Sci U S A *102*, 11236-11241.

Tsodikov, O.V., Ivanov, D., Orelli, B., Staresincic, L., Shoshani, I., Oberman, R., Scharer, O.D., Wagner, G., and Ellenberger, T. (2007). Structural basis for the recruitment of ERCC1-XPF to nucleotide excision repair complexes by XPA. EMBO J *26*, 4768-4776.

Valen, G. (2004). Signal transduction through nuclear factor kappa B in ischemia-reperfusion and heart failure. Basic Res Cardiol *99*, 1-7.

Van Houten, B., Woshner, V., and Santos, J.H. (2006). Role of mitochondrial DNA in toxic responses to oxidative stress. DNA Repair (Amst) *5*, 145-152.

Van Remmen, H., Ikeno, Y., Hamilton, M., Pahlavani, M., Wolf, N., Thorpe, S.R., Alderson, N.L., Baynes, J.W., Epstein, C.J., Huang, T.T., *et al.* (2003). Life-long reduction in MnSOD activity results in increased DNA damage and higher incidence of cancer but does not accelerate aging. Physiol Genomics *16*, 29-37.

Villeda, S.A., Luo, J., Mosher, K.I., Zou, B., Britschgi, M., Bieri, G., Stan, T.M., Fainberg, N., Ding, Z., Eggel, A., *et al.* (2011). The ageing systemic milieu negatively regulates neurogenesis and cognitive function. Nature *477*, 90-94.

Vivekananthan, D.P., Penn, M.S., Sapp, S.K., Hsu, A., and Topol, E.J. (2003). Use of antioxidant vitamins for the prevention of cardiovascular disease: meta-analysis of randomised trials. Lancet *361*, 2017-2023.

Vo, N., Seo, H.Y., Robinson, A., Sowa, G., Bentley, D., Taylor, L., Studer, R., Usas, A., Huard, J., Alber, S., *et al.* (2010). Accelerated aging of intervertebral discs in a mouse model of progeria. J Orthop Res *28*, 1600-1607.

Wang, J., Clauson, C.L., Robbins, P.D., Niedernhofer, L.J., and Wang, Y. (2012). The oxidative DNA lesions 8,5'-cyclopurines accumulate with aging in a tissue-specific manner. Aging Cell.

Wang, J., Yuan, B., Guerrero, C., Bahde, R., Gupta, S., and Wang, Y. (2011a). Quantification of oxidative DNA lesions in tissues of Long-Evans Cinnamon rats by capillary high-performance liquid chromatography-tandem mass spectrometry coupled with stable isotope-dilution method. Analytical Chemistry (Washington) *83*, 2201-2209.

Wang, J., Yuan, B., Guerrero, C., Bahde, R., Gupta, S., and Wang, Y. (2011b). Quantification of oxidative DNA lesions in tissues of Long-Evans Cinnamon rats by capillary high-performance liquid chromatography-tandem mass spectrometry coupled with stable isotope-dilution method. Anal Chem *83*, 2201-2209.

Wang, Y. (2008). Bulky DNA lesions induced by reactive oxygen species. Chem Res Toxicol *21*, 276-281.

Warner, H.R., and Sierra, F. (2003). Models of accelerated ageing can be informative about the molecular mechanisms of ageing and/or age-related pathology. Mech Ageing Dev *124*, 581-587.

Weeda, G., Donker, I., de Wit, J., Morreau, H., Janssens, R., Vissers, C.J., Nigg, A., van Steeg, H., Bootsma, D., and Hoeijmakers, J.H. (1997a). Disruption of mouse ERCC1 results in a novel repair syndrome with growth failure, nuclear abnormalities and senescence. Curr Biol *7*, 427-439.

Weeda, G., Eveno, E., Donker, I., Vermeulen, W., Chevallier-Lagente, O., Taieb, A., Stary, A., Hoeijmakers, J.H., Mezzina, M., and Sarasin, A. (1997b). A mutation in the XPB/ERCC3

DNA repair transcription gene, associated with trichothiodystrophy. Am J Hum Genet *60*, 320-329.

Westerveld, A., Hoeijmakers, J.H., van Duin, M., de Wit, J., Odijk, H., Pastink, A., Wood, R.D., and Bootsma, D. (1984). Molecular cloning of a human DNA repair gene. Nature *310*, 425-429.

Wijen, J.P., Nivard, M.J., and Vogel, E.W. (2000). The in vivo genetic activity profile of the monofunctional nitrogen mustard 2-chloroethylamine differs drastically from its bifunctional counterpart mechlorethamine. Carcinogenesis *21*, 1859-1867.

Wilcox, C.S. (2010). Effects of tempol and redox-cycling nitroxides in models of oxidative stress. Pharmacol Ther *126*, 119-145.

Winter, A.G., Samuel, K., Hsia, K.T., and Melton, D.W. (2003). The repair and recombination enzyme ERCC1 is not required for immunoglobulin class switching. DNA Repair (Amst) *2*, 561-569.

Wipf, P., Xiao, J., Jiang, J., Belikova, N.A., Tyurin, V.A., Fink, M.P., and Kagan, V.E. (2005). Mitochondrial targeting of selective electron scavengers: synthesis and biological analysis of hemigramicidin-TEMPO conjugates. J Am Chem Soc *127*, 12460-12461.

Wojcik, M., Burzynska-Pedziwiatr, I., and Wozniak, L.A. (2010). A review of natural and synthetic antioxidants important for health and longevity. Curr Med Chem *17*, 3262-3288.

Wu, Y., Mitchell, T.R., and Zhu, X.D. (2008). Human XPF controls TRF2 and telomere length maintenance through distinctive mechanisms. Mech Ageing Dev *129*, 602-610.

Wullaert, A., Heyninck, K., and Beyaert, R. (2006). Mechanisms of crosstalk between TNF-induced NF-kappaB and JNK activation in hepatocytes. Biochem Pharmacol *72*, 1090-1101.

Xiao, Z.Q., and Majumdar, A.P. (2000). Induction of transcriptional activity of AP-1 and NF-kappaB in the gastric mucosa during aging. Am J Physiol Gastrointest Liver Physiol *278*, G855-865.

Xiong, H., Zhu, C., Li, F., Hegazi, R., He, K., Babyatsky, M., Bauer, A.J., and Plevy, S.E. (2004). Inhibition of interleukin-12 p40 transcription and NF-kappaB activation by nitric oxide in murine macrophages and dendritic cells. J Biol Chem *279*, 10776-10783.

Yamamoto, Y., and Gaynor, R.B. (2001). Role of the NF-kappaB pathway in the pathogenesis of human disease states. Curr Mol Med *1*, 287-296.

Yamamura, K., Ichihashi, M., Hiramoto, T., Ogoshi, M., Nishioka, K., and Fujiwara, Y. (1989). Clinical and photobiological characteristics of xeroderma pigmentosum complementation group F: a review of cases from Japan. Br J Dermatol *121*, 471-480.

Yin, D. (1996). Biochemical basis of lipofuscin, ceroid, and age pigment-like fluorophores. Free Radic Biol Med *21*, 871-888.

Zafeiriou, D.I., Thorel, F., Andreou, A., Kleijer, W.J., Raams, A., Garritsen, V.H., Gombakis, N., Jaspers, N.G., and Clarkson, S.G. (2001). Xeroderma pigmentosum group G with severe neurological involvement and features of Cockayne syndrome in infancy. Pediatr Res *49*, 407-412.

Zelle, B., Berends, F., and Lohman, P.H. (1980). Repair of damage by ultraviolet radiation in xeroderma pigmentosum cell strains of complementation groups E and F. Mutat Res *73*, 157-169.

Zhou, B., Yang, L., Li, S., Huang, J., Chen, H., Hou, L., Wang, J., Green, C.D., Yan, Z., Huang, X.*, et al.* (2012). Midlife gene expressions identify modulators of aging through dietary interventions. Proc Natl Acad Sci U S A.

Zhu, X.D., Niedernhofer, L., Kuster, B., Mann, M., Hoeijmakers, J.H., and de Lange, T. (2003). ERCC1/XPF removes the 3' overhang from uncapped telomeres and represses formation of telomeric DNA-containing double minute chromosomes. Mol Cell *12*, 1489-1498.